UNIVERSITÀ DEGLI STUDI DI UDINE
hic sunt futura

www.uniud.it

UNIVERSITY OF UDINE

Department of Medical Area DAME

PhD course in Biomedical Sciences and Biotechnologies

in agreement with CRO-IRCCS Institute of Aviano (Italy)

XXXIII Cycle

PhD THESIS

Multimerin-2 maintains vascular homeostasis and controls cancer cells dissemination

PhD Student:

Evelina Poletto

Supervisor:

Dr. Paola Spessotto

Co-supervisor:

Dr. Mongiat Maurizio

Discussion Year 2021

TABLE OF CONTENTS

1. ABSTRACT

Angiogenesis, the formation of new blood vessels from pre-existing vasculature, is a hallmark of cancer. In fact, tumor vascularization is required to support cancer growth, supplying oxygen and nutrients to tumor cells, and represents also an important route for metastatization. In this context, Multimerin-2 an extracellular matrix protein specifically deposited along blood vessels, plays an important role. This study started from the observation that in ovarian, breast, gastric and colon cancer samples the expression of Multimerin-2 is lost in a number of vessels. Next, we verified the effects of Multimerin-2 down-regulating its expression in endothelial cells and demonstrating that Multimerin-2 was necessary for proper cell-to-cell contact formation thus exerting a homeostatic function. In particular, Multimerin-2 loss led to the dismantlement of VE-cadherin lining, causing a strong increase of cell permeability to small molecules. Mechanistically, Multimerin-2 knockdown triggered the phosphorylation of VEGFR2 at Y951, leading to Src activation, and, ultimately VE-cadherin phosphorylation at Y568, which in turn is targeted for internalization and degradation. These results were corroborated *in vivo* exploiting the *Multimerin-2*$^{-/-}$ mouse model, since blood vessels from *Multimerin-2*$^{-/-}$ mice displayed abnormal VE-cadherin lining and increased vascular leakage. Furthermore, B16F10 tumor-bearing *Multimerin-2*$^{-/-}$ mice showed impaired tumor vasculature, characterized by increased permeability and reduced perfusion. As a consequence, the compromised tumor vessels functionality in *Multimerin-2*$^{-/-}$ mice associated with impaired drug delivery and decreased chemotherapy efficacy. Given that blood vessels represent an important route for the dissemination of cancer cells, we next verified if the loss of Multimerin-2 could affect cancer cell dissemination. Indeed, we found that Multimerin-2 depletion favoured cancer cells transmigration through the endothelial barrier with a VEGF-A-independent mechanism. Instead, the down-regulation of Multimerin-2 in endothelial cells associated with a strong increase in the adhesion molecule VCAM1 only under tumor conditions. Consistently, the intravenous injection of B16F10 cells in *Multimerin-2*$^{-/-}$ mice led to the formation of a higher number of lung metastatic lesions compared to the *wild type* animals.

Taken together these results pinpoint Multimerin-2 as a key molecule for the maintenance of vascular homeostasis. Depending on the levels of Multimerin-2 loss, these pre-clinical results open the possibility to develop a new prognostic marker to predict clinical outcome of cancer patients.

2. INTRODUCTION

2.1 Angiogenesis

The vascular system, with its unique hierarchical organization, is essential for the distribution of oxygen and nutrients and the clearance of catabolites in the whole body, contributing to tissues homeostasis. Vessels structure varies among different types of vessels depending on their functional requirements. Capillaries, that ensure exchanges between bloodstream and tissues, are formed by an inner layer of endothelial cells (ECs), wrapped by pericytes, mesenchymal-like cells that contribute to vessels stabilization. Both ECs and pericytes contribute to the deposition of the highly specialized basement membrane (BM) of the endothelium. Larger vessels are also invested by smooth muscle cells and an elastin-rich extracellular matrix (ECM), to ensure an higher contractile capability to respond to blood flow fluctuations (Grant and Karsan, 2018).

Blood vessel formation is an early and fundamental step during embryonic development. This process, known as vasculogenesis, begins with the clustering of endothelial progenitor cells (angioblasts) to form a primordial vascular plexus (Kolte et al., 2016). Once formed, vessels can grow through sprouting angiogenesis, in which ECs emerge from pre-existing vasculature to form new tube structures, or through intussusceptive angiogenesis, that allows the insertion of new transcapillary tissue pillars, contributing to the vascular bed formation (Burri and Djonov, 2002). Despite essential, sprouting angiogenesis occurs only during development and in adult, physiologically, takes place in the female reproductive tract or during wound healing, in a very restrictive time window. Indeed, aberrant angiogenesis contributes to the pathogenesis of many diseases, such as arthritis, retinopathy and cancer (Carmeliet, 2003).

Hypoxia is the main driver of sprouting angiogenesis: in fact, low levels of oxygen within a tissue induce the stabilization of HIFs (Hypoxia Inducible Factors) transcription factors which trigger the expression of several angiogenic molecules necessary to guide the angiogenic process (Warmke et al., 2018). Historically, in 1977 Ausprunk and Folkmann (Ausprunk' and Folkman, 1977) were the first to describe the main steps of angiogenesis, as follow (Figure 1):

1. degradation of BM in proximity of the angiogenic stimuli;
2. loss of ECs contacts and their migration toward stimuli;
3. formation of a solid cord of ECs;
4. lumen formation;
5. anastomosis of contiguous tubular sprouts to form functionally capillary loops;
6. stabilization of newly formed vessels through BM deposition and pericytes recruitment.

All these events are built up by the coordination of specialized and activated ECs, termed as tip and stalk cells, whose specification is required for the development of a properly shaped nascent sprout. Tip cells are characterized by a migratory phenotype, they form protrusions and filopodia guiding the nascent blood vessel towards the angiogenic stimulus. Instead, stalk cells display a higher proliferation potential necessary to stabilize and extend the sprouts, also coordinating lumen formation (Gerhardt et al., 2003; Geudens and Gerhardt, 2011). In this context, Vascular Endothelial Growth Factor A (VEGF-A), whose expression is triggered by HIFs, plays a pivotal role in orchestrating vessels formation. It can stimulate the formation of filopodia in tip cell and, represents the most important proliferative cue for stalk cells, which respond to VEGF-A concentration and spatial distribution (Gerhardt et al., 2003).

Upon an angiogenic stimulus, ECs must be "released" through the BM breakdown to allow migration. Tip cells secrete several proteases to digest the surrounding ECM, such as the membrane type 1-matrix metalloproteinase (MT1-MMP) (Arroyo and Iruela-Arispe, 2010) and the urokinase-type plasminogen activator (uPA) (Kolte et al., 2016). The ECM digestion leads to the release of

matrix-bound angiogenic factors, and, on the other hand, also anti-angiogenic molecules, to ensure a balanced angiogenic response. Local increase of angiogenic cytokines, including Angiopoietin-2 (Ang-2) is instrumental to pericytes detachment from the emerging sprouts. Specification of leading tip cells and proliferative stalk cells is determined by a mechanism of "lateral inhibition", involving the Notch and VEGF-A/VEGFR2 signalling pathways (Phng and Gerhardt, 2009), that establish the two distinct ECs phenotypes (Figure 1). Once the sprout is formed, in order to be functional, it must be perfused to prevent regression. Lumen formation can take place in two distinct way:

- cell hollowing, occurring through the coalescence of intracellular vacuoles between adjacent ECs;
- cord hollowing, established through the shaping of ECs' junctions to form a lumen (Strilić et al., 2009).

New vessels loops can be further completed by the merge of tip cells coming from different sprouts. Finally, stabilization is achieved through the deposition of BM components and the recruitment of pericytes allowing ECs to enter a quiescent state (Potente et al., 2011).

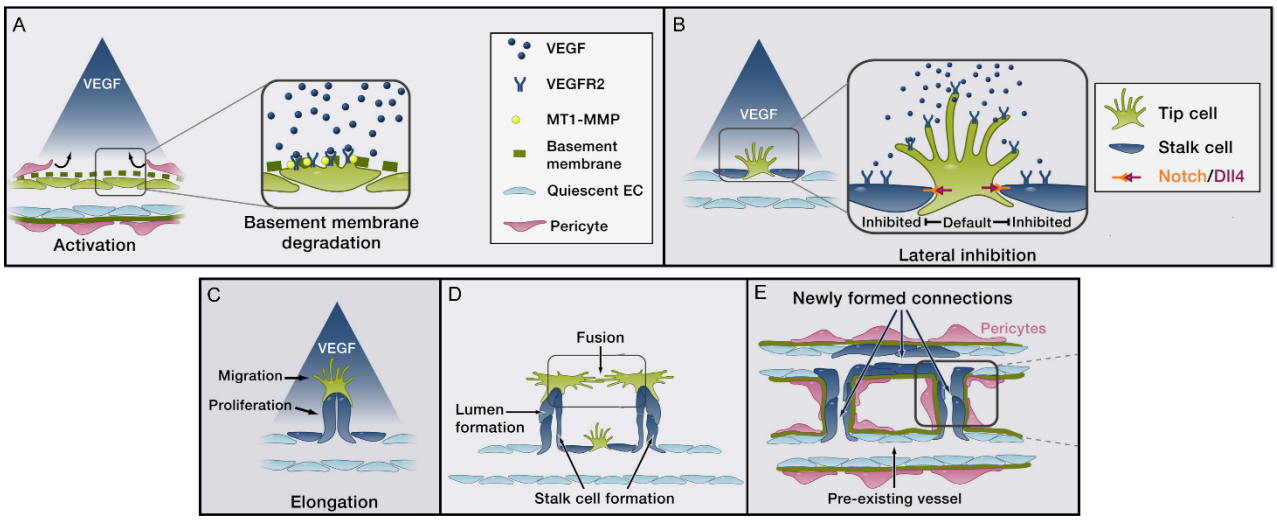

Figure 1. Schematic representation of the key step of sprouting angiogenesis. *(A) Upon angiogenic stimuli ECs degrade the BM. (B) Tip and stalk cells are committed through different sensing of the angiogenic stimulus. (C) Tip cells form filopodia and migrate whereas stalk cells proliferate and elongate the sprouts. (D) Lumen is formed and adjacent sprouts can fuse. (E) Newly formed vessels are stabilized with BM deposition and pericytes recruitment (adapted from Potente, 2011).*

2.1.1 Endothelial cells act as a barrier

Quiescent endothelium, formed by the so-called phalanx ECs, constitutes a dynamic barrier between blood and tissues in the whole body, controlling the exchange of fluids, small molecules and transmigration of immune cells. Physiologically, small solutes and molecules (less than 40kDa) can leak outside of the vessels without affecting endothelium integrity, in a process defined as vascular permeability (Claesson-Welsh, 2015). This tightly regulated process is achieved through the establishment of a specialized junctional compartment between ECs, formed by different transmembrane adhesive proteins which connect adjacent cells through homophilic interactions. Above all, vascular permeability is mediated by two main junction types: adherens junctions (AJs) and tight junctions (TJs) that are intermingled along the cleft (Dejana, 2004) (Figure 2). TJs form dense structures, visible by electron microscopy, which juxtapose very close to the membranes of

adjacent cells. Many classes of proteins participate to TJs formation: occludins, claudins and junctional adhesion molecules (JAMs), which are transmembrane proteins connected to intracellular adapters called *zonula occludens* (ZO-1, ZO-2 and ZO-3) (Gavard, 2009). Of note, claudin-5 is a typical TJs' protein exclusively expressed by ECs and its absence leads to an altered permeability of brain barrier (Nitta et al., 2003). Instead, AJs in cell-to-cell contacts are formed through the interactions of Ca^{2+}-dependent transmembrane proteins called cadherins. ECs mainly express VE-cadherin, exclusively present in the endothelium, and N-cadherin also expressed by neuronal cells and smooth muscle cells (Bazzoni and Dejana, 2004). VE-cadherin is essential for developing of vascular system since the gene knockout leads to early embryonic lethality due to severe vascular defects (Carmeliet et al., 1999). Importantly, at cytoplasmatic levels both TJs and AJs are connected to the actin cytoskeleton, further supporting their stability and orchestrating the EC barrier (Bazzoni and Dejana, 2004).

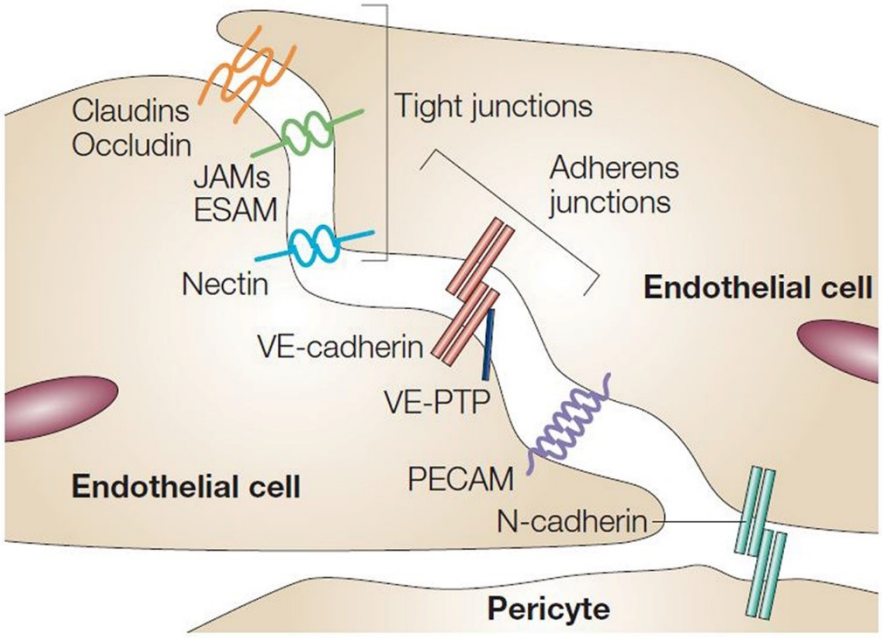

Figure 2. ECs junctions. *ECs are characterized by a specialized junctional compartment formed by TJs (claudins, occludins and JAMs) and AJs, mainly represented by VE-cadherin (from Dejana, 2004).*

Interestingly, the organization of the endothelial junctions varies among the vessels of different organs, reflecting the special needs of each tissue. For example, capillaries in the blood brain barrier are characterized by tightly connected ECs with a high amount of junctional proteins to protect the brain from edema. Instead, hormone-producing organs, like pancreas, show a fenestrated endothelium with fewer junctions to allow the passage of several molecules (Claesson-Welsh, 2015). These evidences support the idea that ECs' junctions are not mere glue between cells, but they form a specific signalling unit that, finely tunes ECs responses. Indeed, junctional proteins can trigger several signals inside the cells to communicate cell position, growth arrest and apoptosis, thus contributing to vascular homeostasis (Dejana, 2004). For example, VE-cadherin can interact with different GTPase to create a dynamic crosstalk with the cytoskeleton and through the engagement of β-catenin can

modulate gene expression, defining its localization. Moreover, upon an angiogenic signal, VE-cadherin modifications can potentiate the activation of several growth factor receptors. For instance, VEGF-A stimulation can trigger the phosphorylation of Y568 Y685 and Y731 of VE-cadherin, peculiar post-translational modifications associated to increased vascular permeability (Y568 and Y685) and favoured leukocytes extravasation, for Y731 (Orsenigo et al., 2012; Wessel et al., 2014).

2.1.2 VEGFR2 coordinates endothelial cells behaviours

In physiological conditions, the EC' quiescent state is maintained by a proper equilibrium between activators and inhibitors of angiogenesis, including growth factors, proteases, ECM components, cytokines and chemokines. Under certain conditions, like hypoxia, angiogenesis is switched on mainly due to increased levels of VEGF-A.

The VEGF protein family includes five members: placental growth factor (PGF), VEGF-A, VEGF-B, VEGF-C and VEGF-D, exerting different functions through ligand-specific transmembrane receptors (Carmeliet, 2005). Four different isoforms of VEGF-A, generated by alternative splicing, have been described: $VEGF_{121}$, $VEGF_{165}$, $VEGF_{189}$, and $VEGF_{206}$. These proteins can be either secreted as soluble cytokines in the microenvironment or be bound within the ECM (apart from $VEGF_{121}$), thus confining them closely to EC surface (Ferrara, 2010). VEGFs can bind three membrane tyrosine-kinase receptors, VEGFR1, VEGFR2 and VEGFR3, which show overlapping but distinct expression patterns. VEGFR1 is mainly expressed by monocytes and smooth muscle cells, VEGFR2 by ECs and VEGFR3 by lymphatic ECs (Koch and Claesson-Welsh, 2012). Gene depletion of all VEGFRs causes embryonic death at early stages, due to severe defects of the vascular system (Sullivan and Brekken, 2010). Apart from VEGFR3, both VEGFR1 and VEGFR2 can bind VEGF-A triggering different cellular responses (Figure 3). VEGFR1 functions as a decoy receptor since it can bind VEGF-A with higher affinity respect to VEGFR2, but has a very weak kinase activity, which impedes a full activation of the receptor (Ito et al., 1998). Thus, VEGFR1 sequesters VEGF-A, preventing and controlling VEGFR2 activation in ECs. VEGFR2 is typically expressed by ECs and through the binding of VEGF-A, it regulates most of the essential activities of the endothelium. Indeed, VEGFR2 is the main inducer of angiogenesis mediating EC survival, proliferation migration and permeability. VEGF-A engagement causes the autophosphorylation of VEGFR2 in several tyrosine residues; the most important are Y1175, Y1214 and Y951, which can be recognized by many signalling transducers. For example, phosphorylated Y1175 can activate the PLCγ and RAS/RAF/MAP kinase cascades to sustain EC proliferation, whereas phosphorylated Y1214 promotes migration through the activation of the Cdc42 and p38/MAPK signalling pathways (Koch and Claesson-Welsh, 2012). The VEGF-A/VEGFR2 axis can control vascular permeability in two distinct ways: on one hand it induces the expression of endothelial nitric oxide synthase (eNOS), thus increasing the NO levels, and, on the other hand, it causes VE-cadherin phosphorylation by Src, losing the EC junctions (Li et al., 2016; Wallez et al., 2007). VEGFR2 responses are controlled through the interaction with other transmembrane receptors, such as Neuropilin-1 (NRP1) and integrins, to fine-tune the EC' responses (Koch and Claesson-Welsh, 2012; Peach et al., 2018).

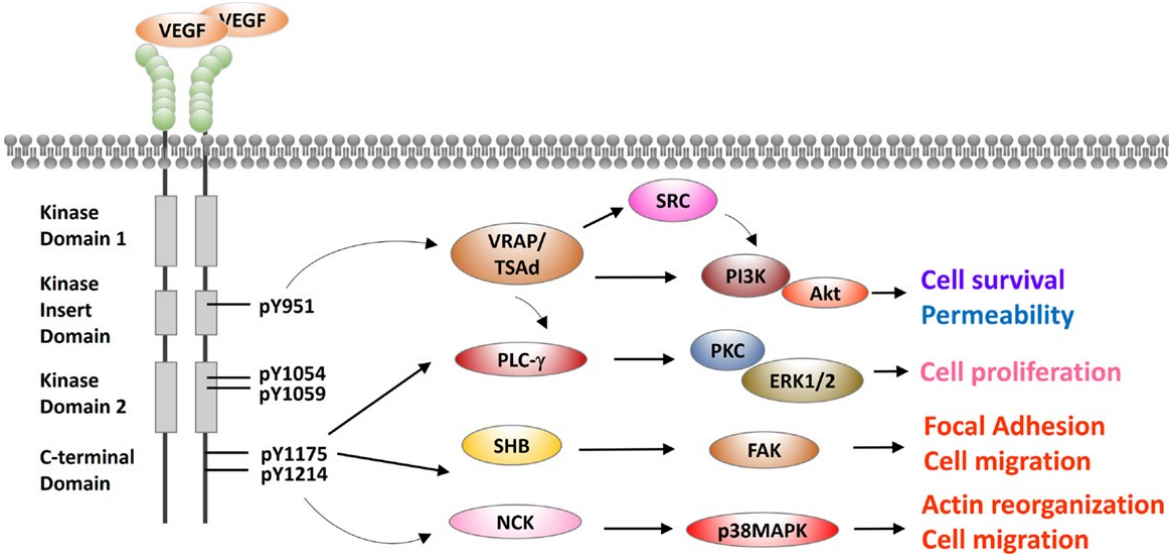

Figure 3 VEGFR2 functions in ECs. *Different sites of phosphorylation induce the recruitment of distinct signal transducers, which in turn trigger several cellular response (from Zhu and Zhou, 2015).*

2.2 Tumor angiogenesis

Like any other normal organs, to survive tumors need nutrients and oxygen as well as the clearance of catabolites. Thus, the formation of new vessels is a crucial step during tumor progression and it is considered a hallmark of cancers (Hanahan and Weinberg, 2011). In adults, physiological angiogenesis is a tightly controlled process lasting in a limited time window and being promptly switched off due to an overbalance of anti-angiogenic factors. Instead, tumors are characterized by a pathological continuously persisting angiogenesis.

Initially, tumors have very small dimensions (0,2-2mm diameter) and they are not vascularized, since the uptake of oxygen and small molecules occurs via diffusion from the nearby vessels, resting in a dormant state (Ribatti, 2013). In 1971, Folkman was the first to hypothesize that, in order to sustain their growth, cancer cells must induce the formation of new vessels through the production of angiogenic factors (Folkman et al., 1971). Indeed, to keep proliferating, tumors must trigger the so-called "angiogenic switch", disrupting the finely tuned balance between pro- and anti-angiogenic factors (Carmeliet, 2005), thus inducing blood vessel formation. This switch is caused by concomitant events. On one hand, oncogene activation, besides inducing the hyperproliferation of cancer cells also stimulates the expression of several angiogenic factors, such as VEGF-A, PDGF, and FGF2. On the other hand, due to the rapid growth, the inner part of tumor is exceedingly hypoxic, condition recognized as a main driver of sprouting angiogenesis. Moreover, in the tumor microenvironment (TME), augmented levels of pro-angiogenic molecules are maintained by immune cells infiltrates as well as by cancer associated fibroblasts (CAFs) (Ribatti, 2013).

Escape from dormancy and tumor-associated vessels formation can be achieved through different mechanisms (Figure 4):

- sprouting angiogenesis, where the VEGF-A/VEGFR2 pathway is fundamental, as observed during the development of the vascular system;
- recruitment of endothelial progenitor cells (EPCs) that initiates vasculogenesis within the tumor mass;

- vascular mimicry, when highly aggressive cancer cells can phenocopy ECs behaviours forming tube-like structures;
- trans-differentiation of cancer stem cells (CSCs) in ECs or smooth muscle cells for de novo generation of tumor vasculature (Lugano et al., 2020).

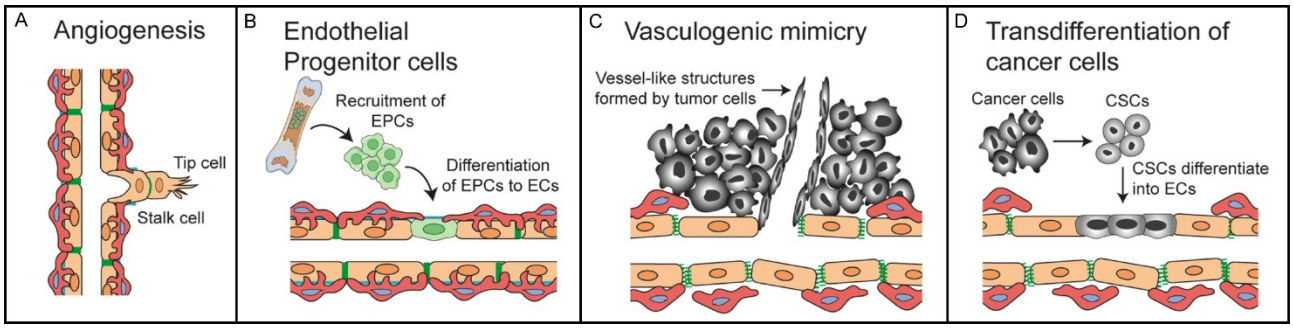

Figure 4. Formation of tumor-associated vessels*. (A) Sprouting of new vessels from pre-existing ones. (B) Recruitment of progenitors ECs (EPCs) that can initiate vasculogenesis. (C) Cancer cells phenocopy ECs to form vessels like structures. (D) CSCs transdifferentiate into ECs and smooth muscle cells to form new vessels (from Lugano et al., 2020).*

The unceasing presence of pro-angiogenic factors hinder the stabilization and maturation of newly formed tumor-associated vessels. In fact, tumor vessels are abnormal, being extremely tortuous and often displaying collapsed or enlarged lumens. Their distribution is highly chaotic being characterized by adjacent vessels-rich and vessels-poor regions. ECs lose their typical cobblestone shape, are poorly interconnected with weakened junctions and occasionally are multi-layered (Potente et al., 2011). The BM is abnormal, both in terms of thickness and composition impeding a proper attachment of pericytes and smooth muscle cells. These morphological defects affect vessels functionality, and thus cancer pathophysiology, in terms of growth, metastasis and response to drug treatments. Heterogeneous distribution of tumor-associated vessels profoundly alters the blood flow and the discontinuous ECs barrier allows increased leakiness of plasma proteins and other molecules (Goel et al., 2011). The excess of tumor vascular permeability strictly contributes to the increase of the interstitial pressure, boosting mechanical stress to both cancer cells and ECs that are forced to collapse into the vessel lumen, further compromising their functionality and increasing tumor tissue hypoxia (Figure 5).

Importantly, the intrinsically inefficient tumor vasculature gravely impairs drug therapy. On one hand, high interstitial pressure impedes an homogeneous drug distribution in the tumor and, on the other,the increased tumor stiffness, observed in many solid cancers, can compress vessels, causing the collapse of their lumen, further affecting drug delivery (Claesson-Welsh, 2015; Goel et al., 2011).

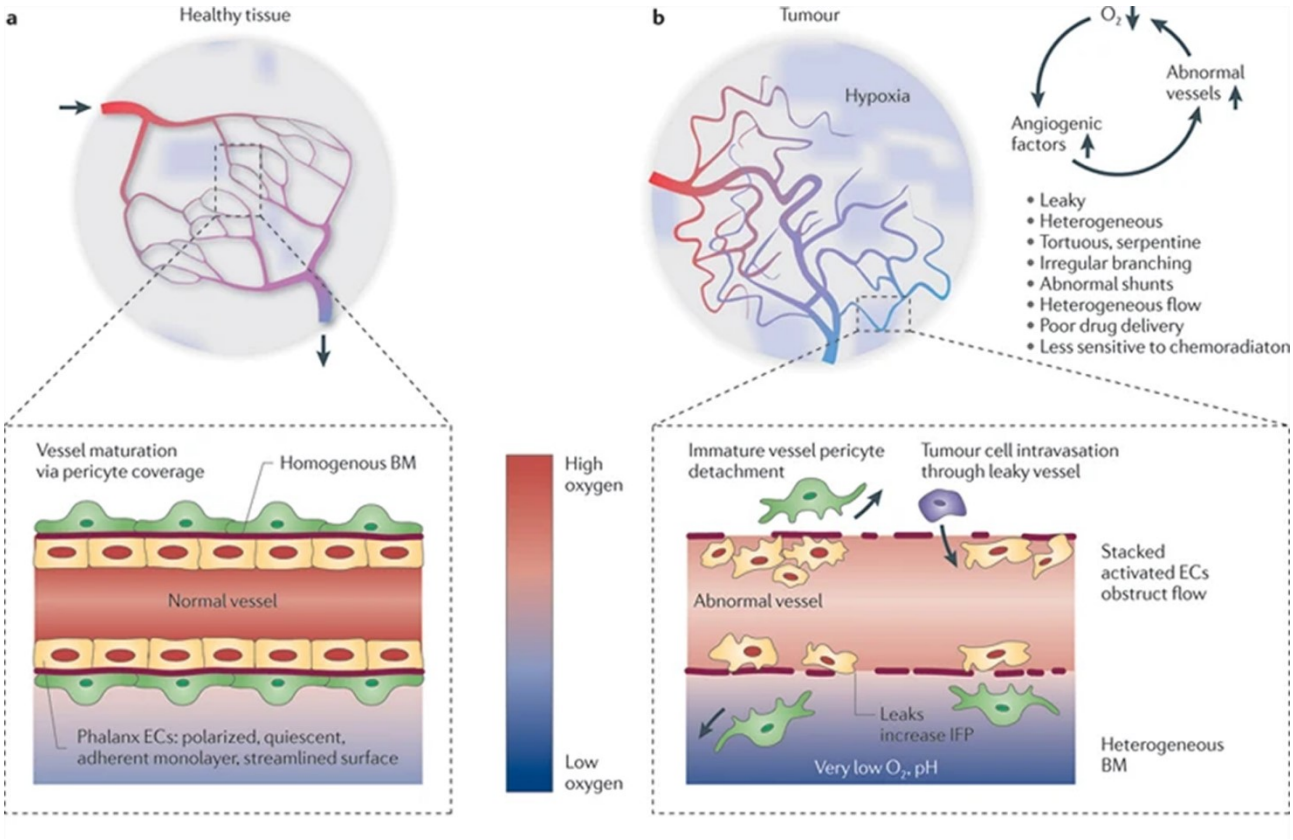

Figure 5. Tumor-associated vessels are structurally and functionally abnormal. *(a) In healthy tissue, a regularly patterned and functional vasculature is characterized by a hierarchical organization, normal vessel wall and tightly connected ECs. (b) In tumors the vasculature and ECs barrier are significantly impaired in terms of structure and functionality (from Carmeliet and Jain, 2011).*

2.2.1 Anti-angiogenic therapy for cancer treatment

In 1971, with his seminal work, Dr. Judah Folkman was the first to hypothesize that the identification of the molecules able to block tumor angiogenesis could raise the possibility to induce cancer cell starvation and death.

VEGF-A over-expression has been reported as a common feature in many cancers, and correlates with tumor progression, vascular density, invasiveness, metastasis and recurrence (Apte et al., 2019). Therefore, VEGF-A represents a suitable and attractive target for anti-angiogenic therapies. In 1993, Dr. Ferrara's lab developed the first neutralizing monoclonal antibody able to block VEGF-A, subsequently called bevacizumab, and halt tumor growth *in vivo* (Kim et al., 1993). Almost ten years later, bevacizumab was approved for the treatment of metastatic colon cancer (Hurwitz et al., 2004), following clinical trials which showed increased progression free survival of the patients treated with this drug combined with conventional therapy. Currently, bevacizumab is used for the therapy of several cancer types, such as non-small cells lung cancer, glioblastoma, renal cancer and ovarian cancer. Moreover, many other anti-angiogenic drugs able to inactivate major angiogenic cytokines or inhibit their receptors have been developed. These compounds can either be blocking monoclonal antibodies (e.g. ramucirumab for VEGFR2), tyrosine kinase inhibitors (e.g. sunitinib and imatinib) or chimeric decoy proteins (e.g. aflibercept).

Unfortunately, so far anti-angiogenic therapy did not meet the expectations since increased progression-free survival has been observed only for a restricted number of tumor types; and, however

the anti-angiogenic therapy does not affect the overall survival. This may in part because tumor-vessels regression besides inducing cancer cells starvation, also affects the blood flow hindering proper drug delivery and, thus, chemotherapy efficacy (Goel et al., 2011). Moreover, anti-angiogenic therapy and the consequently increased intratumoral hypoxia establishes a selective pressure favouring the development of more aggressive tumor phenotypes displaying increased tumor cell invasiveness and metastatic potential. Furthermore, the putative benefits from the anti-angiogenic therapy are also circumvented by the engagement of vessel co-option or vascular mimicry, as well as by the over-expression of angiogenic molecules obviating the VEGF-A function (Lugano et al., 2020). The "vessels normalization hypothesis" (Jain, 2001), takes into account these problems and proposes that a more efficacious anti-angiogenic therapy instead of inducing vascular disruption should reduce the intratumoral vascular network and simultaneously normalize the vessels in order to improve drug delivery and reduce tumor hypoxia. Indeed, the combination of chemotherapy and anti-angiogenics in delimited time window ameliorates the cancer patients progression free survival, enhancing tumor oxygenation and inhibiting metastasis (Jayson et al., 2012). Tumor vessels normalization could be achieved overcoming the imbalanced presence of pro-angiogenic factors, through the stimulation of the physiological anti-angiogenic counterpart, as schematically shown in Figure 6.

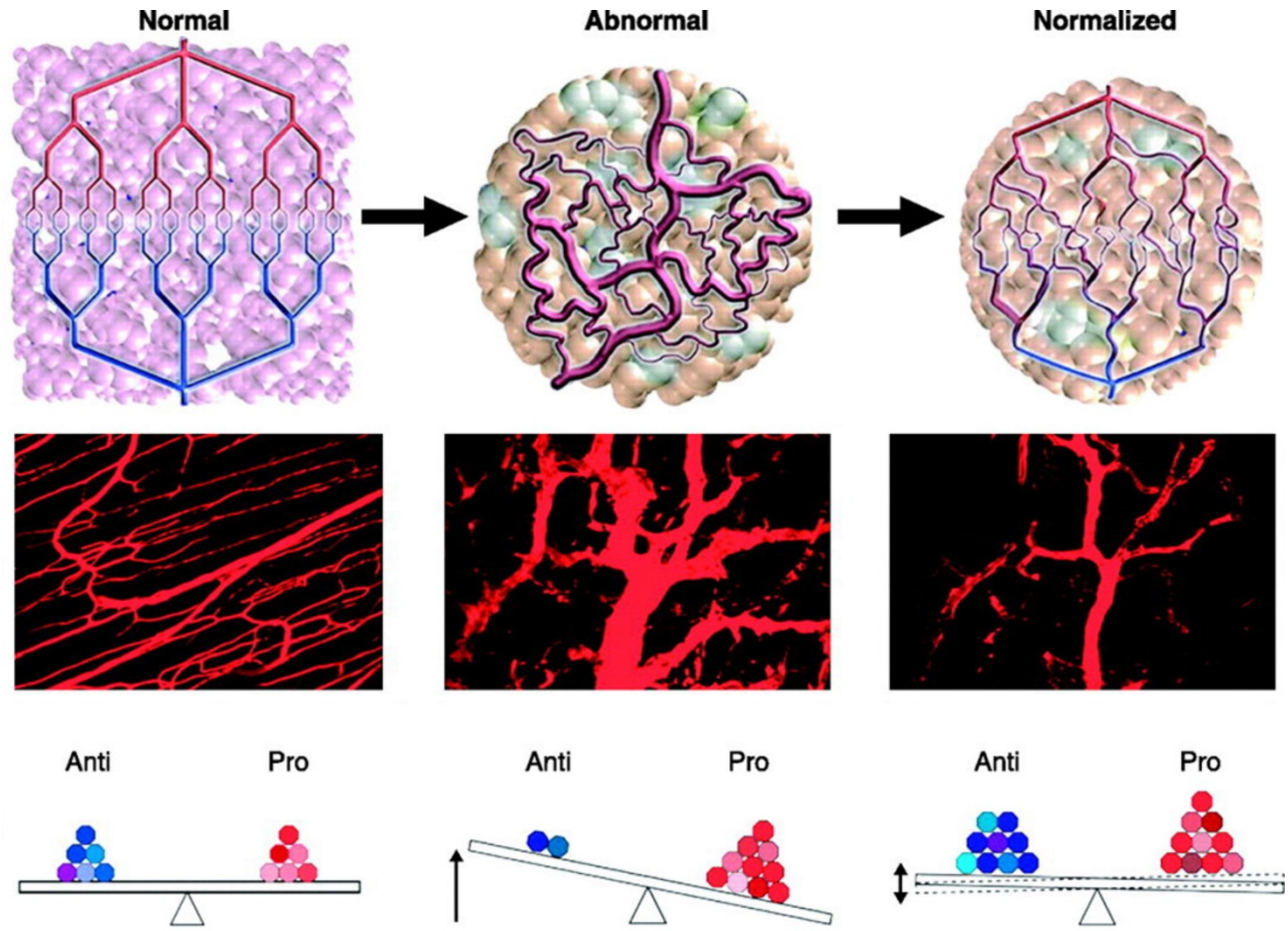

***Figure 6**. **Schematic representation of the tumor vessel normalization concept.** Tumor vasculature is structurally and functionally abnormal. The image shows the dynamics of vascular normalization induced by VEGFR2 blockade at an early time window in a mouse model; these modifications may reflect changes in the balance of pro- and antiangiogenic signaling in the tissue (adapted from Goel et al., 2011).*

Many strategies have been proposed to induce tumor vessels normalization:

1. Rethinking of timing and dosing of available anti-angiogenic drugs to potentiate chemotherapy, also modulating the TME towards a better response to immunotherapy (Cantelmo et al., 2017; Huang et al., 2012).
2. Setting up dual targeting of main angiogenic pathways; indeed, inhibition of Ang2/TIE2 axis, which sustains vessels destabilization, together with VEGF-A/VEGFR2 blocking improves ECs junction strengthening and decreases metastasis (Koh et al., 2010).
3. Modulating the hypoxia-induced molecules; in fact the PDH2 (prolyl hydroxylase that modulate HIFs activities) haplodeficiency associates to improved EC barrier and reduced vessels leakage and tortuosity (Mazzone et al., 2009).
4. Induction of Notch signalling to induce EC quiescence during drug treatment (Maes et al., 2014).
5. Metabolic rewiring of tumor ECs metabolism, since it has been reported that the specific inhibition of the glycolytic activator PFKFB3 induces tumor vessel normalization favouring pericytes recruitment (Cantelmo et al., 2016).

Therefore, improvement of anti-angiogenic therapy in cancer patients could benefit from a deeper understanding of the different molecular phenotypes and biological features between tumor ECs and normal EC. Moreover, the development of novel biomarkers able to predict patients' response, could help to discern the patients that would benefit from anti-angiogenic therapy.

2.2.2 Tumor angiogenesis and metastatic dissemination

As previously mentioned, the intrinsic inefficiency of the tumor vasculature contributes to maintenance of a hypoxic TME that, in turn, favours the acquisition of invasive capabilities by cancer cells, which undergo to epithelial-to-mesenchymal transition (EMT). Once this aggressive phenotype is achieved, cancer cells use the vascular system to develop metastasis, which occurs through three main steps: intravasation in the primary tumor, survival in the blood stream and extravasation to a distant site (Figure 7).

High interstitial pressure, generated by both over-proliferative cancer cells and poor drainage by tumor-associated vessels, can squeeze neoplastic cells inside vessels lumen (Ribatti, 2013). Despite this "passive intravasation", metastatic cancer cells can actively migrate toward vessels, attracted by growth factors gradients (Bockhorn et al., 2007). Moreover, tumor cells express large number of metalloproteases (MMPs) able to digest the vessels BM and adhesion molecules to better interact with ECs. On the other hand, tumor cells can shape the surrounding microenvironment to favour intravasation. For example, tumor cells activate CAFs to remodel the ECM, thus sustaining their migration (Hale et al., 2013). Cancer cells can also mimic functions mediated by immune cells: Tavora and colleagues nicely demonstrate that Toll-Like Receptor 3 (TLR3) expression in tumor cells modulates the activation of ECs to allow intravasation (Tavora et al., 2020).

Once reached the lumen, cancer cells must survive in a hostile environment, withstand to anoikis, shear stress and immune cell attack. One of the most studied survival mechanisms consists in the platelets shielding, which helps to resist the blood flow and prevent natural killer cells recognition (Stegner et al., 2014).

Finally, to allow colonization at distant sites, cancer cells extravasate from vessels. This event usually takes place in small capillaries, where circulating tumor cells (CTCs) remain physically trapped. Here, neoplastic cells, to remain firmly attached, closely interact with ECs through the

engagement of several adhesion molecules. Interestingly, CTCs hijack the same adhesion machinery used by lymphocytes during rolling and diapedesis. During the initial steps of adhesion, CTCs, directly or indirectly, stimulate the expression of E-selectin by ECs that in turn engages other adhesion molecules on the cancer cell surface (e.g. CD44) (Reymond et al., 2013). Next, other types of molecules contribute to strengthen the adhesion, including EC specific transmembrane protein, such as VCAM1(Wieland et al., 2017), and integrins receptors in both ECs and CTCs. Interestingly, the establishment of these interactions is also mediated by immune cells, such as macrophages and neutrophils, which, together with cancer cells, secrete various cytokines able to induce ECs' junctions opening (Wolf et al., 2012). Once the extravasation is completed, tumor cells can persist very close to the peri-vascular niche, mimicking pericytes, through the engagement of L1CAM, another EC specific adhesion molecule (Er et al., 2018).

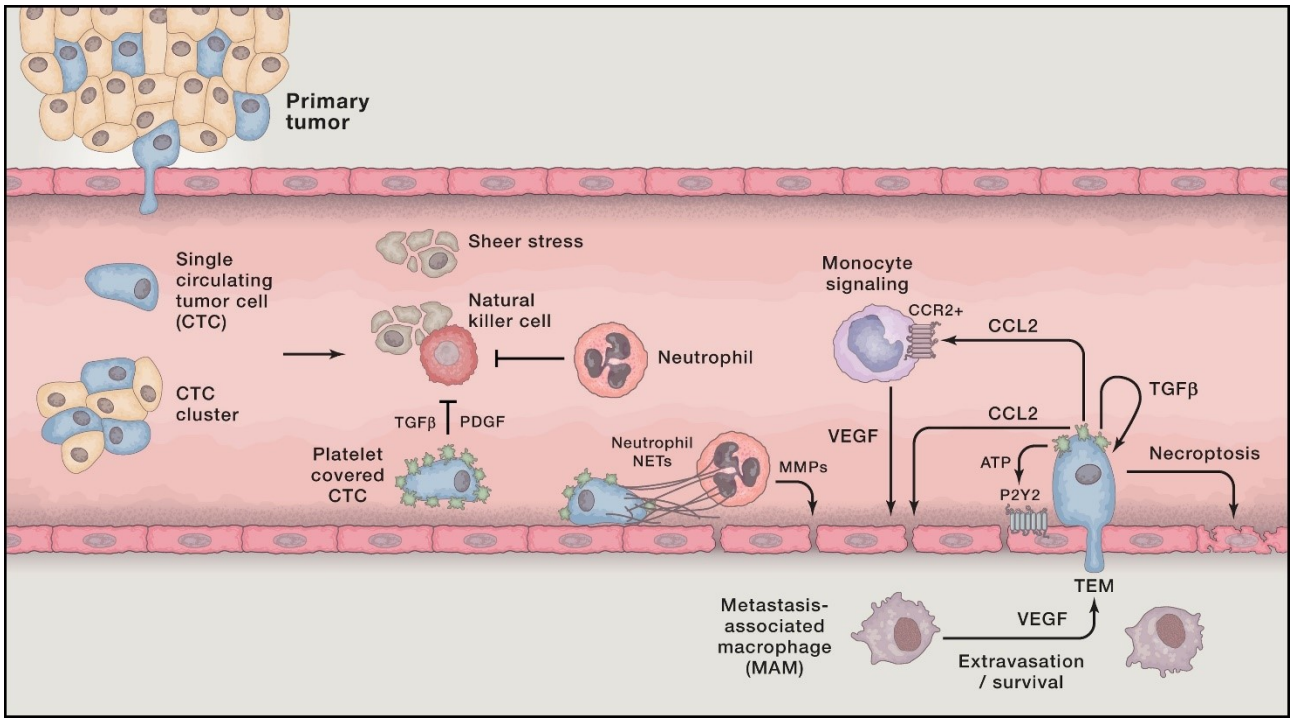

Figure 7. Main steps of metastatic dissemination. *Cancer cells escape from primary tumors and intravasate into the circulation, either as single CTCs or CTCs clusters. The bloodstream represents a hostile environment for CTCs and to survive tumor cells gain physical and immune protection engaging the coating by platelets. Once lodged in a capillary, activated platelets and cancer cells secrete a number of bioactive factors that can act mainly on ECs, and promote the transendothelial migration of cancer cells (from Lambert et al., 2017).*

2.3 The extracellular matrix

The ECM represents the non-cellular component of all tissues and organs; it guarantees the physical and mechanical support to the cells and controls several cellular functions, contributing to tissue homeostasis. ECM deposition occurs in the early stages of embryonic development: indeed, loss of function of several ECM components has been linked to embryonic lethality, demonstrating their fundamental role in the tissue biology (Bonnans et al., 2014). So far, around 300 of "core matrisome" proteins have been identified as ECM proteins and glycoproteins. In addition, remodelling enzymes, ECM-bound growth factors and other ECM-interacting proteins (such as cell surface receptors) can be included as ECM components (Hynes and Naba, 2012). Two main types of

ECM components can be distinguished: fibrous-forming proteins, such as collagens, elastin, fibronectin, laminins and proteoglycans (PGs), and glycosaminoglycans (GAGs), which mainly contribute to tissue hydration (Theocharis et al., 2016). These constituents form two main categories based on their distribution and composition: interstitial connective tissue matrix forming the scaffold for cells in the various tissues, and BM (or pericellular matrix), a specialized ECM that structurally sustains and defines all epithelial tissues (Bonnans et al., 2014). Collagen is the most abundant fibrous ECM protein in our body and with its fibrils defines the tensile strength of tissues, favours cell adhesion, migration and directs tissue development (Rozario and DeSimone, 2010). Importantly, collagens interact with elastin, another important ECM molecule which confers elastic property to the tissues. Also fibronectin aids the fibrillogenesis of collagen fibers, and plays a crucial role triggering different signals by mechanotransduction, since it can be differentially processed in the microenvironment and recognized or not by integrin receptors (Humphrey et al., 2014).

Importantly, beyond their physical function, many ECM components closely interact with the adjacent cells through surface receptors (i.e. integrins) modulating cell adhesion, migration, proliferation, apoptosis and differentiation (Hynes, 2009). Moreover, the ECM controls the spatial distribution of several growth factors. Many ECM proteins can bind cytokines, such as VEGF-A, FGF2 and TGF-β, defining their availability for the corresponding cell receptors (Hynes, 2009). The ECM is a highly dynamic structure since it is constantly remodelled by the action of specific oxidases and MMPs, ADAMs and ADAMTS (Theocharis et al., 2016).

In fact, the ECM is constantly shaped in terms of composition, abundance, and organization of its components, thus defining a highly specific biochemical and biomechanical environment, affecting cell fate. Therefore, the ECM remodelling is a tightly regulated process and plays a crucial role in the maintenance of tissue homeostasis. Not surprisingly, pathological conditions, such as cancer, are characterized by an extensive alteration of the ECM that promote the early steps of tumorigenesis, as well as cancer progression and metastasis formation (Kai et al., 2019; Pickup et al., 2014).

2.3.1 ECM remodelling and tumor angiogenesis

Tumor cells can reshape the microenvironment through an aberrant activation of the surrounding CAFs, which secrete large amount of collagen and remodelling enzymes increasing tissue stiffness. Moreover, CAFs, in synergy with cancer cells, produce high amounts of cytokines and prepare “the road” for the de novo formation of tumor-associated vessels. Indeed, matrix remodelling significantly affects ECs activation. For instance, increased ECM stiffness triggers VEGFR2 expression thus promoting angiogenesis (Mammoto et al., 2009). Moreover, several ECM components and fragments generated during remodelling deeply affect the aberrant formation of the tumor vasculature. For example, fibronectin expression is required during developing vasculature and its deposition is switched off once the vessels are formed; however, in tumor-associated vessels its expression, and in particular, the EDB-fibronectin isoforms, is switched on (Coltrini et al., 2009; Van Obberghen-Schilling et al., 2011). Similarly, other ECM proteins, like perlecan, biglycan, hyaluronan and laminins are up-regulated in cancers (Andreuzzi et al., 2020). Besides the increased stiffness, the TME displays aberrantly elevated levels of proteases, which act locally and lead to the release of several matrix-bound angiogenic cytokines, further sustaining tumor angiogenesis (Mohan, 2020). For instance, MMP9, one of the prominent enzymes involved during active angiogenesis, prompts the angiogenic switch through VEGF-A freeing (Bergers et al., 2000).

2.3.2 The EMILIN protein family

EMILINs are a family of ECM glycoproteins characterized by the presence of the cysteine-rich EMI domain at the N-terminus and many proteins of this family also display a gC1q-like domain at C-terminus (Colombatti et al., 2012). Three subgroups can be identified among EMILINs:

- The first group includes the major family members EMILIN1 (Colombatti et al., 1985), EMILIN2 (Doliana et al., 2001), Multimerin-1 (Hayward et al., 1991) and Multimerin-2 (Sanz-Moncasi et al., 1994).
- The second is formed by only one protein, EMILIN3, which shares a similar structure with the members of the first group, but lacks the gC1q domain (Leimeister et al., 2002); EMILIN-3 acts in the ECM milieu regulating TGF-β availability and plays a pivotal function during notochord formation (Corallo et al., 2013; Schiavinato et al., 2012).
- The third group includes Emu1 and Emu2 (Leimeister et al., 2002), small collagenous proteins which, except for the EMI domain, do not share structural similarities with the other members and whose functions are still undefined.

The structures and the domains organization of main EMILINs are shown in Figure 8.

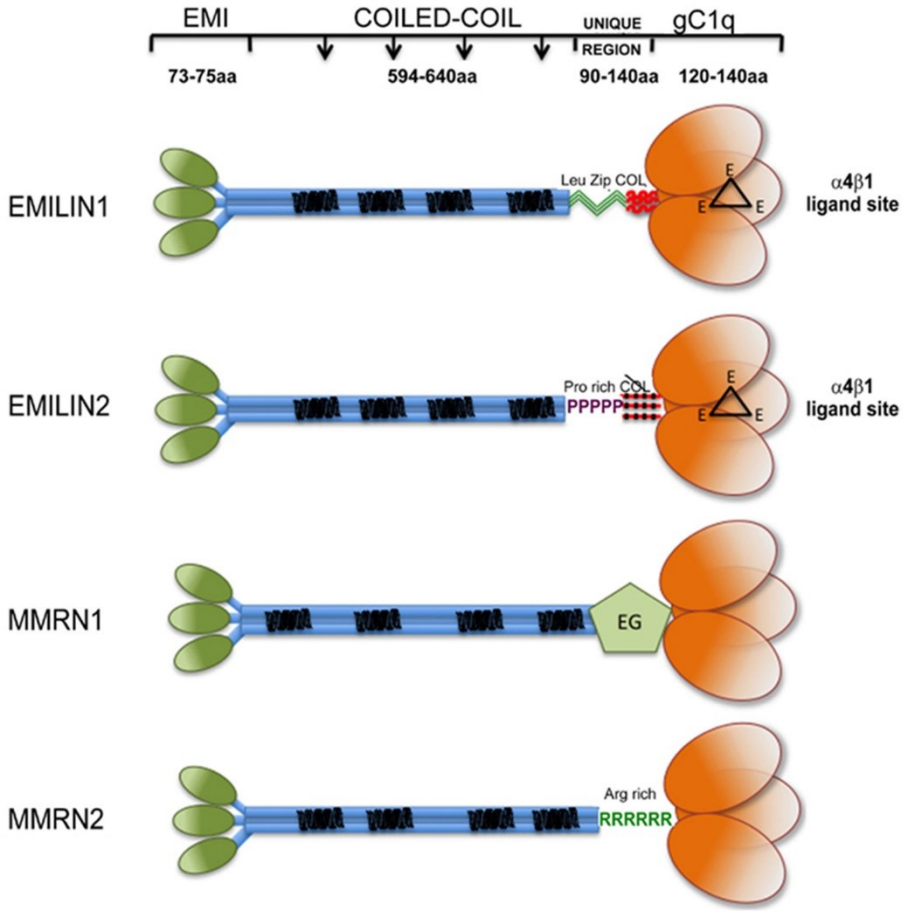

Figure 8. Graphical representation of the structure of the main components of the EMILINs protein family members. *(EMI) EMI domain; Coiled-coil region; (C1q) gC1q-like domain; (Pro rich) prolin-rich domain; (EG) region with partial similarity with EGF domain; (RR) arginine-rich domain; (from Colombatti et al., 2012).*

2.3.2.1 EMILIN1

EMILIN1, the archetype of the EMILINs protein family, was first identified following the characterization of the ECM components associated with the elastic fibers (Bressan et al., 1993). In fact, EMILIN1 (Elastin Microfibrils Interface Located proteIN) is a 115 kDa glycoprotein located at the interface between amorphous elastin surface and microfibrils. EMILIN1 is widely expressed within the connective tissue of several organs and it is abundant in the wall of large vessels (Colombatti et al., 1985). Expression analysis carried during mouse embryo development revealed that EMILIN1 is highly expressed in blood vessels wall and in the perineuronal mesenchyme. The protein was also detected in the mesenchyme of different organs, such as lungs and liver, and in the mesenchymal condensation of limb bud and branchial arches (Braghetta et al., 2002). Finally, at late gestation, EMILIN1 is widely expressed in the in the interstitial connective tissue and in smooth muscle-rich tissues.

Emilin1$^{-/-}$ mice are characterized by hypertensive phenotype, with increased blood pressure, augmented peripheral resistance and reduced vessels size. EMILIN1 is necessary for a proper control of TGF-β maturation and availability, an essential processes linked to hypertension (Zacchigna et al., 2006). Moreover, *Emilin1*$^{-/-}$ mice show a defective lymphatic system, characterized by hyperplasia, enlargement and irregular pattern of visceral and superficial lymphatic vessels (Danussi et al., 2008). Molecularly, EMILIN1 engages the α4β1 and α9β1 integrins through the gC1q domain favouring cell adhesion, migration and halting cell proliferation (Danussi et al., 2011; Spessotto et al., 2003). In fact, *Emilin1*$^{-/-}$ mice display an accelerated formation of skin tumors due to uncontrolled proliferation and show increased lymph node metastasis (Danussi et al., 2012). Likewise, the defective drainage capability of *Emilin1*$^{-/-}$ mice, impaired the inflammatory resolution during colon carcinogenesis by lymphatic vessels, thus promoting tumor outgrowth (Capuano et al., 2019).

2.3.2.2 EMILIN2

EMILIN2 was originally identified exploiting a two-hybrid system and using the EMILIN1 gC1q domain as a bait (Doliana et al., 2001). Differently from EMILIN1, this protein is characterized by a prolin-rich sequence between the coiled coil region and the collagenous stalk. Also, their expression pattern is distinct: EMILIN2 is present in high amount in the fetal heart and in adult lungs; intermediate expression has been detected in peripheral leukocytes, placenta and spinal cord. At low levels, EMILIN2 is present in the adult aorta, small intestine and appendix (Doliana et al., 2001; Braghetta et al., 2004). Moreover, EMILIN2 is an important component of the BM of the cochlea (Amma et al., 2003). Interestingly, the *Emilin2* gene is inactivated by methylation in many cancer types, such as breast, lung and colon cancers, and the decreased expression correlates with poor outcome for the patients (Hill et al., 2010). In accordance, with this finding EMILIN2 overall exerts tumor suppressive functions. In fact, in cancer cells, EMILIN2 triggers the extrinsic apoptotic pathway through the engagement of the death receptors DDR4 and DDR5 (Mongiat et al., 2007). EMILIN2 can also directly interact with Wnt1 ligand, impinging on LRP6 phosphorylation and β-catenin nuclear localization (Marastoni et al., 2013). Consistently, ectopic expression of EMILIN2 significantly reduces tumor growth *in vivo*, however, and surprisingly EMILIN2-treated tumors display increased angiogenesis (Mongiat et al., 2010). Indeed, EMILIN2 has been identified as an important component of the microenvironment able to modulate ECs functions (Bronisz, 2012). Interestingly, we found that EMILIN2 is downregulated in gastric cancer patients, altering tumor associated vessels and affecting ECs behaviours *in vitro* (Andreuzzi et al., 2020; Andreuzzi et al., 2018). Indeed, our group demonstrated that EMILIN2, mainly produced by fibroblast (FB) in the

microenvironment, can directly bind EGFR expressed on the cell surface of FB and EC, stimulating the expression of IL-8 through Jak2/STAT3 pathway, and thus, the proliferation and migration of ECs (Figure 9). Moreover, tumors grew in *Emilin2*$^{-/-}$ mice have lower vessel density, compromised vascular perfusion and poor response to chemotherapy treatment (Paulitti et al., 2018). Currently, our laboratory is collecting additional evidences suggesting that EMILIN2 aids vessel maturation and stabilization mediating the recruitment of pericytes on ECs layer. This could be achieved acting simultaneously on pericytes, where EMILIN2 can modulate $\alpha_5\beta_1$ and $\alpha_6\beta_1$ integrin pathways, and on ECs, boosting the expression platelet-derived growth factor (PDGF), a key molecule for the recruitment of pericytes (unpublished observations).

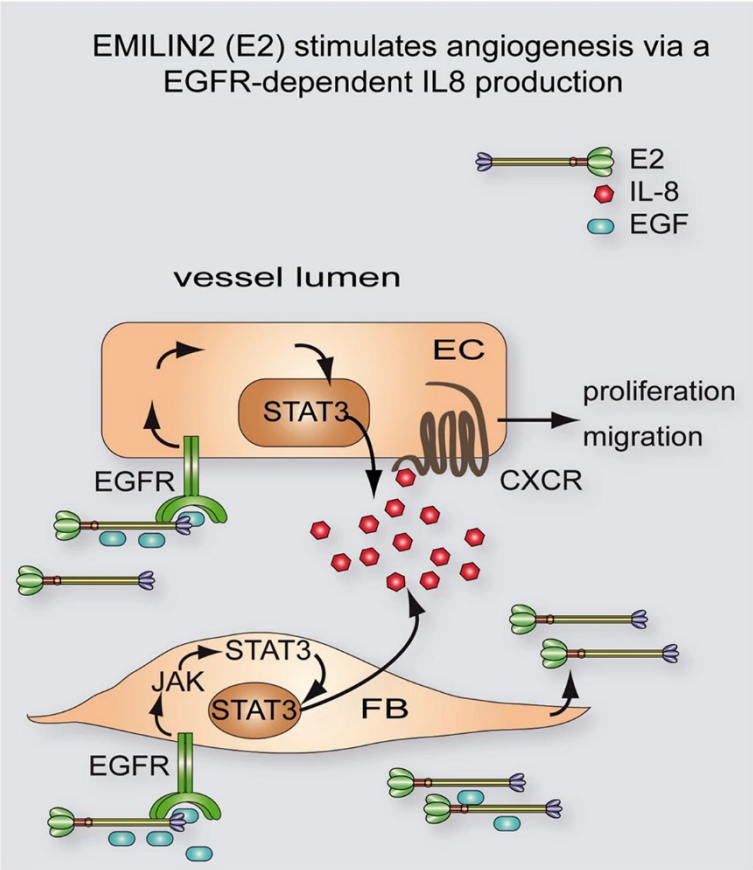

Figure 9. EMILIN2 affects ECs behaviour. *The molecule activates EGFR through a direct binding to EGFR and EGF leading to the activation of Jak2 and STAT3 and the over-production of IL-8. The mechanism takes place both in ECs and FBs (from Paulitti et al., 2018).*

2.3.2.3 Multimerin-1

Multimerin-1 forms S-S linked soluble homopolymers that are mainly stored in platelets, megakaryocytes and ECs or can be embedded in the ECM of ECs forming fibrillar structures (Hayward et al., 1998). Multimerin-1 can modulate the adhesion of platelets, neutrophils and ECs involving the interaction with integrins $\alpha_{IIb}\beta_3$ and $\alpha_V\beta_3$ (Adam et al., 2005). Moreover, Multimerin-1 enhances platelets adhesion and thrombus formation through the binding to fibrillar collagen and von Willebrand factor (Leatherdale et al., 2020). In platelets, Multimerin-1 is stored within α-granules, where it is associated with high affinity to factor V, at the site required during factor V activation;

thus delaying thrombin generation by activated factor V (Jeimy et al., 2008). Taken together these findings suggest an important homeostatic role of Multimerin-1 during platelet activation and consequent aggregation.

2.3.2.4 Multimerin-2

Multimerin-2, firstly named EndoGlyx-1, was identified during the screening for new EC specific markers employing monoclonal antibodies produced against human umbilical vein ECs (HUVEC) (Sanz-Moncasi et al., 1994). The Multimerin-2 molecular structure differs from the other EMILIN members, for the presence of a short cluster of charged amino acids (10 out of 27 residues) located between the coiled-coil region and the C1q-like domain. Multimerin-2 is specifically deposited along the vessels of all organs, from capillaries to large vessels, with the only exception represented by hepatic and splenic sinusoids. Multimerin-2 is also deposited along tumor capillaries, including in the areas designated as "hot spots" of neo-angiogenesis (Sanz-Moncasi et al., 1994). The protein shows a diffuse and continuous localization along the ECs lining of the blood vessels, showing an increased abundance on the abluminal side (Figure 10) (Christian et al., 2001).

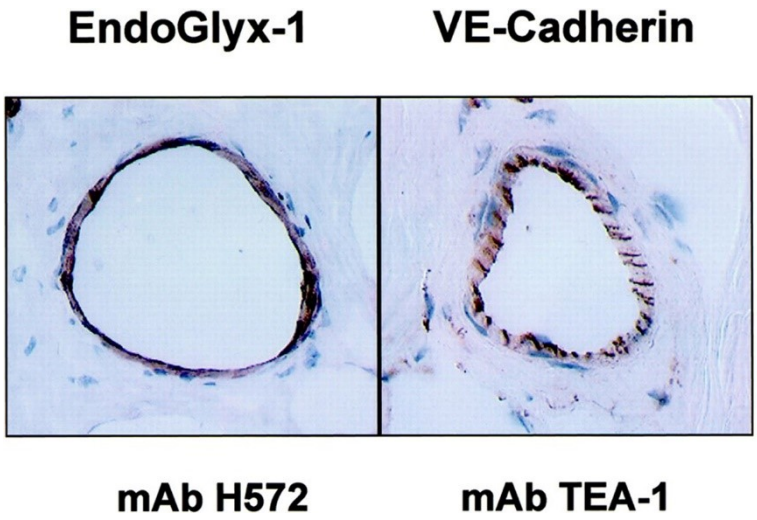

Figure 10. Immunohistochemical staining of Multimerin-2 in human blood vessels. *Sections of normal breast tissue stained with the H572 mAb detecting MMRN2 or with TEA-1 mAb detecting VE-Cadherin (from Christian S. et al., 2001).*

Our group was the first to describe the function of Multimerin-2 and the molecular mechanisms by which it affects EC behaviour. Multimerin-2 inhibits ECs migration and counteracts sprouting angiogenesis *in vivo* (Lorenzon et al., 2012). These effects depend on its capability to sequester VEGF-A, subtracting the cytokine for the binding to VEGFR2 receptor, thus halting its activation (Colladel et al., 2016). Indeed, Multimerin-2 can bind VEGF-A, and other members of the VEGF cytokine family, through the glycosylated N-terminus. Once ectopically overexpressed in the microenvironment, Multimerin-2 or its active fragment impair tumor growth possibly reducing its vascularization (Colladel et al., 2016; Lorenzon et al., 2012). Consistent with the hypothesis that Multimerin-2 exerts an angiostatic function (Figure 11) the protein is depleted during active angiogenesis. This occurs via two distinct mechanisms: on one hand EC challenged with angiogenic cytokines display decreased Multimerin-2 mRNA levels, on the other hand, in the TME, during active angiogenesis, Multimerin-2 is degraded through the action of MMP9, and with a lesser degree MMP2.

Indeed, the analyses performed on sections derived from colon cancer patients showed that the presence of active MMP9 correlated with extensive degradation of Multimerin-2 (Andreuzzi et al., 2017). Consistently, Multimerin-2 deposition is also impaired in tumor associated vessels of gastric cancer patients (Andreuzzi et al., 2018).

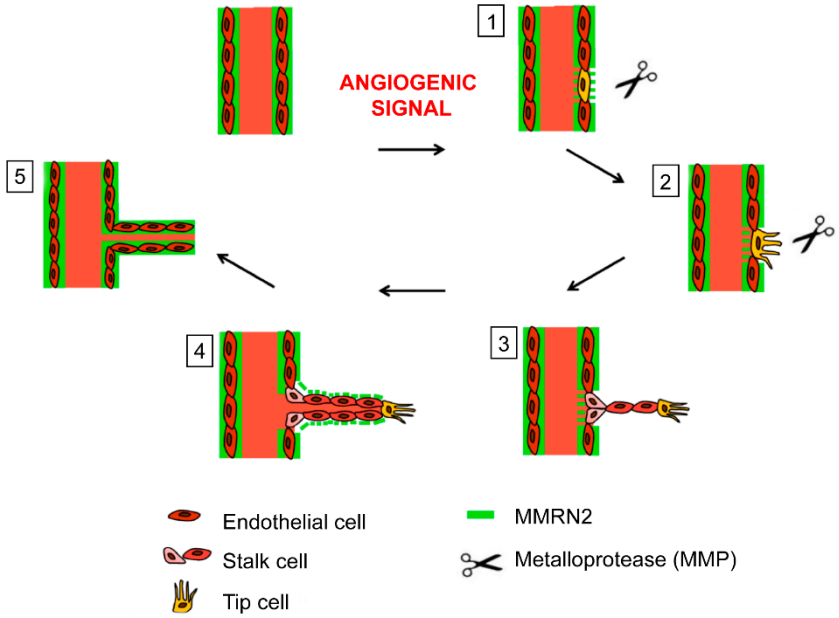

Figure 11. Schematic representation of the expression and degradation of Multimerin-2 during sprouting angiogenesis. *(1) Following an angiogenic stimuli Multimerin-2 is degraded by MMPs. (2) Tip cells, which drive angiogenesis are formed. (3) Stalk cells proliferate to form the new vessel. (4) Lumen is formed and Multimerin-2 is deposited to stabilize vessel. (5) The quiescent EC state is restored (from Mongiat et al., 2016).*

Multimerin-2 can also exert a positive action during sprouting angiogenesis through the interaction with the tumor EC marker C-type lectin transmembrane receptor CLEC14A (Noy et al., 2015). More recently, Multimerin-2 was also shown to bind to other C-type lectin family members namely CD93 and CD248, thus affecting EC behaviours (Galvagni et al., 2017; Khan et al., 2017). In particular, CD93, which is predominantly expressed by tumor ECs, co-localizes with Multimerin-2 in the blood vessels of several human tumors. Abrogation of this interaction reduces ECs adhesion and migration *in vitro* and affects sprouting capability in *ex vivo* models (Galvagni et al., 2017; Tosi et al., 2020). Mechanistically, Multimerin-2 through CD93 stabilization, favours the activation of β_1 integrin and fibronectin fibrillogenesis in ECs, thus enhancing vessel maturation during tumor angiogenesis *in vivo* (Lugano et al., 2018). Despite the overall impact of Multimerin-2 function during vessels maturation is not completely unravelled, these data suggest that hampering the Multimerin-2/CD93 interaction could be a novel strategy to target tumor angiogenesis.

3. AIMS OF STUDY

Angiogenesis is a hallmark of cancer and in fact this process must be switched on to nourish cancer cell growth.

Since the first ground-breaking hypothesis, it took several decades of collective efforts to develop anti-angiogenic therapies able to halt tumor progression. However, despite several anti-angiogenic drugs have been approved for the treatment of a number of tumor types, the clinical outcome of these patients did not meet the expectations.

Thus, it is of upmost importance to better understand the mechanisms regulating angiogenesis and vascular efficiency and to develop new predictive biomarkers able to identify the patients that would benefit from anti-angiogenic therapy.

In this context Multimerin-2 may represent a key molecule. Multimerin-2 is an ECM protein specifically deposited along the blood vessels and exerts an angiostatic function mainly through the sequestration of VEGF-A, negatively affecting VEGFR2 activation.

The ectopic expression of Multimerin-2 in cancer cells leads to impaired vascularization and decreased tumor growth when implanted in nude mice.

More recently, we discovered that Multimerin-2 expression is lost in a number of vessels associated to gastric and colon tumors, possibly due to MMP9/MMP2-driven degradation. These compelling evidences prompted us to further elucidate the role of Multimerin-2 in mediating EC function.

In particular the aims of this PhD project were to:

1. Verify the effects of Multimerin-2 loss and the impact on EC functionality *in vitro* and *in vivo* and dissect the molecular mechanism involved;

2. Asses the relevance of Multimerin-2 loss in cancer growth as well as in drug delivery and chemotherapy efficacy;

3. Verify if the loss Multimerin-2 could associate with an altered capability of cancer cells to disseminate through the EC barrier.

4. RESULTS

4.1 Multimerin-2 is frequently lost in tumor-associated vessels

In order to better understand the role of Multimerin-2, we firstly assessed its deposition along the tumor-associated vessels. To this end, immunohistochemistry analyses were performed on sections derived from formalin fixed, and paraffin-embedded cancer patients' samples. Ovarian cancer samples derived from the MITO16A project, which aimed at clarifying the molecular mechanisms affecting the efficacy of bevacizumab in combination with conventional platinum-based chemotherapy. Instead, triple-negative breast cancer and colon cancer sections were kindly provided by the Pathology Unit of CRO-IRCCS Institute of Aviano (Italy). Multimerin-2 was stained with a specific anti-human Multimerin-2 affinity-purified polyclonal antibody followed by incubation with alkaline phosphatase-conjugated secondary antibodies, whereas blood vessels were stained with an antibody recognizing CD34, a pan-endothelial cell marker and developed with the peroxidase method. As expected, the tumor tissues were highly vascularised as detected with the anti-CD34 antibody (Figure 1). Interestingly, in all the tumor type investigated we observed that, despite many of the tumor-associated vessels expressed Multimerin-2 (Christian et al., 2001), a number of vessels displayed discontinuous deposition of the molecule and some vessels showed no or faint Multimerin-2 staining, even though with a high variability among the patients (Figure 1). These evidences prompted us to verify the effects of Multimerin-2 loss in ECs and better clarify the role of Multimerin-2 in tumor angiogenesis.

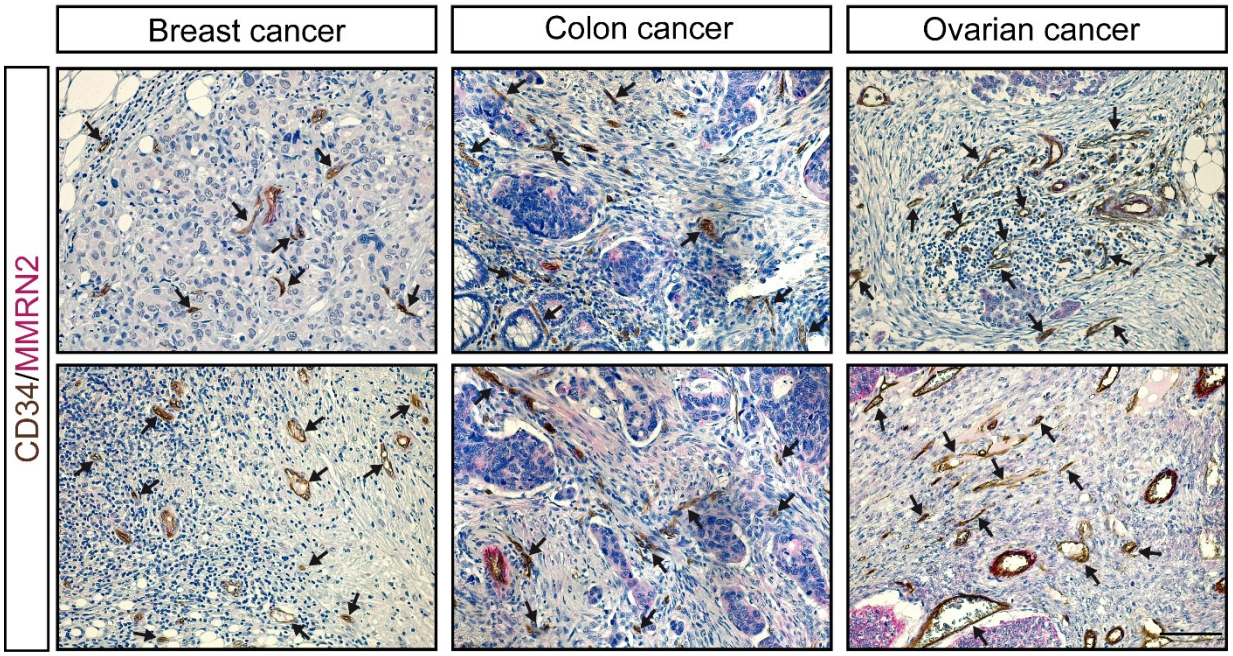

Figure 1. Multimerin-2 expression is frequently lost in tumor-associated vessels. *Representative immunohistochemistry images of tumor sections stained for Multimerin-2 (MMRN2) (purple) and CD34 (brown) to highlight vessels; two images are reported for each tumor type analysed, corresponding to different patients; breast cancer on the left, colon cancer in the middle and ovarian cancer on the right; scale bar 50 µm.*

4.2 Multimerin-2 loss affects ECs morphology and causes the dismantlement of adherens junctions

Previously, our group reported that Multimerin-2 down-modulates VEGFR2 activation through the sequestration of VEGF-A (Colladel et al., 2016). These findings, together with the observation that Multimerin-2 is frequently lost in tumor-associated vessels, prompted us to better characterize the role of Multimerin-2 in EC homeostasis. Thus, taking advantage of an adenoviral siRNA construct previously generated by our laboratory (Lorenzon et al., 2012), we first decided to down-regulate Multimerin-2 in HUVEC cells. Following adenoviral transduction, Multimerin-2 expression was down-modulated with high efficiency (above 90%) (Figure 2A). Confluent HUVEC cells silenced for Multimerin-2, failed to form a stable monolayer since adjacent cells often displayed large gaps, as shown in Figure 2B and 2C. This result suggested that Multimerin-2 could play a role in the maintenance of endothelial cell-to-cell contacts.

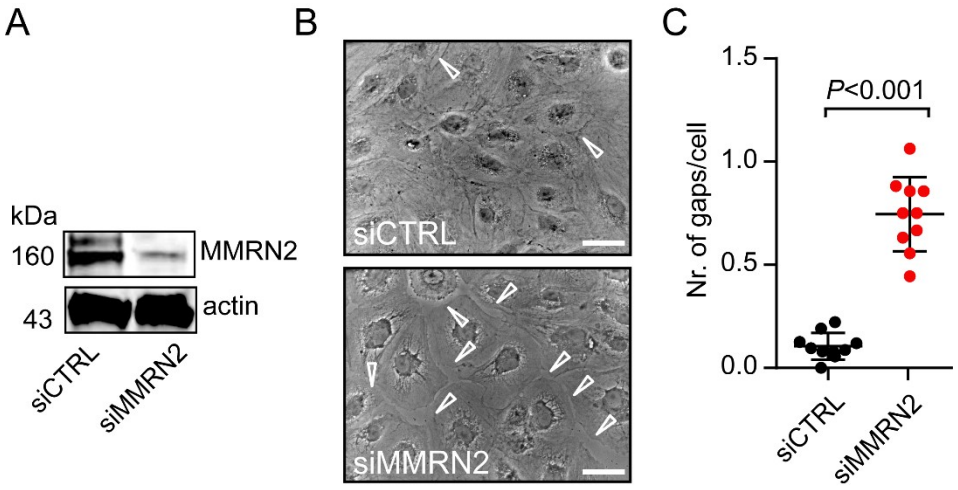

Figure 2. Multimerin-2 knockdown perturbs the formation of the EC monolayer*. (A) Western blot analysis showing the downregulation of Multimerin-2 upon adenoviral transduction with the scrambled control (siCTRL) or Multimerin-2 (siMMRN2) siRNA constructs; actin was used as protein loading control. (B) and (C) Representative images and relative quantification of inter-endothelial gaps (white arrowheads) following transduction with control (siCTRL) or Multimerin-2 (siMMRN2) siRNA constructs; scale bar 50 µm; n=10. P values were obtained using Mann-Whitney Rank Sum test.*

Thus, upon Multimerin-2 silencing we decided to better investigate the junctional ECs compartment. Transmission electron microscopy (TEM) analyses, performed in collaboration with Dr. Patrizia Sabatelli (Institute of Molecular Genetics, CNR, Bologna, Italy) revealed that HUVEC cells depleted of Multimerin-2 showed altered morphology of the cell-cell contacts, where intercellular clefts (IC) were more convoluted and displayed increased interdigitations (Figure 3A and 3B). In addition, the number of adherens junctions was lower in Multimerin-2 silenced cells respect to the control (Figure 3A and 3C). Based on these results, we decided to investigate the expression and localization of VE-cadherin, the main component of ECs AJs. Following Multimerin-2 knockdown in HUVEC cells, immunofluorescence analyses showed a strong impairment of the VE-cadherin lining, accompanied with increased actin stress fiber formation, as assessed with the use of

phalloidin (Figure 3C and 3D).

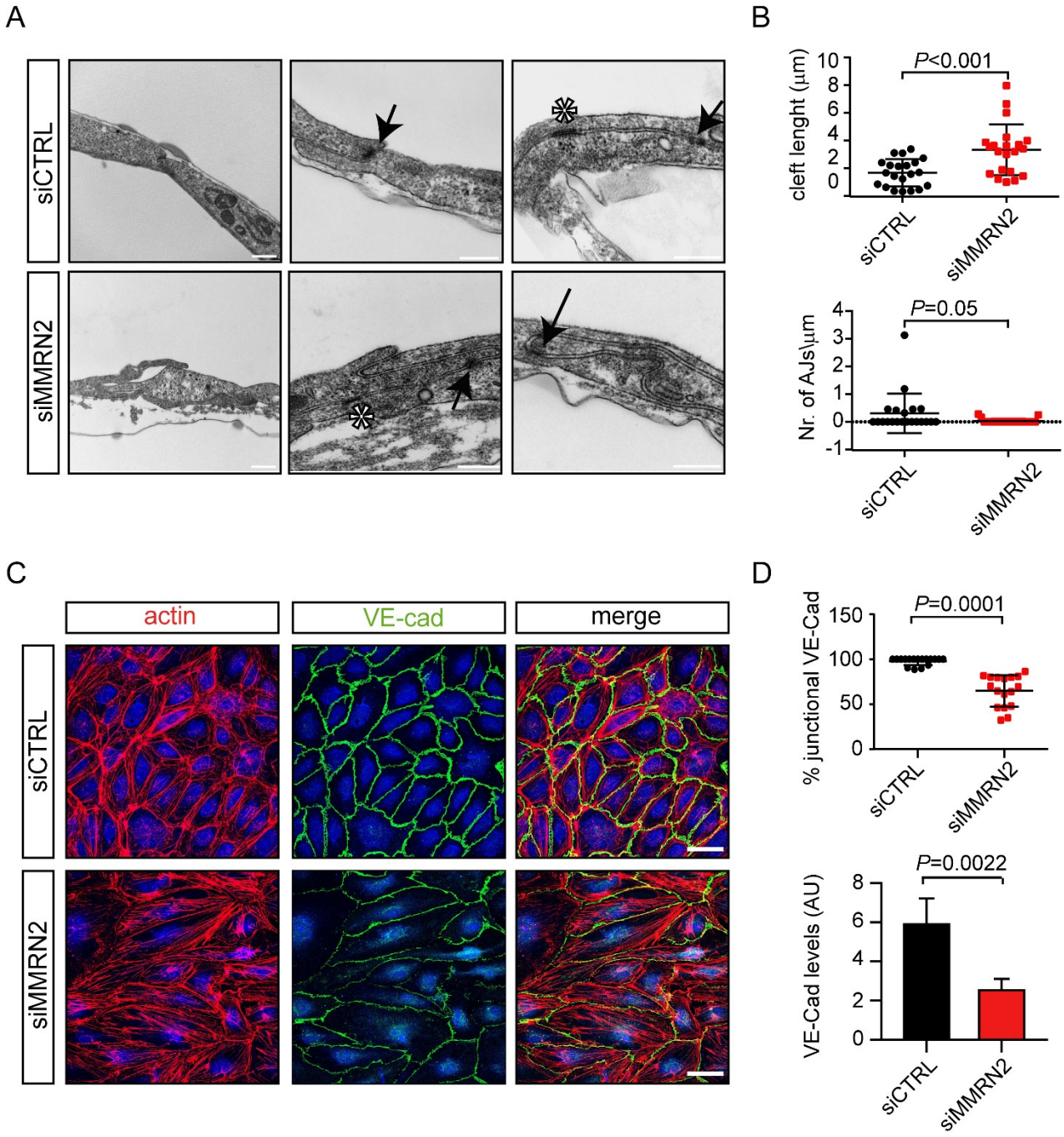

Figure 3. Multimerin-2 loss halts EC adherens junction stability. *(A) TEM images of HUVEC cells following transduction with control (siCTRL) or Multimerin-2 (siMMRN2) siRNA constructs; AJs and TJs are indicated with asterisks and arrows, respectively; scale bar 300 nm. (B) Quantification of the intercellular clefts (to) and AJ number (bottom) (n=20). (C) Immunofluorescence representative images of VE-cadherin (green), actin (red) and nuclei with TO-PRO (blue) following transduction with control (siCTRL) or Multimerin-2 (siMMRN2) siRNA constructs; scale bar 50µm. (D) Quantification analysis of junctional VE-cadherin (top) and overall signal intensity (bottom); n=16. P values were obtained using Mann-Whitney Rank Sum test.*

In light of the observed alteration of the actin bundles (Figure 3A), we evaluated the Myosin Light Chain (MLC) phosphorylation, an indicator of actin remodelling involved in EC contractility (Shen et al., 2010). Following Multimerin-2 silencing we found an increased phosphorylation of MLC at

the Ser19 residue, as confirmed by Western blot (Figure 4A and 4B) and immunofluorescence analyses (Figure 4C and 4D).

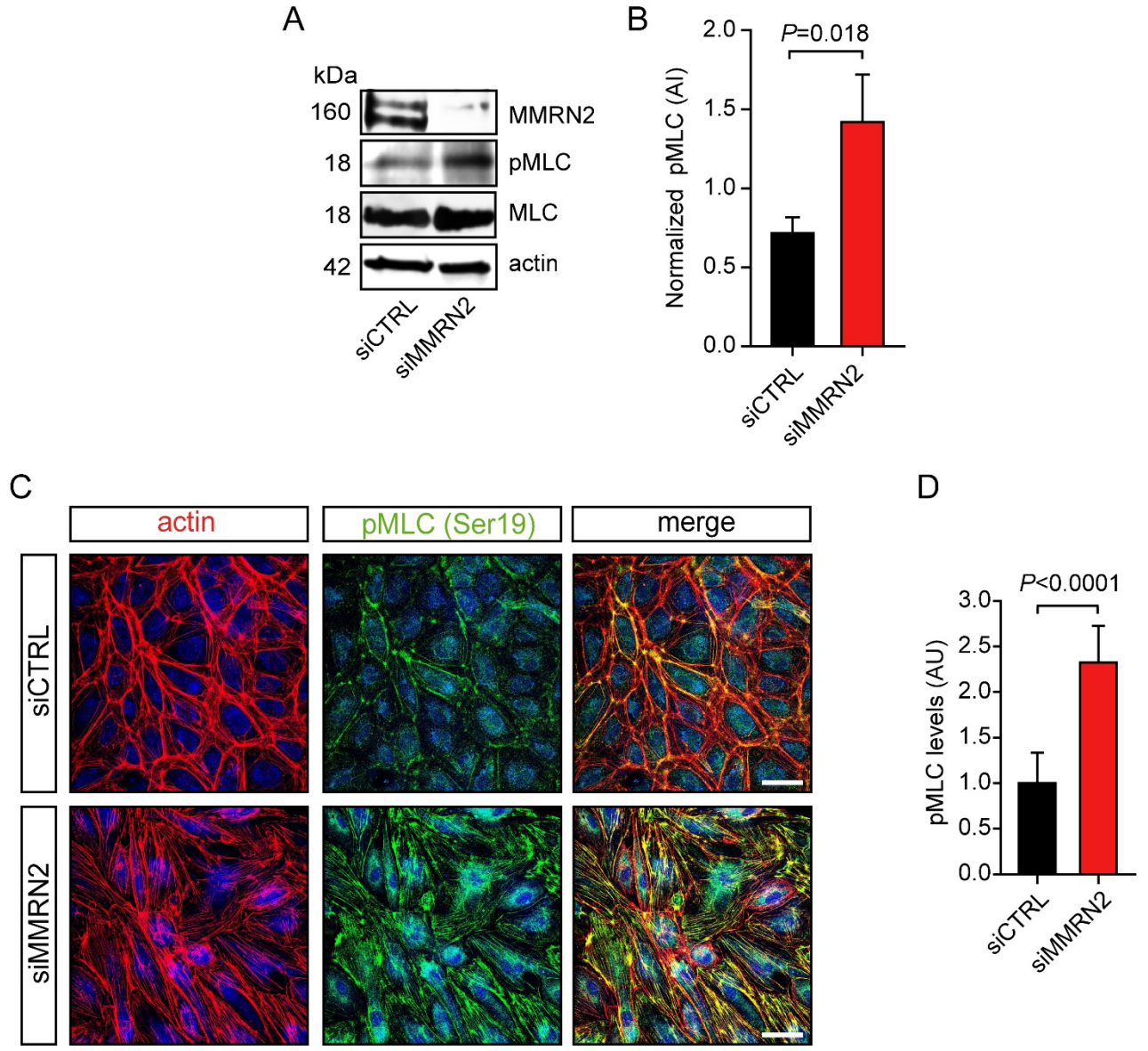

Figure 4. Multimerin-2 silencing induces MLC phosphorylation. *(A) Western blot analysis showing increased phosphorylation of MLC (Ser19) following transduction of HUVEC cells with control (siCTRL) or Multimerin-2 (siMMRN2) siRNA constructs; actin was used as protein loading control. (B) Quantification of the phospho-MLC levels, referred to total MLC and normalized to actin; n=3. (C) Representative immunofluorescence images of phospho-MLC (green), actin (red) and nuclei with TO-PRO (blue) following transduction of HUVEC cells with the control (siCTRL) or Multimerin-2 (siMMRN2) siRNA construct. (D) Quantification of the phospho-MLC levels; scale bar 50μm; n=16. P values were obtained using the paired Student's T-test.*

4.3 Multimerin-2 depletion elicits VEGFR2 phosphorylation affecting EC permeability

As mentioned in the introduction section, the activation of the VEGFR2 signalling pathway can affect the integrity of ECs adherens junctions. In particular, phosphorylation of Y951 of VEGFR2 has been linked to increased phosphorylation of VE-cadherin by Src kinase (Li et al., 2016). Since Multimerin-2, through the sequestration of VEGF-A, down-regulates VEGFR2 phosphorylation at Y1175 and Y1214 (Colladel et al., 2016; Lorenzon et al., 2012), we assessed if Multimerin-2 could affect VE-cadherin stability impinging also on VEGFR2 phosphorylation at Y951. Strikingly, Multimerin-2 knockdown in HUVEC cells caused an increased phosphorylation of VEGFR2 at this residue (Figure 5A and 5B); accordingly, Multimerin-2 silenced HUVEC cells displayed increased levels of Src phosphorylation at Y418 and led to enhanced VE-cadherin phosphorylation at Y568 (Figure 5C-E), a post-translational modification linked to its internalization and degradation (Orsenigo et al., 2012).

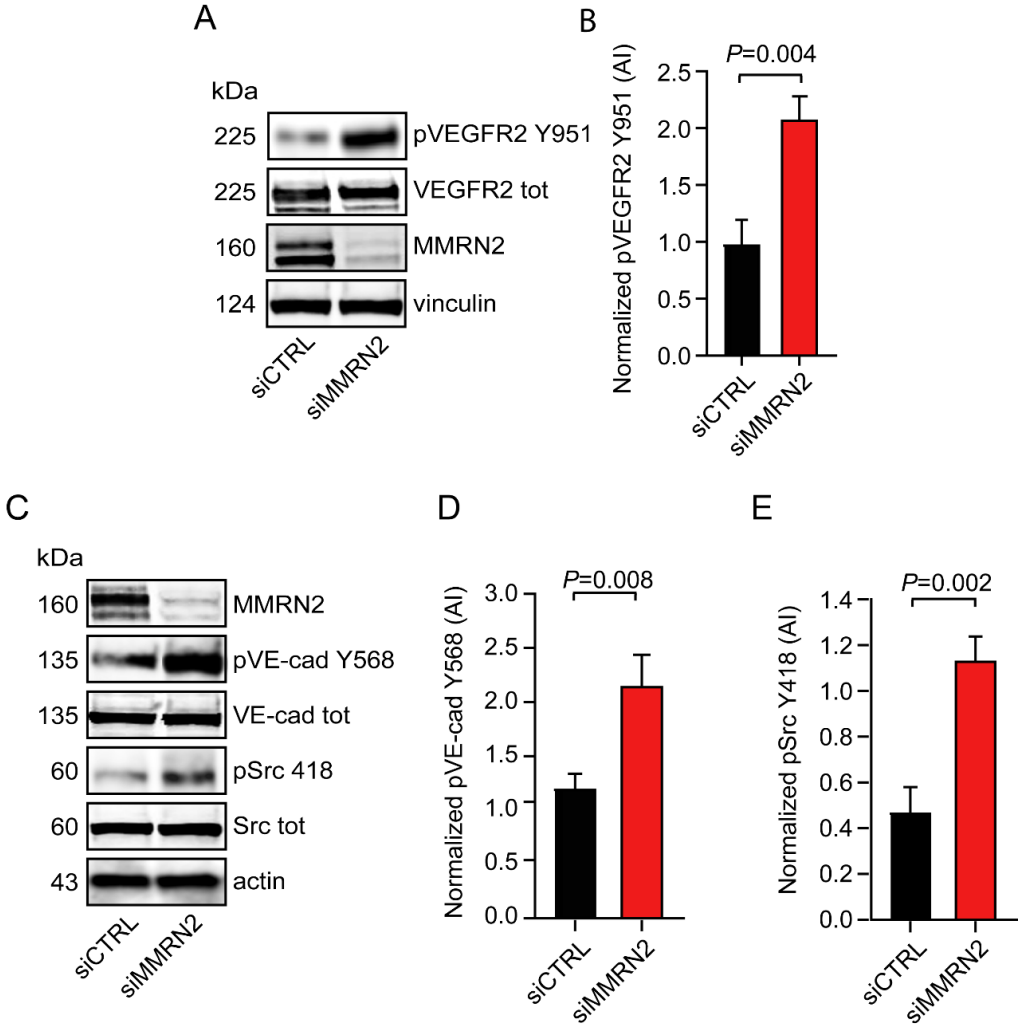

Figure 5. Loss of Multimerin-2 associates with increased phospho-VEGFR2 levels at Y951 affecting VE-cadherin phosphorylation. *(A) Western blot analysis showing increased phospho-VEGFR2 levels at Y951 following transduction of HUVEC cells with control (siCTRL) or Multimerin-2 (siMMRN2) siRNA constructs; vinculin was used as protein loading control. (B) Quantification of the phospho-VEGFR2 levels referred to total VEGFR2 and normalized to vinculin; n=3. (C) Western blot analysis showing increased phospho-VE-cadherin levels at Y568 and phospho-Src levels at Y418 following transduction of HUVEC cells with control (siCTRL) or Multimerin-2 (siMMRN2) siRNA constructs; actin was used as protein loading control. (D) and (E) Quantification of the phospho-VE-cadherin levels at Y568 and phospho- Src levels at Y418, referred to total VE-cadherin and total Src, respectively, both normalized to actin; n=3. P values were obtained using paired Student's T-test.*

Morphological alterations and rearrangement of ECs adherens junctions are functionally linked to altered ECs permeability. Thus, given the striking effects of Multimerin-2 loss in the stability of the VE-cadherin lining we assessed if it could in turn affect EC permeability. To this end, manipulated confluent HUVEC cells were tested for the permeability to FITC-Dextran (70 kDa). As expected, Multimerin-2 silenced ECs were significantly more permeable to the FITC-dextran tracer compared to the control cells (Figure 6A), further supporting the hypothesis that Multimerin-2 expression is required for the proper maintenance of ECs homeostasis. We also observed a possible compensatory mechanism to overcome this increased permeability. Indeed, following Multimerin-2 depletion and exploring other mechanisms involved in the regulation of vascular permeability, we found that Tie2 was up-regulated whereas the expression of Ang2 was down-regulated (Figure 6B and 6C). Indeed, the engagement of Tie2 by Ang2 is known to induce vascular permeability (Thomas and Augustin, 2009).

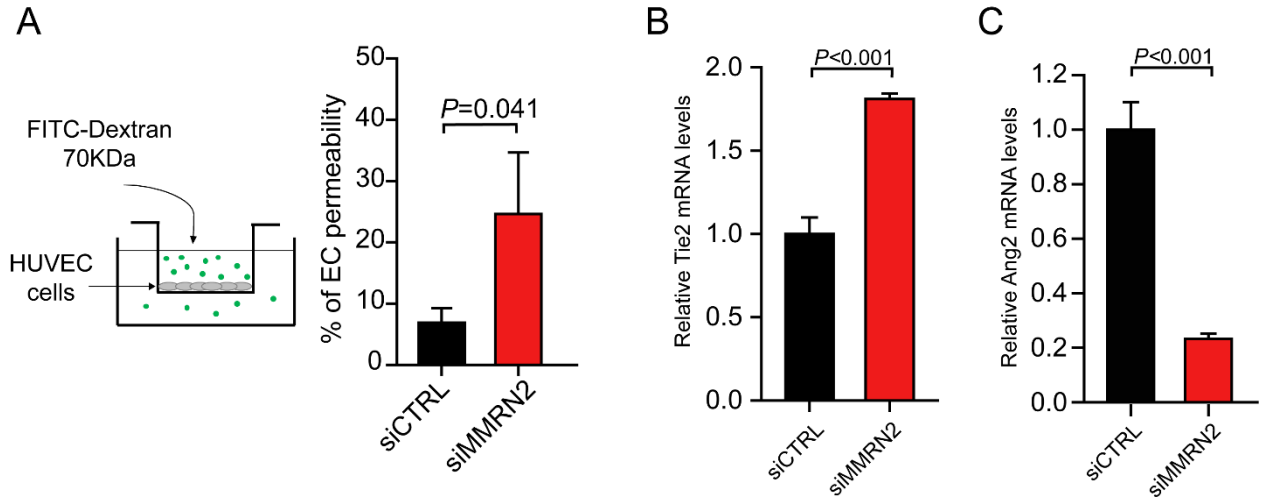

Figure 6. Multimerin-2 loss induces an increase in EC permeability. *(A) Schematic representation of the EC permeability assay (left); measurements of EC permeability to FITC-dextran (right) following transduction of HUVEC cells with control (siCTRL) or Multimerin-2 (siMMRN2) siRNA constructs; n=3. (B) and (C) Real-time PCR analyses of the relative mRNA levels of Tie2 and Ang2 in HUVEC cells following transduction with control (siCTRL) or Multimerin-2 (siMMRN2) siRNA constructs; n=3. P values were obtained using the paired Student's T-test.*

4.4 Generation and validation of the *Multimerin-2*$^{-/-}$ mouse model

To study the role of Multimerin-2 in vascular homeostasis *in vivo* we took advantage of the *Multimerin-2*$^{-/-}$ mouse model generated by our collaborators Dr. Paolo Bonaldo and Dr. Paola Braghetta (Department of Molecular Medicine, University of Padua, Italy). The knockdown of the *Multimerin-2* gene was obtained substituting the first exon with the neo^{R} cassette, according to the scheme reported in Figure 7A. Gene editing efficiency was assessed by Southern blot, quantitative PCR and Western blot analyses, showing complete abolishment of Multimerin-2 expression (Figure 7B-D).

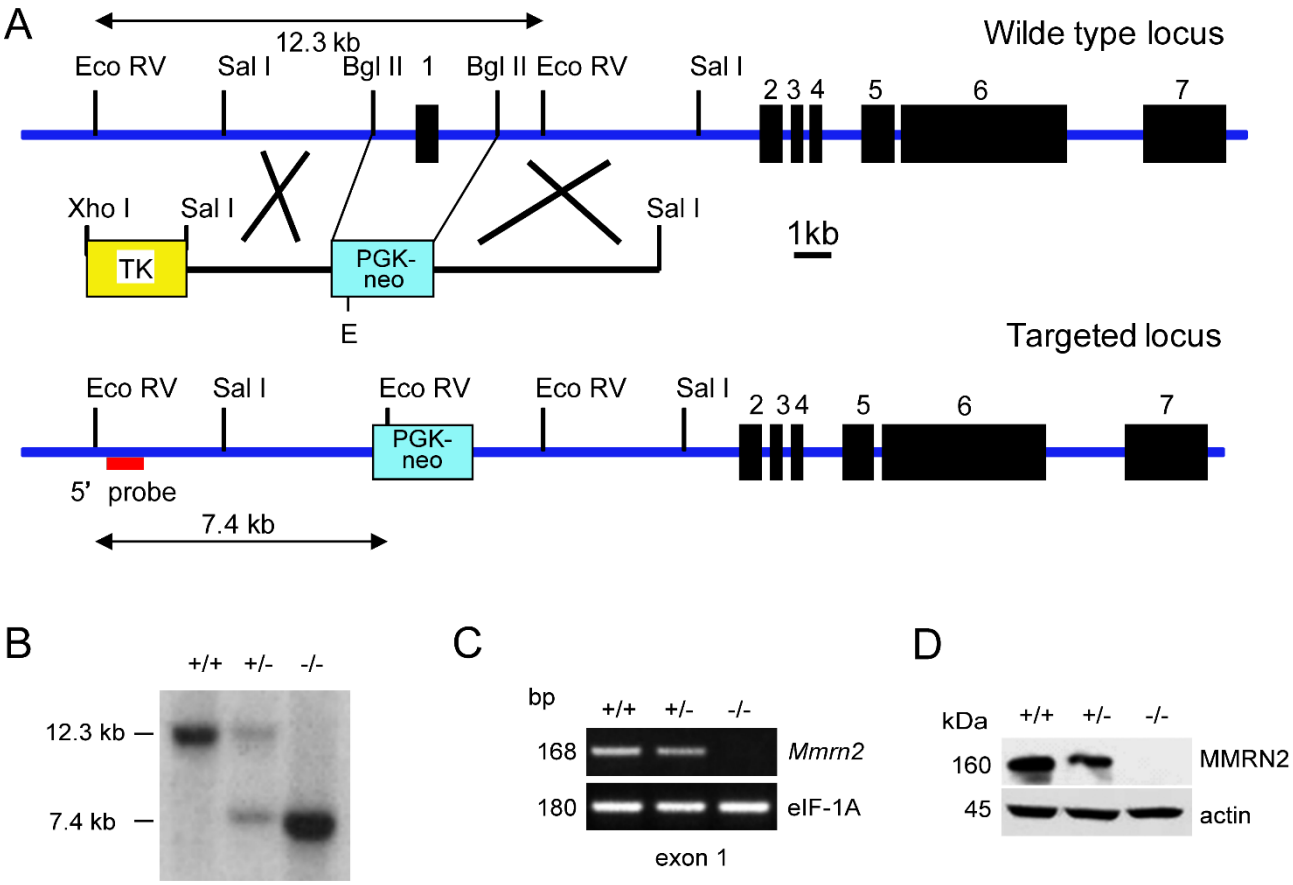

Figure 7. Generation of the Multimerin-2$^{-/-}$ mouse model. *(A) Schematic representation reporting the strategy employed for the Multimerin-2 gene knockout; black boxes = Multimerin-2 exons; yellow box = Thymidine kinase (TK); light blue box = LacZ-PGK-neo cassette; the restriction enzyme sites used for the editing are indicated; the red bar indicates the probe position used to detect the homologous recombination events. (B) Southern Blot analysis of the genomic DNA extracted from the murine tails and digested with EcoRV enzyme, showing the expected pattern of migration: the wt band at 12,3 Kb and Multimerin-2$^{-/-}$ band at 7,4 Kb. (C) RT-PCR analysis performed on the RNA extract from the mouse tails, using primers encompassing the first exon of Multimerin-2 gene; as opposed to the Multimerin-2$^{-/-}$(-/-) mice where no band was detected, the expected band at 168 kDa could be amplified in samples collected from wt mice (+/+). (D) Western blot analysis of the protein extracts from wild-type (+/+), Multimerin-2$^{+/-}$ (+/-) and Multimerin-2$^{-/-}$(-/-) mice, showing lack of Multimerin-2 expression in Multimerin-2$^{-/-}$ animals. (figure from Pellicani et al., 2020).*

The mouse model was further validated through immunofluorescence analyses performed on a number of organs isolated from *wild-type* and *Multimerin-2*$^{-/-}$ mice confirming the specific deposition of the molecule along the blood vessels counterstained with an anti-CD31 antibody (Figure 8A-C). In addition to the spleen and skin vessels, we also analysed the sprouting vessels of the retina, a model extensively exploited in the field of angiogenesis. In line with the hypothesis that Multimerin-2 is required to stabilize the newly formed vessels during angiogenesis (Figure 11 of Introduction section), several tip cells of the sprouting front of the retinal vessels from the *wild-type* P5 pups, displayed no Multimerin-2 staining (Figure 8B).

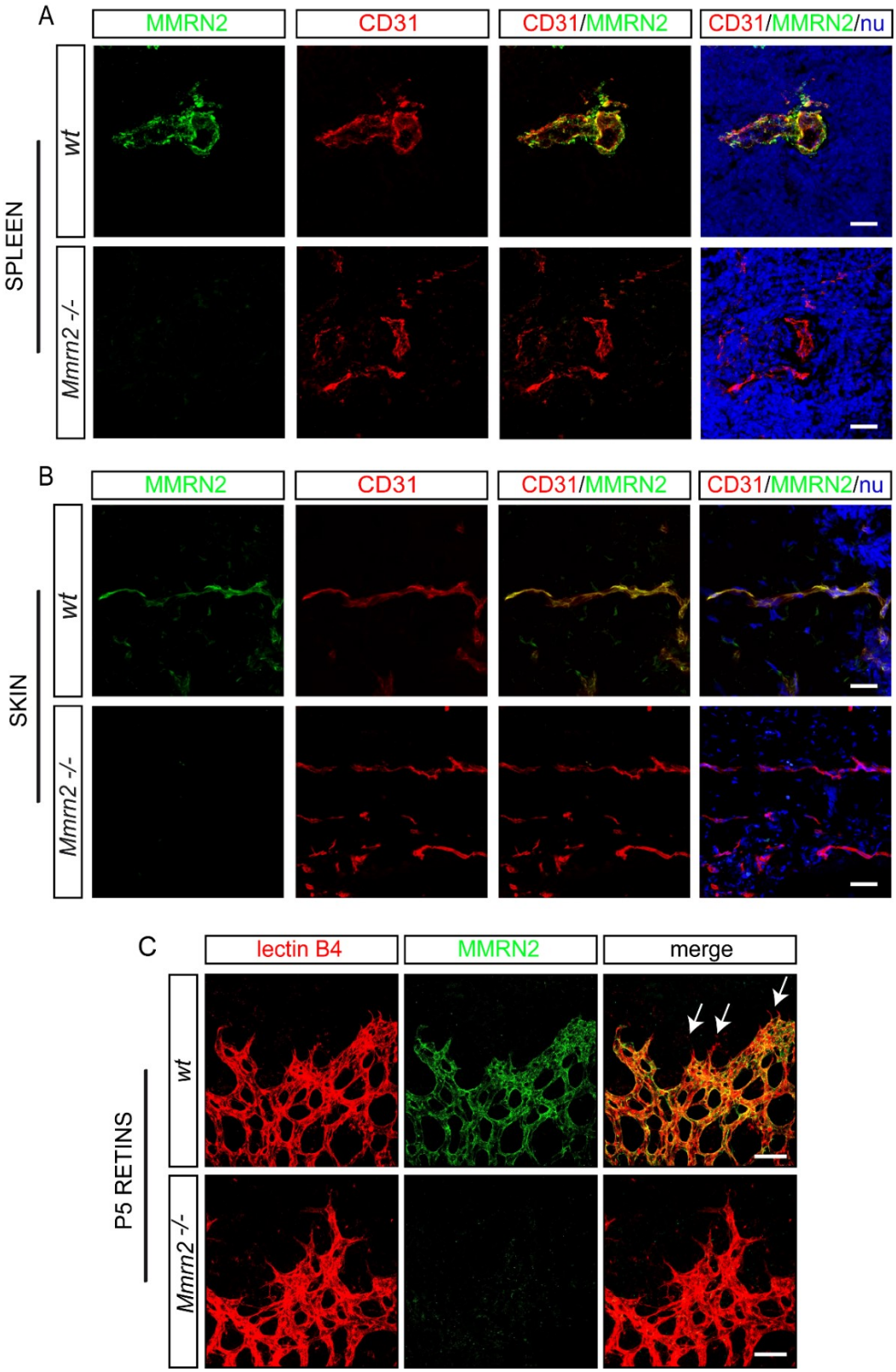

Figure 8. Multimerin-2 is deposited along the blood vessels. *(A) Representative images of the immunofluorescence analyses performed on spleen sections isolated from wild type (wt) and Multimerin-2$^{-/-}$ (Mmrn2$^{-/-}$) mice; Multimerin-2 (green), vessels with CD31 (red) and nuclei with TO-PRO (blue). (B) Representative images of the immunofluorescence analyses performed on skin sections isolated from wild type (wt) and Multimerin-2$^{-/-}$ (Mmrn2$^{-/-}$) mice; Multimerin-2 (green), vessels with CD31 (red) and nuclei with TO-PRO (blue). (C) Representative images of the immunofluorescence analyses performed on P5 whole-mounted retinas isolated from P5 wild-type (wt) and Multimerin-2$^{-/-}$ (Mmrn2$^{-/-}$) pups; Multimerin-2 (green); vessels are stained with isolectin B4 (red) and nuclei with TO-PRO (blue); arrows indicate tip cells devoid of Multimerin-2 deposition; scale bar 50 µM.*

4.5 Retinal vessels' ECs from *Multimerin-2*$^{-/-}$ mice display junctional defects

The retina model is one of the most widely used tools in the study of angiogenesis since retinal vessels rise after birth from the optic nerve, progressively irradiating towards retina margins and completing their maturation after 3 weeks allowing to assess over time the angiogenic process *ex vivo*.

Taking advantage of the retina model we examined VE-cadherin organization in retinal blood vessels from *wild-type* and *Multimerin-2*$^{-/-}$ mice. Adding value to our previous *in vitro* results, we found that *Multimerin-2*$^{-/-}$ mice displayed aberrant VE-cadherin distribution (Figure 9A). In particular, VE-cadherin staining was frequently intracellular and condensed, encumbering the possibility to clearly distinguish the cell-cell contacts (high magnification of Figure 9A). Consistently, retinal vessel from *Multimerin-2*$^{-/-}$ mice were characterized by increased phosphorylation of VEGFR2 at the Y949 residue (the murine counterpart of the human Y951) respect to the *wild-type* littermates.

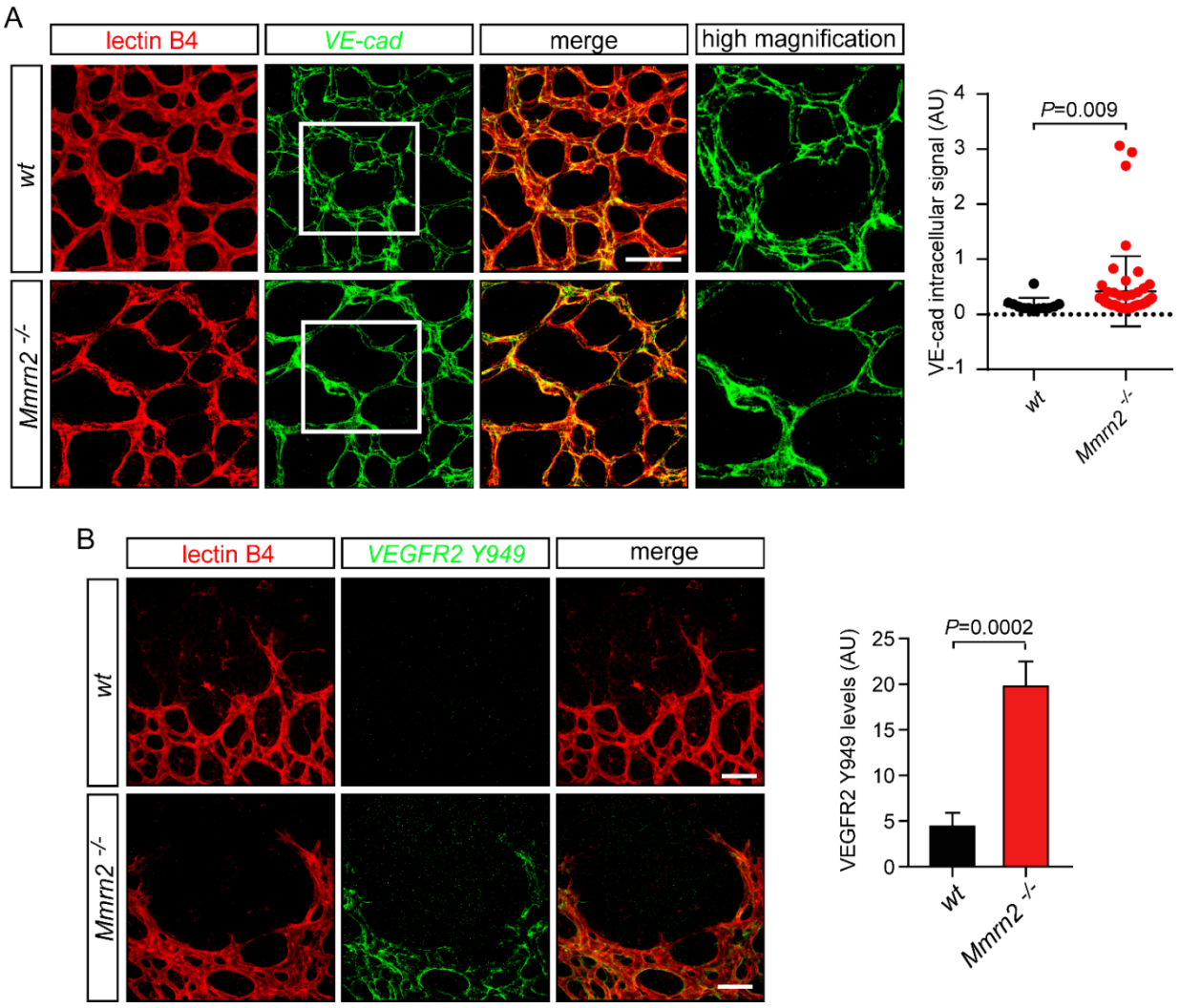

Figure 9. Vessels from Multimerin-2$^{-/-}$ display impaired VE-cadherin lining and increased levels of phospho-VEGFR2 (Y949). *(A) Representative immunofluorescence images of P9 retinal vessels of wild type (wt) and Multimerin-2$^{-/-}$ (Mmrn2$^{-/-}$) pups; VE-cadherin (green); vessels are counterstained with isolectin B4 (red); the graph on the right indicates the relative quantification of the VE-cadherin intracellular signals; n=6. (B) Representative immunofluorescence images of P5 retinal vessels from wild type (wt) and Multimerin-2$^{-/-}$ (Mmrn2$^{-/-}$) pups; phospho-VEGFR2 (Y949) is highlighted in green; vessels are counterstained with isolectin B4 (red); the graph on the right indicates the relative quantification of the phospho-VEGFR2 (Y949) signals; n=5; scale bar 50 μM. P values were obtained using Mann-Whitney Rank Sum test in (A) or the paired Student's T-test in (B).*

4.6 *Multimerin-2*$^{-/-}$ mice display increased vascular permeability

Given the striking effects of Multimerin-2 loss in the proper maintenance of the ECs barrier functionality, we queried if Multimerin-2 loss could also affect vascular permeability *in vivo*. To this aim two different tests were set up to determine the extent of vascular leakage in *wild-type* and *Multimerin-2*$^{-/-}$ mice. First, upon VEGF-A stimulation in the ear dermis, we performed ear permeability assays assessing the leakage from the vessels of retro-orbitally injected FITC-dextran (Figure 10A). In support of our hypothesis, we found that Multimerin-2 depletion led to increased vascular permeability. To corroborate this finding, we next carried out Miles permeability assays through the retro-orbital injection of the Evans blue dye followed by the injection of VEGF-A in the dorsal skin to induce vascular permeability. Also in this experimental setting, we demonstrated that the ablation of Multimerin-2 causes a significant increase of the vascular permeability, as assessed by the spectrophotometric quantification of the leaked Evans blue dye (Figure 10B).

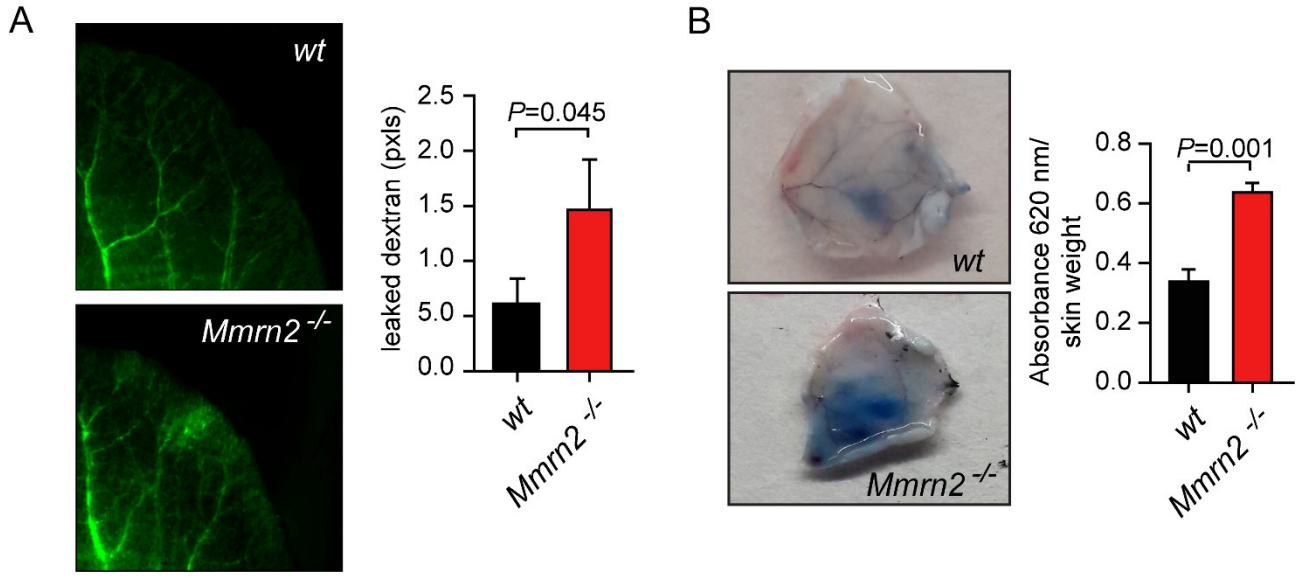

Figure 10. Multimerin-2 loss affects vascular permeability. *(A) On the left the representative images of ear permeability assay following the injection of FITC-dextran in wild type (wt) and Multimerin-2*$^{-/-}$ *(Mmrn2*$^{-/-}$*) mice; on the right the relative quantification graph is reported; n=10. (B) On the left, the representative images of the Miles permeability assay, performed on the dorsal skin of wild type (wt) and Multimerin-2*$^{-/-}$ *(Mmrn2*$^{-/-}$*) mice; on the right the graph of the relative quantification of the leaked Evans blue dye is reported; n=10. P values were obtained using the paired Student's T-test.*

4.7 Multimerin-2 depletion associates with altered tumor-associated vasculature

Once established the important role of Multimerin-2 in the maintenance of vascular homeostasis, we explored if its loss could also impact on tumor growth. To this end, we subcutaneously injected B16F10 syngeneic melanoma cells in *wild-type* and *Multimerin-2*$^{-/-}$ mice. Despite tumor growth was only slightly, but not significantly, impaired in *Multimerin-2*$^{-/-}$ mice (Figure 11A), a significant alteration of the vascular network was detected. In fact, tumors grown in *Multimerin-2*$^{-/-}$ mice displayed an increased number of vessels, with a higher density of small vessels, compared to the *wild-type* littermates (Figure 11B). Moreover, the analyses of the tumor vasculature performed on thick tumor sections (50 µm) revealed that *Multimerin-2*$^{-/-}$ mice were also characterized by an altered shape of the tumor vessels (Figure 11C). The vessels morphology was further assessed through TEM analyses performed in collaboration with dr. Patrizia Sabatelli (Institute of Molecular Genetics, CNR, Bologna, Italy). These analyses showed that tumor vessels from *Multimerin-2*$^{-/-}$ mice were frequently characterized by altered morphology and collapsed lumen (Figure 11D).

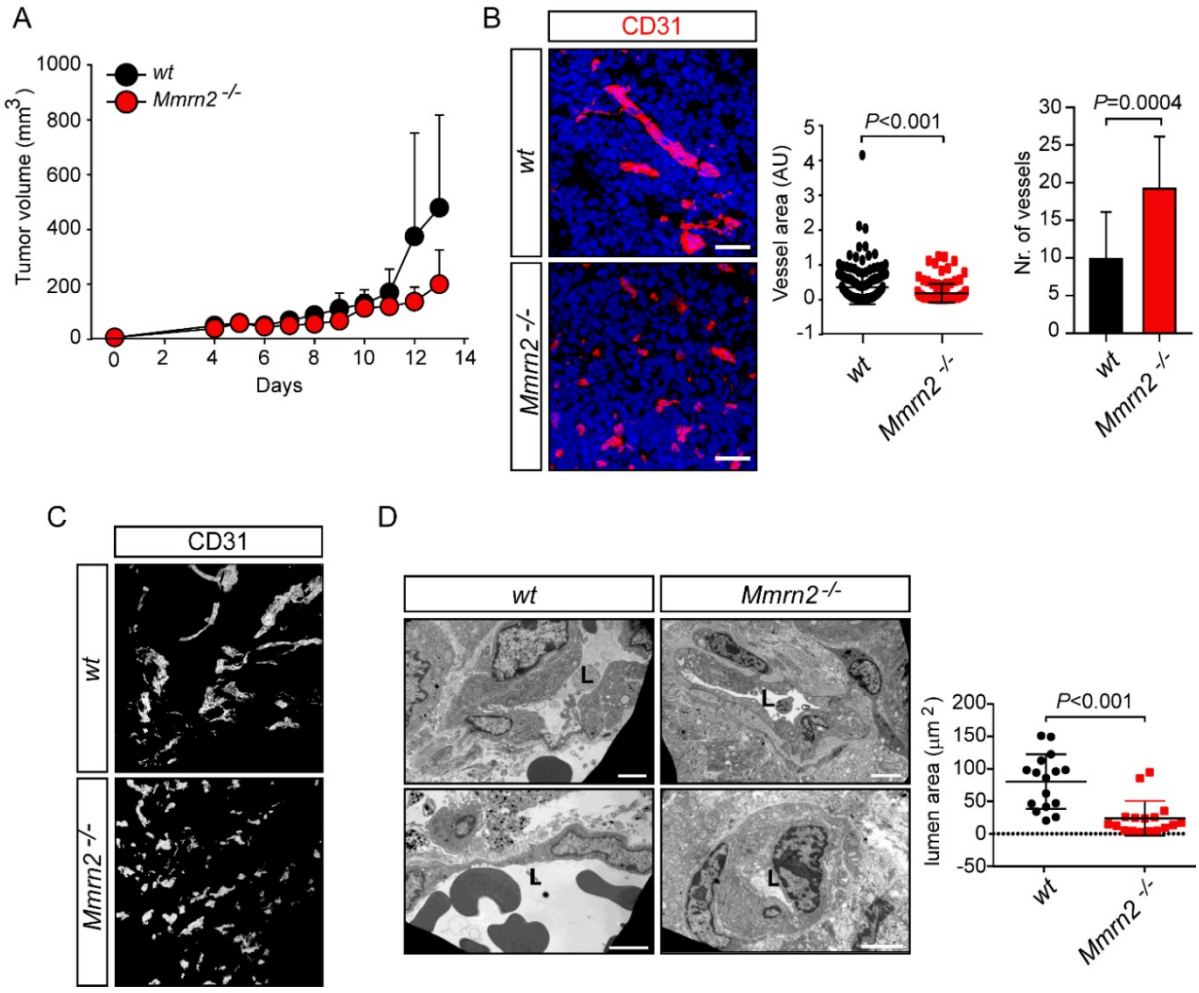

Figure 11. Multimerin-2 depletion alters the tumor-associated vasculature. *(A) B16F10 tumor growth curve in wild type (wt) and Multimerin-2*$^{-/-}$ *(Mmrn2*$^{-/-}$*) mice; n=10. (B) Representative immunofluorescence images of the vessels in B16F10 tumor sections; vessels were stained with the anti-CD31 antibody (red) and nuclei with TO-PRO (blue); scale bar 50 µM; on the right the relative quantification of the vessels area and number of vessels per field are reported; n=10. (C) Representative immunofluorescence images of B16F10 tumor vessels in 50 µm thick sections; vessels were stained with the anti-CD31 antibody. (D) Representative TEM images of the B16F10 tumor-associated vessels from wild type (wt) and Multimerin-2*$^{-/-}$ *(Mmrn2*$^{-/-}$*) mice; scale bar 2 µm; on the right the relative quantification graph of lumen dimensions is reported; n=12. P values were obtained using paired Student's T-test in (A) or the Mann-Whitney Rank Sum test in (B) and (D).*

These results suggested that tumor-associated vessels from *Multimerin-2*$^{-/-}$ mice were more inefficient compared to the vessels from *wild-type* animals, thus contributing to hypoxia in TME. In fact, we found that tumors developed in a Multimerin-2-deficient environment were characterized by augmented levels of GLUT1, a well-known marker of hypoxia (Hoskin et al., 2003), as shown in Figure 12A. Moreover, tumor associated vessels from *Multimerin-2*$^{-/-}$ mice displayed increased levels of VEGFR2 phosphorylation at Y949 (Figure 12B), further confirming the molecular mechanism elicited also under normal conditions.

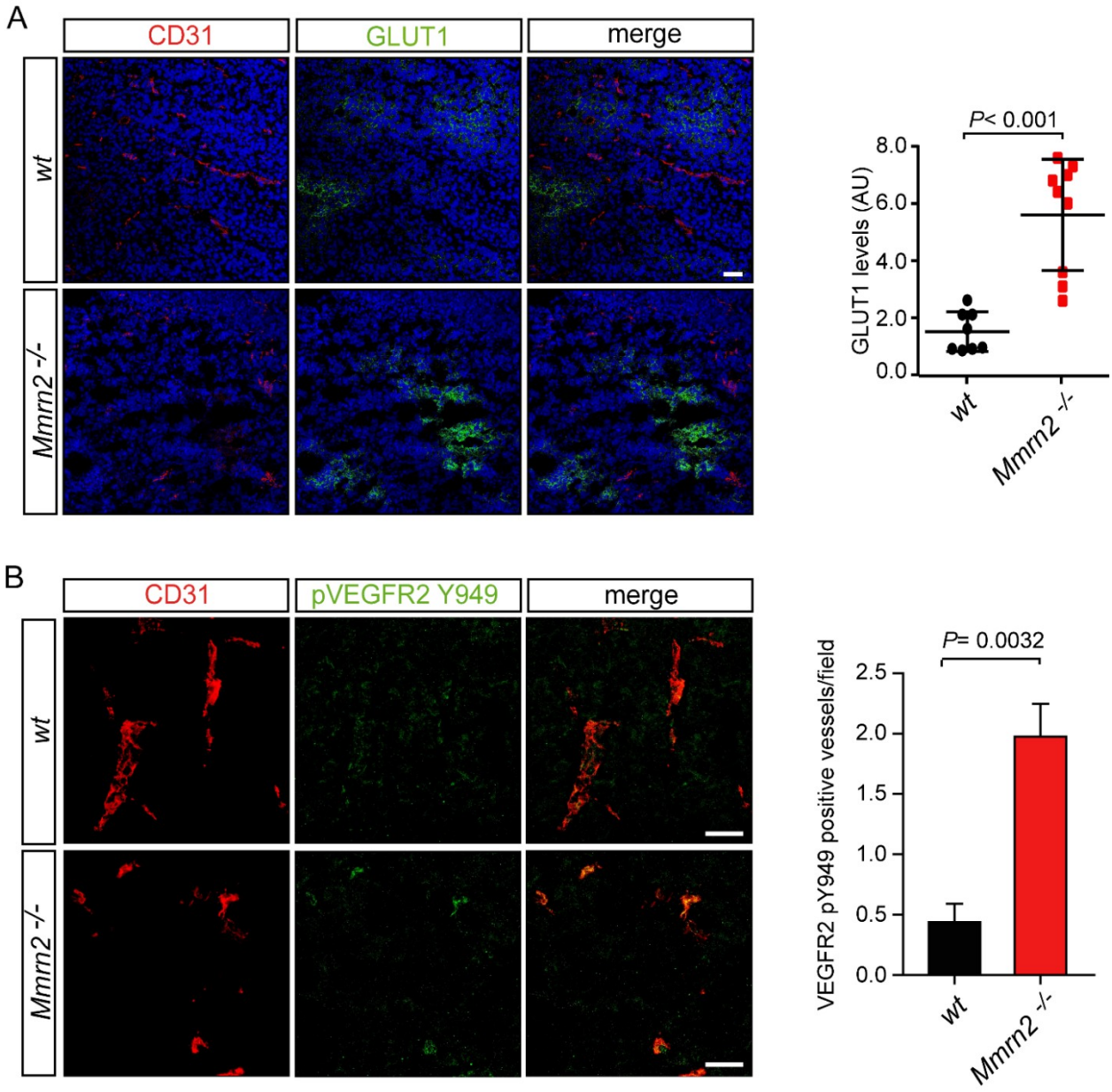

Figure 12. Tumors from Multimerin-2$^{-/-}$ mice display increased hypoxia and augmented levels of phospho-VEGFR2 (Y949). *(A) Representative images of B16F10 tumor sections from wild type (wt) and Multimerin-2$^{-/-}$ mice stained with the hypoxia marker GLUT1 (green), vessels are stained with an anti-CD31antibody (red), and nuclei with TO-PRO (blue); on the right the graph of the relative quantification of the GLUT1 signals is reported; n=8 (wt), n=9 (Mmrn2$^{-/-}$). (B) Representative images of B16F10 tumor sections from wild type (wt) and Multimerin-2$^{-/-}$ (Mmrn2$^{-/-}$) mice stained for phospho-VEGFR2 (Y949) (green), vessels were stained with an anti-CD31 antibody (red), and nuclei with TO-PRO (blue); on the right the relative quantification graph of the percentage of phospho-VEGFR2 positive vessels is reported; n=8; scale bar 50 µm. P values were obtained using the paired Student's T-test.*

4.8 Multimerin-2 loss impacts on the efficiency of the tumor-associated vessels

The altered morphology of the tumor-associated vessels from *Multimerin-2*$^{-/-}$ mice, in conjunction with the VEGFR2 state and the elevated hypoxic conditions, prompted us to better investigate the role of Multimerin-2 in the regulation of vascular efficiency. To this aim, tumor-bearing *wild-type* and *Multimerin-2*$^{-/-}$ mice were retro-orbitally injected with FITC-dextran and tomato-lectin, to assess tumor vessels permeability and vessels perfusion, respectively. As shown in Figure 13A, FITC-dextran partially colocalized within the CD31-stained vessels (blue structures) only in *wild-type* mice, whereas in *Multimerin-2*$^{-/-}$ mice the FITC-dextran compound mainly leaked outside the tumor vessels. Quantification of the intravascular FITC-dextran signal is reported in Figure 13B. The use of tomato-lectin revealed that also vessel perfusion was significantly impaired in *Multimerin-2*$^{-/-}$ mice, since the marker did not reach most of the tumor vessels, as opposed to what observed in *wild-type* animals (Figure 13A and C). Taken together, these results demonstrate that the loss of Multimerin-2 in tumors associates with increased vascular permeability and poor perfusion of the vessels, thus significantly compromising the vascular efficiency.

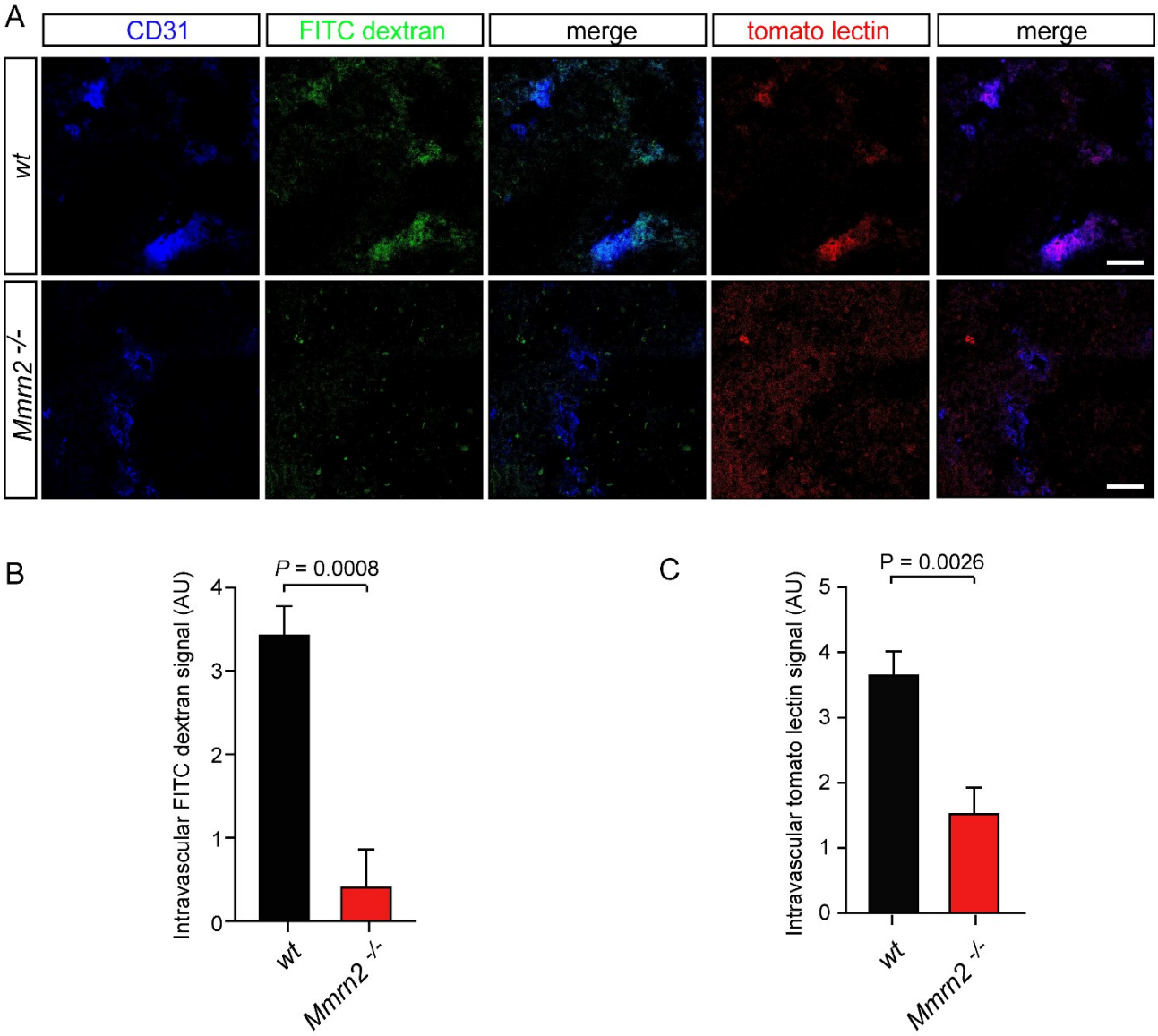

Figure 13. Loss of Multimerin-2 associates with increased permeability and poor perfusion of tumor-associated vessels. *(A) Representative images of B16F10 tumors grown in wild type (wt) and Multimerin-2$^{-/-}$ (Mmrn2$^{-/-}$) mice following the injection of FITC-dextran and tomato-lectin; vessels are stained with an anti-CD31 antibody (blue); scale bar 50 µM. (B) Graph reporting the quantification of the intravascular FITC-dextran signal relative to the vascular density; n=8. (C) Graph reporting the quantification of the intravascular tomato-lectin signal relative to the vascular density; n=8. P values were obtained using the paired Student's T-test.*

4.9 Loss of Multimerin-2 associates with impaired drug delivery and therapy efficacy

Next, we asked if the compromised vasculature of tumors grown in *Multimerin-2*$^{-/-}$ mice could affect chemotherapy efficacy. To address this question, we subcutaneously injected *wild-type* and *Multimerin-2*$^{-/-}$ mice with B16F10 melanoma cells and once tumors reached the volume of ~ 100mm^3 animals were treated with *cis*-platin every other day. The tumor growth curve shown in Figure 14A, highlighted that the treatment was significantly less effective in reducing tumor growth in *Multimerin-2*$^{-/-}$ mice. Given the intrinsic inefficiency of the intratumoral vessels in *Multimerin-2*$^{-/-}$ animals, we hypothesized that this result could be due to impaired drug delivery within the tumor mass. Indeed, using an antibody able to specifically recognize the *cis*-platin-DNA adducts, we demonstrated that drug delivery was significantly impaired in tumors grown in *Multimerin-2*$^{-/-}$ animals, since the number of adducts was significantly lower. (Figure. 14B). Taken together these results demonstrate the loss of Multimerin-2 in intatumoral vessels associates with decreased drug delivery and efficacy of the treatments.

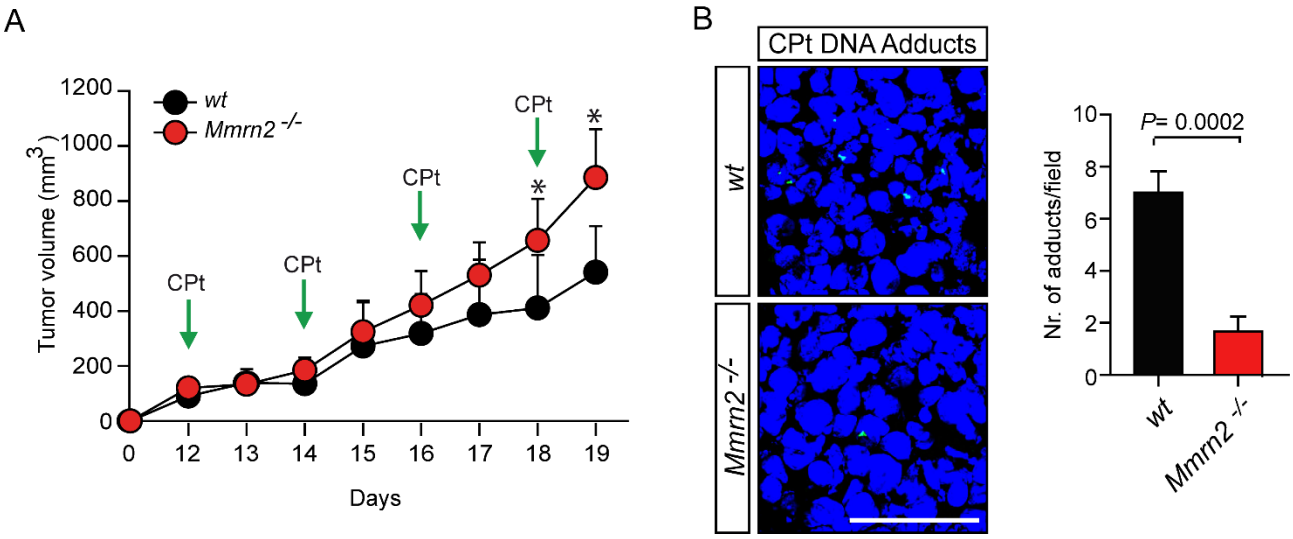

Figure 14. Multimerin-2 depletion hinders chemotherapy efficacy due to impaired drug delivery. *(A) B16F10 tumor growth curve in wild type (wt) and Multimerin-2*$^{-/-}$ *(Mmrn2*$^{-/-}$*) mice under cis-platin treatment regimen (injections are indicated with green arrows); n=8; *, P≤0,02. (B) Representative images of the cisplatin (CPt)-DNA adducts (green) in B16F10 tumors grown in wild type (wt) and Multimerin-2*$^{-/-}$ *(Mmrn2*$^{-/-}$*) mice; nuclei were stained with TO-PRO (blue); on the right the graph indicating the quantification relative to the number of nuclei is reported; n=10. P values were obtained using the paired Student's T-test.*

4.10 The loss of Multimerin-2 facilitates cancer cell transmigration through ECs barrier

Once established the role of Multimerin-2 in the proper maintenance of the EC junctions and in the regulation of the permeability to small molecules, we asked if these alterations could also promote cancer cells transmigration, thus favouring metastatic dissemination.

Given the high metastatic potential of the triple-negative breast cancer cell line MDA-MB-231 we decided to employ these cells to carry out the transmigration assays. First, to trace the cells following transmigration, MDA-MB-231 cells were engineered to constitutively express the GFP reporter. Following transduction with the control or Multimerin-2 siRNA vectors, HUVEC cells were seeded on the top of transwells membrane and MDA-MB-231-GFP cells let migrate through a stable EC monolayer (Figure 15A). Strikingly, the knockdown of Multimerin-2 significantly promoted the transmigration of cancer cells through the ECs monolayer, as opposed to what observed control HUVEC cells expressing normal levels of Multimerin-2 (Figure 15B). To verify the molecular mechanisms involved, we first focused of the VEGF-A/VEGFR2 signaling pathway, known to be down-regulated by Multimerin-2 through the sequestration of VEGF-A (Colladel et al., 2016; Lorenzon et al., 2012). To this end, the transmigration assay was performed in the presence or not of bevacizumab, a VEGF-A blocking antibody. As shown in Figure 15C, the use of bevacizumab lowered the transmigration of MDA-MB-231 cells to the levels of control cells, however, it also blocked the transmigration in control ECs suggesting that Multimerin-2 may affect transendothelial cancer cell migration through VEGF-A-independent mechanisms.

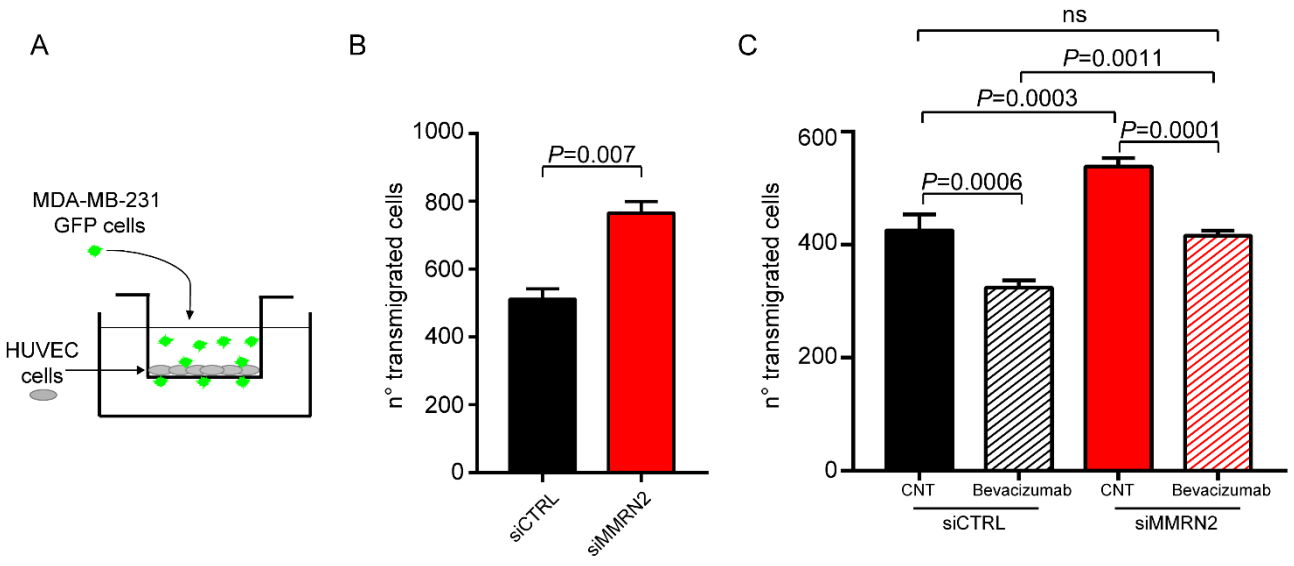

Figure 15. Multimerin-2 loss promotes cancer cell transmigration through the endothelium. *(A) Schematic representation of the transmigration assay. (B) Graph reporting to the number of MDA-MB-231-GFP (MB231-GFP) cells transmigrated through the HUVEC cell monolayer on the bottom side of the transwell membrane, following transduction with control (siCTRL) or Multimerin-2 (siMMRN2) siRNA constructs; n=3. (C) Graph reporting to the number of MDA-MB-231-GFP (MB231-GFP) cells transmigrated through the HUVEC cell monolayer on the bottom side of the transwell membrane, following transduction with control (siCTRL) or Multimerin-2 (siMMRN2) siRNA constructs in the presence of bevazizumab or trastuzumab (CNT) as control; n=3. P values were obtained using the ANOVA test for multiple comparison.*

4.11 Multimerin-2 depletion associates with altered VCAM1 expression in ECs under tumor conditions

Transmigration of cancer cells through the endothelial barrier is governed by a complex crosstalk between neoplastic cells and ECs, also involving ECM remodelling and recruitment of immune cells. To adhere, intra- and extra-vasate through the blood vessels, cancer cells frequently exploit the same molecular machinery employed by immune cells to reach inflamed tissues. Several molecules take part in this process, including selectins, integrins and also endothelial-specific molecules such as the vascular cell adhesion molecule 1 (VCAM1) (Schlesinger and Bendas, 2015). In particular, since VCAM1 over-expression associates with increased metastatic dissemination and poor prognosis for cancer patients (Deok-Hoon Kong et al., 2018), we asked if the loss of Multimerin-2 could be linked to increased VCAM1expression levels in ECs. In contrast to our hypothesis, Multimerin-2 silenced HUVEC cells did not display any change in the VCAM1 protein levels (Figure 16A), whereas the VCAM1 mRNA levels were significantly lower compared to control-silenced cells (Figure 16B). We next wondered if the loss of Multimerin-2 could affect the expression of VCAM1 under tumor conditions. To this end, manipulated ECs were challenged with the conditioned media (CM) from MDA-MB-231 cancer cells (Figure 16C), and the expression of VCAM1 was assessed under this experimental setting. As shown in Figure 16D and 16E, both the VCAM1 protein and mRNA levels were significantly higher in Multimerin-2-silenced HUVEC cells, when challenged with CM from-MDA-MB-231 cells. This result further highlights the importance of the crosstalk between tumor and ECs during the metastatic dissemination and pinpoints Multimerin-2 as a key cue in this context.

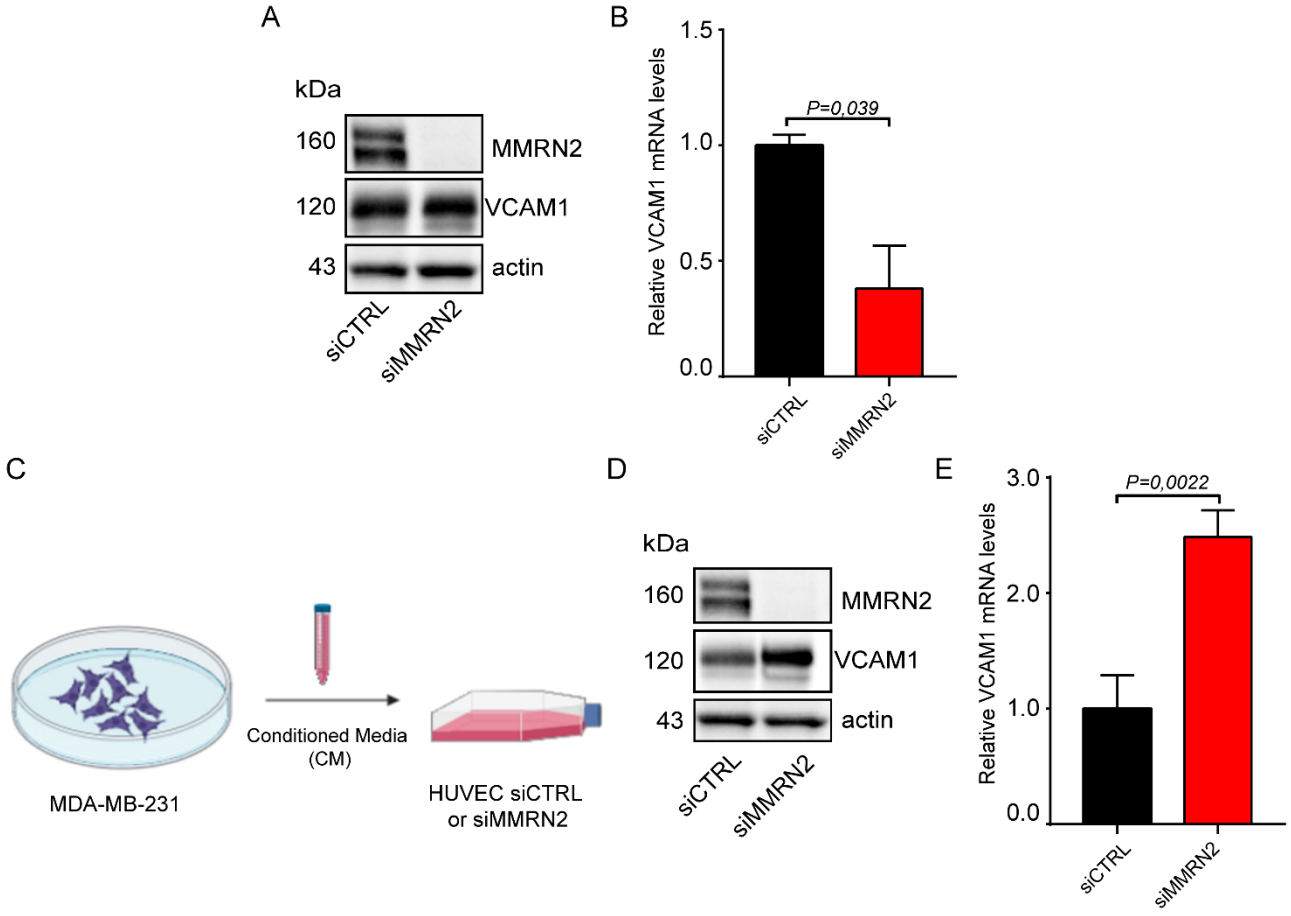

Figure 16. Multimerin-2 loss triggers VCAM1 overexpression in EC under tumor conditions*. (A) Representative image of Western blot analyses of VCAM1 expression following transduction of HUVEC cells with the control (siCTRL) or Multimerin-2 (siMMRN2) siRNA constructs; actin was used as protein loading control; n=3. (B) Real-time PCR analysis of the relative mRNA levels of VCAM1 in HUVEC cells upon transduction with the control (siCTRL) or Multimerin2 (siMMRN2) siRNA constructs; n=3. (C) Schematinc representation of the experimental setting employed to simulate a tumor environment by challenging HUVEC cells with conditioned media (CM) from MDA-MB-231 cells. (D) Representative image of Western blot analyses of VCAM1 expression in HUVEC cells challenged with MDA-MB-231-derived CM and transduced with the control (siCTRL) or Multimerin-2 (siMMRN2) siRNA constructs; actin was used as protein loading control; n=3. (E) Real-time PCR analysis of the relative VCAM1 mRNA levels in HUVEC cells challenged with MDA-MB-231-derived CM and transduced with the control (siCTRL) or Multimerin-2 (siMMRN2) siRNA constructs; n=3. P values were obtained using the paired Student's T-test.*

Since angiogenesis represents a major hallmark of most of cancer types, and different cancer cells exploit common molecular mechanisms for blood-born metastatization, we asked if Multimerin-2 loss could associate with increased VCAM1 expression levels, independently from the tumor type. To this end, manipulated HUVEC cells were challenged with CM from several cancer cell lines. As indicated by the Western blot analyses, all the breast cancer cell lines employed (MDA-MB-231; MDA-MB-435; MDA-MB-468 and MCF7) triggered a higher expression VCAM1 in Multimerin-2-silenced HUVEC cells, despite with a different extent (Figure 17A). Similar results were obtained challenging manipulated HUVEC cells with conditioned media from cancer cells isolated from melanoma cancer patients Mel-272, Mel-380, Mel-514, Mel-593, kindly provided by Dr. Elisabetta Fratta (CRO-IRCCS Aviano, Italy) (Figure 17B). Consistent results were also obtained with the use of CM from the colon cancer cell lines HT29, HCT116, SW480, SW620, with the only exception of the SW620 cell line (Figure 17C).

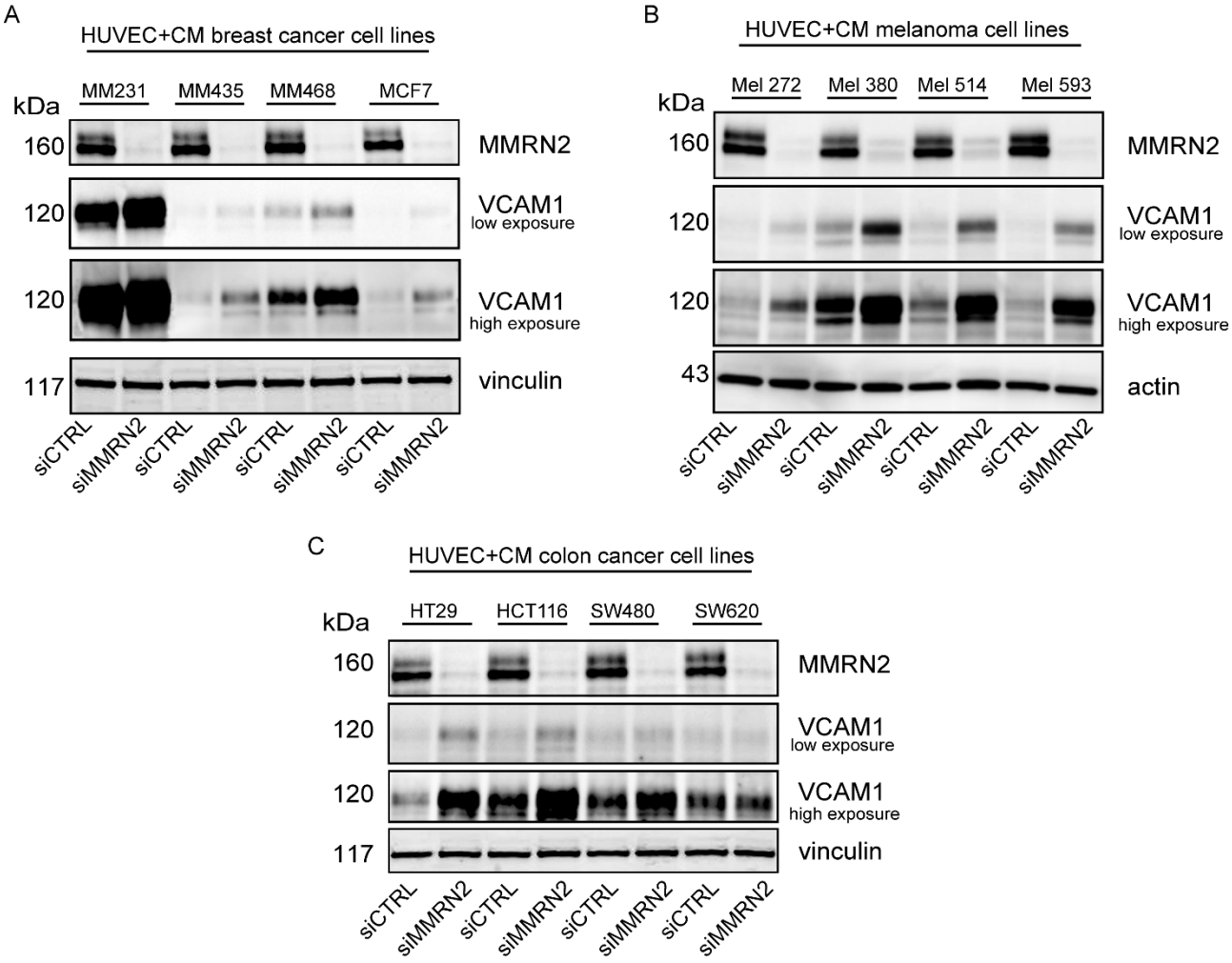

Figure 17. Multimerin-2-silenced HUVEC cells display higher VCAM1 expression when challenged with CM from different tumor types. *(A) Representative image of the Western blot analyses of VCAM1 expression in HUVEC cells transduced with the control (siCTRL) or Multimerin-2 (siMMRN2) siRNA constructs and challenged with CM from different breast cancer cell lines; vinculin was used as protein loading control; MM231 stands for MDA-MB-231; MM435 stans for MDA-MB-435; MM468 stands for MDA-MB-468; n=3. (B) Representative image of the Western blot analyses of VCAM1 expression in HUVEC cells transduced with the control (siCTRL) or Multimerin-2 (siMMRN2) siRNA constructs and challenged with CM from the Mel-272, Mel-380, Mel-514, Mel-593 melanoma cell lines; actin was used as protein loading control; n=3. (C) Representative image of the Western blot analyses of VCAM1 expression in HUVEC cells transduced with the control (siCTRL) or Multimerin-2 (siMMRN2) siRNA constructs and challenged with CM from the HT29, HCT116, SW480 and SW620 colon cancer cell lines; vinculin was used as protein loading control; n=3.*

A different outcome was obtained in the context of ovarian cancer, with the only exception of the OVASHO cell line, which induced a slightly higher expression of VCAM1 in Multimerin-2 silenced HUVEC cells (Figure 18).

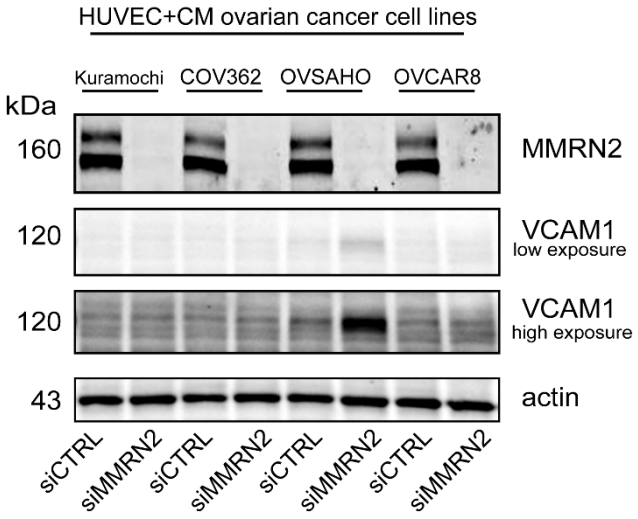

Figure 18. The majority of the ovarian cancer cell lines tested do not increase VCAM1 expression upon Multimerin-2 loss. *Representative image of the Western blot analyses of VCAM1 expression in HUVEC cells transduced with the control (siCTRL) or Multimerin-2 (siMMRN2) siRNA constructs and challenged with CM from the ovarian cancer cell lines Kuramochi, COV362, OVSAHO and OVCAR8; actin was used as protein loading control; n=3.*

4.12 Multimerin-2 loss favours tumor cells intravasation *in vivo*

Finally, we aimed at verifying if Multimerin-2 loss could affect tumor cell metastasis *in vivo*. To this end, we analysed the extra-vasation process through the retro-orbital injection of luciferase positive B16F10 melanoma cells in *wild-type* and *Multimerin-2*$^{-/-}$ mice. Mice were periodically scrutinized for the presence of lung metastasis using the *in vivo* imaging instrument IVIS®-Lumina. *In vivo* imaging of the thorax revealed the presence of higher luciferase signals in *Multimerin-2*$^{-/-}$ mice, respect to the *wild-type* littermates (Figure 19A and 19B), suggesting that the rate of cancer cell extravasation was elevated in these animals. This result was confirmed at the endpoint of the experiment by counting the number of metastatic foci in the isolated lungs (Figure 19C and 19D), further supporting the hypothesis that the loss of Multimerin-2 further exacerbates the inability of the endothelium to efficiently counteract tumor cell dissemination.

Taken together the results presented in this thesis suggest that loss of Multimerin-2 expression often observed in tumor vessels, may associate with poor vascular efficiency, drug delivery and efficacy. Furthermore, the vessels displaying low or absent Multimerin-2 expression may represent the preferential route for metastatization.

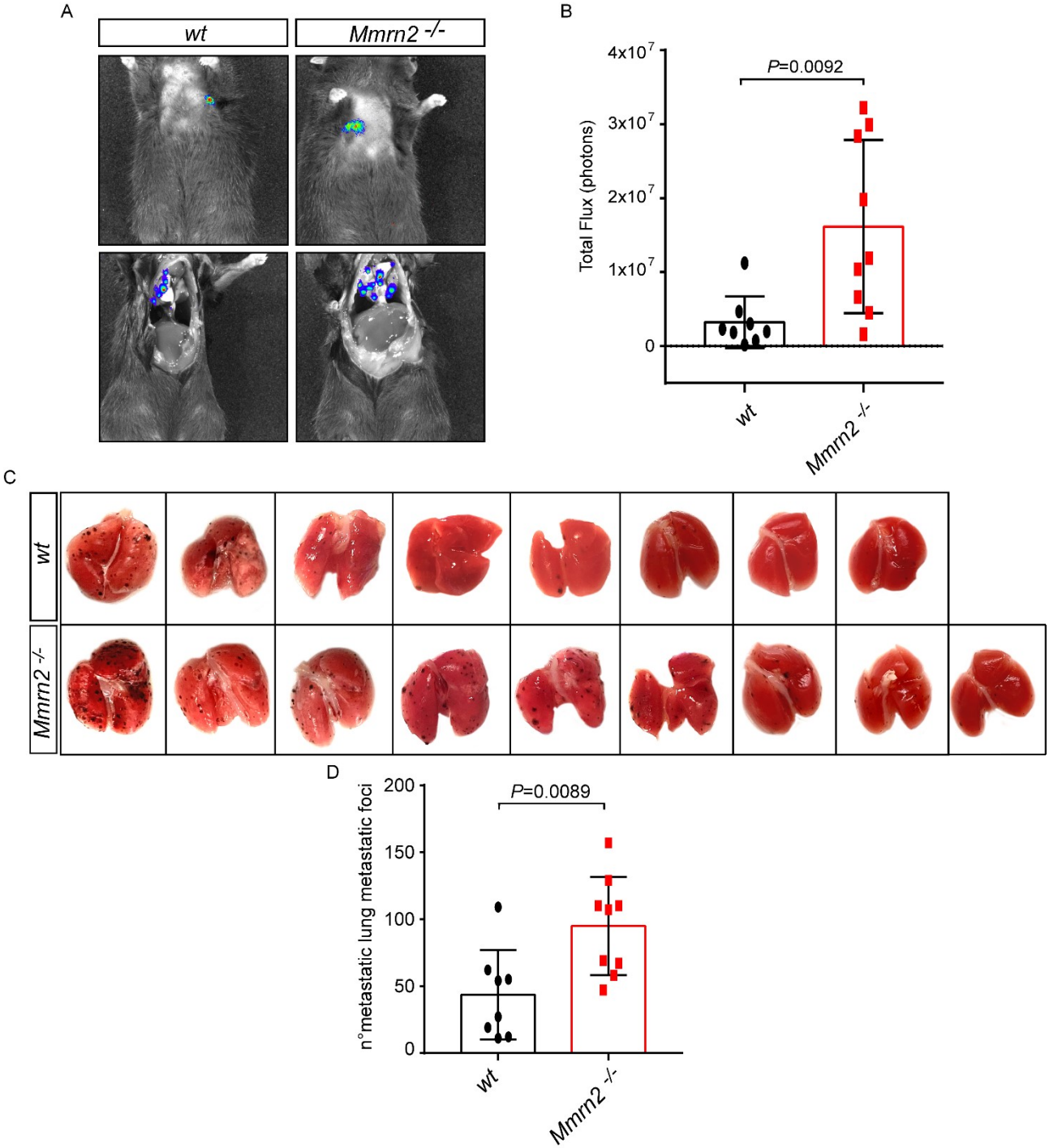

Figure 19. Multimerin-2 loss promotes tumor cell intravasation in vivo. *(A) Representative images of the photon signals from wild-type (wt) and Multimerin-2$^{-/-}$ (Mmrn2$^{-/-}$) mice, following the retro-orbital injection of luciferase positive B16F10 cells, as assessed with the IVIS®-Lumina instrument. (B) Graph reporting the quantification of the results obtained with the experiments reported in A (lower panels). (C) Images of lung metastatic lesions in wild type (wt) or Multimerin-2$^{-/-}$ (Mmrn2$^{-/-}$) mice following the retro-orbital injection of luciferase positive B16F10 cells; metastatic foci were easily recognizable as dark dots. (D) Quantification graph reporting the number of lung metastatic foci in wild type (wt) or Multimerin-2$^{-/-}$ (Mmrn2$^{-/-}$) mice following retro-orbital injection of luciferase positive B16F10 cells; metastatic lesions were manually counted after lungs dissection and fixation; n=8 wt, n=9 Mmrn2$^{-/-}$. P values were obtained using the paired Student's T-test.*

5.DISCUSSION

In this thesis work, we demonstrate that Multimerin-2 deposition along the blood vessels is required for the maintenance of ECs homeostasis. In particular, we found that, through the stabilization of the endothelial cell-cell junctions, Multimerin-2 controls the vascular permeability under physiological conditions, and that its loss exacerbates the malfunction of the tumor-associated vasculature. In fact, our results demonstrate that the homeostatic role of Multimerin-2 is critical especially under pathological conditions, such as cancer. During cancer growth and progression Multimerin-2 expression is frequently lost, and, despite the down-regulation of Multimerin-2 does not associate with a significantly altered tumor growth, it severely worsens the efficiency of the tumor-associated vasculature hindering drug delivery and, thus, chemotherapy efficacy. These results have been recently published by the Matrix Biology journal (Pellicani et al., 2020). Furthermore, in this thesis we also report exciting preliminary data suggesting that the loss of Multimerin-2 in the tumor-associated vasculature, possibly affecting VCAM1 expression, may facilitate the intra- and extra-vasation processes engaged by cancer to metastasize to different sites.

In the first part of this thesis, we provide consistent evidences indicating that the expression of Multimerin-2 is required to maintain the stability of the ECs monolayer and that its loss associates with impaired VE-cadherin lining stability and compromised AJs formation (Figure 3, Results section). We found that Multimerin-2 loss associated with increased phosphorylation of VEGFR2 at Y951, which in turn activates Src kinases inducing VE-cadherin phosphorylation at Y568, a site linked to its recycling/degradation (Figure 5, Results section). Of note, this molecular axis has been reported as one of the major players in the control of the integrity of the ECs barrier upon VEGF-A stimulation (Li et al., 2016). Considering that Multimerin-2 can sequester VEGF-A in proximity of the EC surface, we can infer that this ECM protein is necessary to finely tune VEGFR2 activation, preserving the integrity of AJs. Importantly, VE-cadherin stabilization is achieved also through the action of specific phosphatases, such as the vascular endothelial protein tyrosine phosphatase (VE-PTP). In particular, in the activated endothelium VE-PTP dephosphorylates VE-cadherin preventing its internalization. Recently, it was demonstrated that in the quiescent endothelium VE-PTP stabilizes VE-cadherin junctions independently of its phosphatase activity and in particular by inhibiting the RhoGEF GEF-H1 and modulating RhoA activity, ultimately affecting the organization of the cytoskeleton anchored to the VE-cadherin junctions (Juettner et al., 2019). Since the loss of Multimerin-2, besides impairing the VE-cadherin lining, also impacts on the actin stress fiber formation (Figure 4, Results section), it would be interesting to assess if Multimerin-2 affects the expression of VE-PTP.

The down-regulation of Multimerin-2 in ECs associates with increased phosphorylation of MLC (Figure 4, Results section), thus affecting the organization of the actin cytoskeleton. Consistently, the role of myosin in the control of cell-cell junctions is well established (Bertet et al., 2004), and, in agreement with our findings, increased MLC phosphorylation associates with augmented EC permeability (Komarova et al., 2017). In addition, elevated matrix stiffness in ECs can promote the phosphorylation of MLC, leading to cancer cell adhesion and dissemination (Reid et al., 2017). However, our preliminary data (not included in this thesis) indicate that at least the expression of fibronectin, one of the major components of the ECs BM, is not affected by Multimerin-2, suggesting that increased phospho-MLC levels upon Multimerin-2 loss are primarily the consequence of unstable AJs.

Altered vascular leakage is frequently accompanied by unbalanced levels of angiogenic cytokines. Among them, Ang-2, whose expression increases during sprouting angiogenesis, has been proposed as possible target for anti-angiogenic therapy in alternative to the blockage of the VEGF-A/VEGFR2

signalling axis. In fact, combined inhibition of Ang-2 and activation of Tie-2 promotes tumor vessels normalization, alleviates hypoxia and enhance drug delivery (Park et al., 2016). In contrast to our hypothesis, Multimerin-2 loss associates with lower Ang-2 and higher Tie2 expression levels (Figure 6, Results section). Despite the activation of this signalling axis in the context of Multimerin-2 expression needs further investigations, we can speculate that the altered expression of Ang-2 and Tie-2 represent a compensatory mechanism engaged by ECs to overcome the increased permeability associated with Multimerin-2 loss.

The use of the *Multimerin-2*$^{-/-}$ mouse model allowed to demonstrate that loss of Multimerin-2 associates with increased tumor hypoxia, increased levels of VEGFR2 phosphorylation at Y949 and, consistently, compromised functionality of the vessels in terms of permeability and perfusion (Figure 12 and Figure 13, Results section). In line with our previous observations (Andreuzzi et al., 2018; Andreuzzi et al., 2017), in this study we report consistent results obtained from the analyses of different tumor types indicating that the expression Multimerin-2 is frequently lost in tumor-associated vessels (Figure 1, Results section). In contrast, Multimerin-2 expression was shown to increase in glioblastoma samples, respect to the normal vasculature of healthy individuals (Lugano et al., 2018). Here, high Multimerin-2 correlates with increased expression of CD93, a transmembrane protein considered as a marker of tumor ECs (Orlandini et al., 2014). CD93 and Multimerin-2 are molecular partners (Galvagni et al., 2017; Khan et al., 2017; Tosi et al., 2020) and their interaction is required for proper organization of fibronectin fibrils and the consequent activation of integrin $\alpha_5\beta_1$. Functionally, this complex allows sprouting angiogenesis, stabilizing filopodia formation. Thus Multimerin-2 may exert different functions depending on the activation state of ECs; indeed, these results highlight the need to further investigate the impact of the CD93-Multimerin-2 interaction in the context of the tumor-associated vasculature. We can hypothesize that low Multimerin-2 levels in the initial steps of angiogenesis may be required for fibronectin fibrillogenesis coordinated through the interaction with CD93. Higher Multimerin-2 deposition in the later stages may instead be required to maintain vascular stability and homeostasis, a function also suggested by the fact that Multimerin-2 is universally expressed along the vasculature of most healthy tissues. In contrast, Multimerin-2 expression is lost in a number of tumor-associated vessels possibly due to degradation and/or decreased expression, affecting vascular permeability and functionality.

Our results demonstrate that Multimerin-2 loss leads to increased vascular permeability not only *in vitro* but also *in vivo* (Figure 6 and Figure 10, Results section). This phenotype is likely initiated by aberrant VEGFR2 activation which, in addition to AJs' dismantlement, may favour pericytes detachment from the vessel wall. In fact, vessels from *Multimerin-2*$^{-/-}$ mice display impaired pericytes coverage both in normal developing retinal vessels and in tumor associated vessels (Pellicani et al., 2020; data not shown in the thesis). Besides CD93, Multimerin-2 is also a substrate for the interaction with other two members of the C-type lectin family: CLEC14A and CD248 (Noy et al., 2015). Since CD248, also known as endosialin, is mainly expressed by pericytes, loss of Multltimerin-2 may entail the lack of an important substrate for the engagement of CD248, thus leading to impaired pericyte coverage. Given the important role of pericytes in regulating vascular stability and efficiency, further investigations are necessary to verify the molecular mechanisms by which Multimerin-2 regulates pericyte recruitment by ECs.

VEGFR2 is recognized as the major player in the orchestration of sprouting angiogenesis. The interaction with VEGF-A leads to receptor activation, loosening of the AJs and differentiation of ECs into stalk or tip cells, a process governed by the crosstalk between the VEGF-A/VEGFR2 and the Notch/Ddl4 pathways. In fact, different levels of Notch activation in neighbouring cells mediate a

dynamic turnover of VE-cadherin, allowing the proper coordination of ECs movements (Bentley et al., 2014). In this study, we showed that tip cells at the sprouting front of P5 retinal vessels do not express Multimerin-2 (Figure 8B, Results section), whereas the more mature vasculature in the rear side express high levels of the molecule. In this context, it would be interesting to verify if Multimerin-2 represents an important molecular cue in the crosstalk between the VEGF-A/VEGFR2 and Notch/Ddl4 signalling pathways. Our observations further support the homeostatic/stabilizing role of Multimerin-2 during angiogenesis as previously demonstrated in other experimental settings (Andreuzzi et al., 2017). In our view, the absence of Multimerin-2 in the early stages allows an efficient sprouting of the vessels; once the vessels are formed Multimerin-2 is deposited to stabilize the vasculature.

A better characterization of Notch signalling pathway in the context of the loss of Multimerin-2 may be instrumental also towards the understanding of the molecular mechanisms involved in the up-regulation of VCAM1 in Multimerin-2-silenced ECs challenged with the cancer cells' CM (Figure 17, Results section). In fact, cancer cells increase the levels of N1ICD, the active intracellular domain of Notch1, leading to up-regulation of VCAM1 thus facilitating cancer cell transmigration and increasing metastatic dissemination (Wieland et al., 2017). Thus, it would be interesting to determine if Multimerin-2 takes part in the regulation of this molecular mechanism.

It can also be speculated that the increased VCAM1 expression upon Multimerin-2 loss may be due to the release of the Multimerin-2-bound VEGF-A, a cytokine known to affect VCAM1 expression (Fearnley et al., 2014). Moreover, the up-regulation of VCAM1 associates with increased neutrophils infiltration, which favours cancer cells homing in the metastatic niche (Wieland et al., 2017). Recently, Zhang ad colleagues showed that the presence of M2 macrophages in the TME of ovarian cancer patients affects ascites formation through the over-expression VCAM1 on the ECs surface and the engagement of VLA4 on the macrophages surface (Zhang et al., 2020). This crucial interaction promotes vascular permeability evoking VE-cadherin phosphorylation. As a consequence, the inhibition of VLA4 combined with the use of bevacizumab impairs ascites formation. In contrast, it was also shown that bevacizumab induces higher VCAM1 expression levels in tumor-associated ECs, enhancing T-cell infiltration in the primary tumor and halting their metastatic potential (Wu et al., 2016). Thus, it would be interesting to verify if, through the modulation of VCAM1 expression, Multimerin-2 may play a role also in the regulation of the immune cells infiltration.

One novel emerging aspect of vascular biology is the complexity of ECs heterogeneity and many recent studies have been focused on uncovering these characteristics in health and disease. Indeed, the concept that normal ECs can adapt their morphology and function to specific tissue requirements it is well established, however it has so far being poorly investigated in the tumor context (Potente and Mäkinen, 2017). Recently, Goveia and colleagues carried out single cell RNA-sequencing of human and murine tumor ECs revealing a highly heterogeneous scenario, identifying 17 known and 16 previously unrecognized ECs phenotypes (Goveia et al., 2020). The authors found that only a small fraction of tumor ECs displays the tip-cell signature, whereas others were characterized by the so called 'breach phenotype', putatively instrumental for BM degradation, or by transcriptomic signature putatively favouring immune cell recruitment. Based on the finding that Multimerin-2 expression in tumor-associated vessels is heterogeneous, ranging from high to low/undetectable, it could be of interest to determine which specific ECs signature is triggered by the loss of Multimerin-2. To this end we are planning to isolate ECs from B16F10 tumors grown in *wild-type* or *Multimerin2*$^{-/-}$ mice,and carry out deep sequencing analyses that may potentially be instrumental for the development of more effective anti-angiogenic therapies.

Taken together the results presented in this thesis suggest that Multimerin-2 could represent a useful biomarker to predict the efficacy of conventional and anti-angiogenic therapy. In fact, the study started from the observation that some tumor-associated vessels lack Multimerin-2 expression. This may be due both to the fact that a high angiogenic stimulus down-regulates the Multimerin-2 mRNA expression and to the increased MMP2/MMP9-driven degradation (Andreuzzi et al., 2017). The loss of Multimerin-2 in tumor-associated vessels was demonstrated in different tumor types including gastric cancer (Andreuzzi et al., 2018, Andreuzzi et al., 2020), as well as in colon, breast and ovarian cancer as reported in this thesis. In particular, we are currently evaluating the expression of Multimerin-2 in about 400 sections of ovarian cancer patients enrolled in the MITO16A project, aimed to verify possible markers able to predict the efficacy of bevacizumab in combination with conventional *cis*-platin based chemotherapy. In fact, the identification of a predictive biomarker able to identify the patient who will respond to the anti-angiogenic treatment would spare cancer patients from unnecessary therapies and the resulting side effects. In this context, Multimerin-2 may represent a good candidate for different reasons. First, Multimerin-2 is a reservoir for VEGF-A, the target of bevacizumab. Second, its loss is very variable among the patients and we hypothesize that patients characterized by low levels of Multimerin-2 will respond less to the treatments. In fact, the absence of Multimerin-2 may associate with increased levels of VEGF-A thus halting the efficacy of the anti-angiogenic treatments. Moreover, a higher loss of Multimerin-2 expression and the consequent lower efficiency of the vessels may compromise drug delivery and efficacy (Figure 14, Results section). Third, the putative increased degradation of Multimerin-2 in patients displaying low levels of Multimerin-2 in tumor-associeated vessels, likely leads to the liberation of a Multimerin-2 C-terminal fragment in the body fluids (serum, ascites and urine). To verify the clinical value of this finding we are currently evaluating the levels of this fragment in 400 sera samples from the MITO16A project. Thus, the results presented in this thesis and the current investigations may grant the possibility to develop a biomarker that could allow to better stratify patients that may benefit from conventional as well as anti-angiogenic treatments.

6. MATERIALS AND METHODS

6.1 Cell culture

Human Umbilical Vein Endothelial Cells (HUVEC) were isolated from umbilical cord vein as previously described (Jaffe et al., 1973). Cells were then cultured in ECM media (Science Cells), enriched with 5% Fetal Bovine Serum (FBS), 1% of Endothelial Cell Growth Supplement (ECGS) and 100 I.U./mL of penicillin/streptomycin (PS) (Science Cells). All the other cell line employed for the experiments are listed in Table 1; DMEM, RPMI, FBS, sodium pyruvate and PS were purchased by GIBCO.

Cell Line	Origins	Culture Media
MDA-MB-231	Breast cancer	DMEM 4,5 g/L glucose, Sodium pyruvate 1mM, 10% FBS, 100 I.U./mL PS
MDA-MB-435	Breast cancer	DMEM 4,5 g/L glucose, Sodium pyruvate 1mM, 10% FBS, 100 I.U./mL PS
MDA-MB-468	Breast cancer	DMEM 4,5 g/L glucose, Sodium pyruvate 1mM, 10% FBS, 100 I.U./mL PS
MCF-7	Breast cancer	DMEM 1 g/L glucose, Sodium pyruvate, 10% FBS, 100 I.U./mL PS
HT29	Colon cancer	RPMI, 10% FBS, 100 I.U./mL PS
HCT116	Colon cancer	RPMI, 10% FBS, 100 I.U./mL PS
SW480	Colon cancer	RPMI, 10% FBS, 100 I.U./mL PS
SW620	Colon cancer	RPMI, 10% FBS, 100 I.U./mL PS
Mel-272I	Melanoma	RPMI, 10% FBS, 100 I.U./mL PS
Mel-380I	Melanoma	RPMI, 10% FBS, 100 I.U./mL PS
Mel-514I	Melanoma	RPMI, 10% FBS, 100 I.U./mL PS
Mel-593I	Melanoma	RPMI, 10% FBS, 100 I.U./mL PS
KURAMOCHI	Ovarian cancer	RPMI, 10% FBS, 100 I.U./mL PS
OVSAHO	Ovarian cancer	RPMI, 10% FBS, 100 I.U./mL PS
OVCAR8	Ovarian cancer	RPMI, 10% FBS, 100 I.U./mL PS
COV362	Ovarian cancer	DMEM 4,5 g/L glucose, Sodium pyruvate, 10% FBS, 100 I.U./mL PS
B16F10	Mouse melanoma	DMEM 4,5 g/L glucose, Sodium pyruvate, 10% FBS, 100 I.U./mL PS

Table 1. *List of the cell lines employed for this work. For each cell line is reported the origins and the culture media used.*

All cells were maintained in humified incubator at 37°C and 5% CO_2, and regularly checked for mycoplasma contamination using MycoAlert™ Mycoplasma Detection Kit (Lonza).

6.2 Antibodies and reagents

The polyclonal anti-Multimerin-2 antibody was produced in our laboratory as previously described (Colladel et al., 2016). Antibodies against VE-cadherin, VEGFR2, Src, phospho-Src (Y416), VCAM1 and actin were from Cell Signalling Technologies. Antibodies against murine CD144 (VE-cadherin) and CD31 were from BD Bioscience. Anti-phospho VE-cadherin (Y658) was provided by Thermo Fischer Scientific; anti-phospho-VEGFR2 (Y951) was from EnoGene and anti-GLUT1 was purchased by Millipore. Antibodies against CD34 and vinculin were from Abcam and Santa Cruz Biotechnology, respectively. Secondary antibodies used for immunofluorescence were conjugated with Alexa Fluor 488, 546 and were provided by Invitrogen, as well as the TO-PRO-3 fluorescent dye used for nuclear counterstain. Secondary antibodies used for immunohistochemistry, conjugated

with horse radish peroxidase (HRP) or alkaline phosphatase were from Vector Laboratories. Secondary antibodies used for Western blot were HRP-conjugated (Amersham) or IRDye®-conjugated (Li-COR Biosciences).

FITC-dextran and Evans blue dyes where obtained by Sigma-Aldrich. Biotinylated Isolectin B4 and DyLight®594 Isolectin (tomato-lectin) were from Vector Laboratories., Texas Red-conjugated streptavidin was from Thermo Fisher Scientific. Bevacizumab and trastuzumab blocking antibodies were provided by the pharmacy unit of the CRO-IRCCS Institute of Aviano (Italy).

6.3 RNA extraction, retrotranscription and Real-Time PCR

RNA extraction from cells was performed using TRIzol lysis reagent (Invitrogen) followed by chloroform phase separation and isopropanol precipitation. RNA quantification was obtained using the Nanodrop spectrophotometer and its quality assessed by agarose gel electrophoresis. Retrotranscription was performed with the AMV-RT enzyme (Promega) in the presence of the Random Primer mix (Promega), according to manufacturer instructions. After determination of primer specificity and efficiency, quantitative Real-Time PCR was carried out with iQ™ SYBR® Green Supermix (Bio-Rad) and BIORAD CFX96 Touch™ Real-Time PCR Detection System. Primer sequences are listed in Table 2.

Target gene	Sequence (from 5' to 3')
h-Gapdh	Fw: GAGAGACCCTCACTGCTG
	Rev: GATGGTACATGACAAGGTGC
h-Tie2	Fw: CCTTGGCTCTGCTGGAATGA
	Rev: GCTGGTTCTTCCCTCACGTT
h-Angpt2	Fw: TGGCTGGGAAATGAGTTTGT
	Rev: GGTTGGCTGATGCTGCTTAT
h-VCAM1	Fw: AAAAGCGGAGACAGGAGACA
	Rev: AGCACGAGAAGCTCAGGAGA

Table 2. *List of primers used for Real-Time PCR. For each target genes are reported the corresponding sequence of forward (Fw) and reverse (Rev) primers.*

Since the primer efficiency was ~100%, the $2^{-\Delta\Delta Ct}$ method was used for analysis.

6.4 Western blot

Cells were lysed in ice-cold lysis buffer (1 mM $CaCl_2$, 1 mM $MgCl_2$, 15 mM Tris-HCl pH 7.2, 150 mM NaCl, 1% TrytonX100, 0,1% SDS, 0,1% Na Deoxycholate) supplemented with 25 mM NaF, 1 mM DTT, 1 mM Na_3VO_4 and the protease inhibitors cocktail (Roche). Protein extracts were prepared for electrophoresis with Laemmli Sample Buffer and the samples boiled 10 minutes at 95°C. Samples were loaded in 4-20% Criterion Precast Gels (Bio-Rad) for molecular weight separation and transferred into Hybond-ECL nitrocellulose membranes (Amersham, GE-Healthcare). Membrane saturation was performed with 5% BSA in TBST (100mM Tris-HCl pH 7.5, 0,9% NaCl, 0,1% Tween 20) for 1 hour at room temperature. Primary antibodies were prepared in 5% BSA in TBST and incubated overnight at 4°C. The anti-phosphoVEGFR2 (Y951) and the anti-phospho VE-cadherin (Y568) were used at the final dilution of 1:500; ; The anti-vinculin, anti-Src, anti-actin, anti-VEGFR2 and anti-VE-cadherin antibodies at 1:1000; the anti-phospho-Src antibody at 1:400; the anti-Multimerin-2 antibody was used at a concentration of 1µg/mL. After incubation with the secondary antibodies the membranes were developed using the ChemiDoc Touch Imaging System (Bio-Rad) or the Odyssey infrared imaging system (Li-COR Biosciences).

6.5 Cell transfection and transduction

Endogenous downregulation of Multimerin-2 in HUVEC cells was performed using the Knock-out RNAi System (Clonotech); specifically, we transduced cells with 500 multiplicity of infection (MOI) with adenoviruses carrying this siRNA sequence: 5'-GCAGACAGTGAAGTTCAACACCACATACA-3'. Transduction was performed for 24 or 72 hours, according to experimental design. MDA-MB-231 cells were transfected with pcDNA-eGFP construct, employing Fugene reagent (Promega); eGFP positive cells were selected using neomycin at the concentration of 500 µg/mL. B16F10-Luciferase (B16F10-Luc) cells were generated transducing cells with lentivirus carrying pLENTI-V5-DEST-Luciferase vector (produced in 293FT cells); luciferase expressing cells were selected using 10µg/mL of blasticidin .

6.6 EC's permeability assay

Low passage (2 to 4) HUVEC cells were transduced with the control or Multimerin-2-targetting adenoviral vectors and 24 hours later seeded at the concentration of $1x10^5$ cells per well on 3µm pore size transwell inserts, coated on the upper side with 1% gelatine. The plates were placed in the incubator until cells reached confluency. Next, the media was carefully replaced with 200 µl of fresh medium containing 1 mg/ml FITC-dextran and incubated for 20 min at 37°C. As readout of ECs leakage measurements at the wavelength of 535 nm were obtained using the TECAN spectrophotometer.

6.7 EC's transmigration assay

Low passage (2 to 4) HUVEC cells were transduced and 24 hours later seeded at the concentration of $9x10^4$ cells per well on 8µm pore size transwell inserts, coated on the upper side with 1% gelatine. The plates were placed in the incubator until cells reached confluency. Next, $1x10^4$ MDA-MM-231-GFP cells suspended in ECM serum free media were added on the top of the insert. Complete DMEM was added on the wells and the inserts placed on top and incubated for 14 hours. The number of transmigrated cells on the bottom side of the insert was determined using Leica TCS SP2 confocal microscope. To verify the involvement of VEGF-A in the putative altered transmigration the experiments were also performed in the presence of 1µg/mL of bevacizumab or 1µg/mL trastuzumab, as a control.

6.8 EC's stimulation

Basal level of VEGFR2 activation was favoured by adding 2ng/mL of VEGF-A to confluent HUVEC cells. To enhance VCAM1 expression transduced HUVEC cells were challenged for 12 hours with the ECM serum free CM from different cancer cell lines.

6.9 Immunofluorescence and immunohistochemistry

Transduced HUVEC cells were seeded and grown on cover glass slides placed in 6 well plates. Once reached confluency, cells were fixed in 4% PFA (in PBS) for 15 minutes at room temperature. After 3 washes with PBS (5 min each), permeabilization was performed with 0,1% Triton X-100 for 5 minutes and rinsed with PBS supplemented with 50mM glycine. Cells were next incubated with 2% BSA for 1 hour at room temperature to block aspecific binding followed by overnight incubation at 4°C with primary antibodies (anti-VE-cadherin 1:100 and anti-phospho MLC 1:50).

Immunofluorescence on tumor samples was carried out on serial cryostat section of 7µM or 50µM obtained from OCT embedded tissues. Slices were collected on positively charged glass slides (BDH

Super-Frost Plus), air dried, washed in PBS and then fixed with 4% PFA (in PBS) for 15 minutes at room temperature. Following 3 washes with PBS, sections were permeabilized with 0,3% Triton X-100 for 5 minutes and blocked with2 % BSA for 1 hour at room temperature. Primary antibodies were incubated overnight at 4°C (anti-CD31 1:20; anti-Glut1 1:100; anti-phospho VEGFR2 Y949 1:100).

Secondary antibodies were added at the dilution 1:200 together with TO-PRO-3 and phalloidin conjugated with Alexa Fluor 546, to stain actin cytoskeleton in cells, and incubated for 1 hour at room temperature. Following 3 washes with PBS cover glasses and sections were mounted with Mowiol supplemented with 2,5% 1,4 diazabicyclo-(2,2,2)-octane (DABCO) to preserve fluorescence.

For the analysis of retinal vessels, we employed pups derived from heterozygous *Multimerin-2*$^{+/-}$ mice crosses. P4 pups were marked by clipping the digits from the paws and genotyping was assessed using the collected tissue. At appropriate stages, *wild-type* and *Multimerin-2*$^{-/-}$ pups were sacrificed by decapitation and the eyes were recovered and fixed in 4% PFA for 2 hours at 4°C. Then, retinas were carefully dissected using Leica M205 FA stereomicroscope and permeabilized with 1%BSA/0,3% Triton X-100 in PBS overnight at 4°C. Following 3 washes of 20 minutes with Pblec buffer (1% Triton X-100, 1mM CaCl2, 1mM MgCl2, 1mM MnCl2, pH 6.8), retinas were incubated with biotinylated isolectin B4 1:25 in Pblec for 24 hours. After further washes with Pblec buffer, an incubation with Texas red-conjugated streptavidin antibody (1:100 in blocking buffer) was performed for 2 hours at room temperature. For double staining, retinas were incubated with blocking buffer overnight at 4°C with different primary antibodies (anti-CD144 1:50; anti-phospho VEGFR2 Y949 1:100). After 3 washes with blocking buffer, retinas were incubated for 2 hours at room temperature with the proper Alexa Fluor secondary antibodies (1:100) diluted in blocking buffer. Following several washes, retinas were finally flat mounted at stereomicroscope on glasses with Fluoromount-G (Thermo Fisher Scientific).

Cell immunofluorescence, tumor sections and retinas stainings were acquired with a Leica TCS SP8 Confocal System. Fluorescence intensity and quantification were evaluated by means of the Volocity software.

Immunohistochemistry was performed on paraffin-embedded tumor samples kindly provided by the Pathology Unit of CRO-IRCCS Institute of Aviano (Italy) or by the MITO16A clinical trial. Briefly, sections were firstly deparaffinated with xylene and progressively rehydrated. Following antigen retrieval with citrate buffer pH 6 (20 minutes in boiling buffer), endogenous peroxidase and alkaline phosphatase were saturated with the Bloxall solution (Vector Laboratories). Blocking was performed with 1% BSA/ 2% FBS in PBS for 1 hour at room temperature and primary antibody incubation (anti-Multimerin-2 1:400; anti-CD34 1:3000 in 0,2% BSA/PBS) was carried out overnight at 4°C. Following 3 washes (5 minutes each) with PBS, incubation with secondary antibodies was performed according to manufacturer instructions. Signals were then developed with DAB Substrate Kit (Vector Laboratories) and ImmPACT™ Vector® Red Substrate Kit (Vector Laboratories). After haematoxylin counterstaining, sections were mounted using Bio-Mount HM (Bio-Optica). Images were acquired with light microscope Leica DM 750.

6.10 Transmission Electron Microscopy (TEM)

For TEM analyses, samples were fixed with 2,5% glutaraldehyde in 0.1M cacodylate buffer pH 7.4.

Post-fixation was conducted in 1% osmium tetroxide in 0.1M cacodylate buffer for 1 hour at 4 °C. Samples were then dehydrated in alcohol and included in resin (Epon812). Ultrafine sections were stained with uranyl acetate and Reynold's lead citrate, and analysed with a transmission electron

microscope (TEM, Philips EM400 at 100 kV). More than 100 cells were evaluated for each experimental condition.

6.11 Generation of *Multimerin-2*$^{-/-}$ mouse model

A SalI 14kb *Multimerin-2*$^{-/-}$ gene fragment was isolated from a lambda gt10 mouse genomic library (Clontech) using a probe spanning the 455-1367 mouse *Multimerin-2* coding region, and subcloned into the pBluescript SK vector. A BglII fragment including promoter sequences, the exon1 and part of the first intron was replaced with a lacZ-PGK-neo (neoR) cassette, containing the neomycin resistance gene under the control of the phosphoglycerate kinase promoter and a poly(A) signal. A thymidine kinase (TK) cassette was ligated at the 50 end XhoI site of the construct for negative selection. Thus, the neoR cassette insertion impairs *Multimerin-2* expression by replacing the proximal Multimerin-2 promoter, the signal peptide and the first 32 residues of the mature protein. After transfection and selection of mouse embryonic stem (ES) cells, two positive recombinant clones were identified and checked for correct single integration by Southern blot analyses. The clones were used to generate germ line chimeric mice by injection into C57BL/6NCrl host blastocysts. The resulting male chimeras were bred to C57BL/6NCrl females, to obtain heterozygous F1 mice, which were intercrossed to produce homozygous null mice. For genotype analysis, genomic DNA was isolated from ES cells, embryos, or tail biopsies. DNA was digested with EcoRV, separated on 0.8% agarose gels, transferred to a Gene Screen membrane (Dupont), and hybridized with a 1.0-kb Multimerin-2 fragment used as an external probe. Insertion of the neoR cassette introduced an additional EcoRV site useful to distinguish the wild-type and the targeted alleles by restriction analysis, which produced 12.3 Kb and 7.4 Kb fragments, respectively. The membranes were then rehybridized with neoR and TK probes to verify that a correct single integration had occurred.

6.12 Ear permeability assay

To analyse the VEGF-induced acute permeability responses, 50 µl of PBS or VEGF-A at a final concentration of 4 ng/µl were injected intradermally in the ear of *wild-type* or *Multimerin-2*$^{-/-}$ C57BL/6 mice, followed by retro-orbital injection of 100µl of FITC-dextran (25 mg/ml in PBS). After 30 minutes, mice were sacrificed, ear tissues were excised and fixed with 4% PFA. FITC-Dextran leakage from the vessels was analysed by means of fluorescence stereomicroscope's acquisition.

6.13 Miles vascular permeability assay

To assess the levels of vascular permeability, the Evans blue dye (100 µl of a 0.5% solution in 0.9% NaCl) was retro-orbitally injected in *wild-type* and *Multimerin-2*$^{-/-}$ mice. After 90 min, 50 µl of VEGF-A (100 ng) or sterile PBS were injected intradermally into the pre-shaved back skin. 30 min later, animals were sacrificed, and the areas of skin adjacent to the injection site were excised. Evans blue dye was extracted by immersion in formamide for 48 h at 55°C. Finally, the amount of the dye was quantified at the spectrophotometer at the wavelength of 620 nm and related to the weight of removed skin.

6.14 In vivo tumor growth

6 weeks old *wild-type* and *Multimerin-2*$^{-/-}$ mice were subcutaneously injected with $5x10^5$ B16F10 cells in both flanks. Tumor size was assessed over time using a caliper and the corresponding tumor volume calculated with the following formula: V= (л x length x width^2)/6. Twelve mice per group (*wild-type* and *Multimerin-2*$^{-/-}$) were used to assess tumor vessels functionality through the retro-orbital injection of 100 µL of FITC dextran (25mg/mL, 70 kDa) to determine vascular leakage. To assess vascular perfusion, after 20 minutes mice were retro-orbitally injected with 100 µL DyLight®594 Isolectin (tomato-lectin) (1mg/mL) and 20 minutes later mice were sacrificed. Tumors were dissected, embedded in OCT (Bio-Optica), snap-frozen and stored at -80°C for further immunofluorescence analysis.

To assess the efficiency of drug delivery, 6 weeks old *wild-type* and *Multimerin-2*$^{-/-}$ mice were subcutaneously injected with $5x10^5$ B16F10 cells in both flanks. Once reached the volume of 100mm^3, mice were intraperitoneally injected with *cis*-platin (10mg/Kg) and sacrificed after 6 hours. Tumors were collected, as described above, and analysed for the presence of *cis*-platin adducts.

To assess the drug efficacy 6 weeks old *wild-type* and *Multimerin-2*$^{-/-}$ mice were subcutaneously injected with $2x10^5$ B16F10 cells in both flanks. Tumors were allowed to reach the volume of 100mm^3 and mice were intraperitoneally injected every other day with a submaximal dose of *cis*-platin (2,5 mg/kg) until the endpoint and tumor volumes assessed with a caliper.

6.15 B16F10 metastasis model

6 weeks old *wild-type* and *Multimerin-2*$^{-/-}$ mice were retro-orbitally injected with $6x10^4$ B16F10 cells, stably expressing the luciferase reporter. Quality of injection was assessed including fluorescein in the cells suspension and fluorescence detected with the IVIS®-Lumina instrument (PerkinEmler). Mice were shaved in the chest area and periodically monitored with the IVIS®-Lumina instrument measuring luciferase signal 10 min following the injection of luciferin (10mg/kg). After 14 days mice were sacrificed, lungs were perfused with 4% PFA, dissected and fixed over day with 4% PFA. Following overnight incubation with 2% sucrose (in PBS), lungs were carefully cleaned, and the number of metastatic foci counted on the lungs surface.

6.16 Statistical analyses

Statistical analyses were performed using SigmaPlot or GraphPad Prism software. All values were represented as the mean ± standard deviation, obtained from at least 3 independent experiments. Numbers experiments and animals used for the *in vitro* and *in vivo* experiments are reported in corresponding figure legends. Statistical significance was determined using the two tails Student's t-test for normally distributed values, or the Mann-Whitney Rank Sum Test when the values were not normally distributed. One way ANOVA test was used for multiple comparisons. Differences were considered statistically significant when $P \leq 0,05$.

7. BIBLIOGRAPHY

Adam, F., Zheng, S., Joshi, N., Kelton, D., Sandhu, A., Suehiro, Y., Jeimy, S., Santos, A., Massé, J.-M., Kelton, J., Cramer, E., Hayward, C., 2005. Analyses of cellular multimerin 1 receptors: in vitro evidence of binding mediated by αIIbβ3 and αvβ3. Thromb. Haemost. 94, 1004–1011. https://doi.org/10.1160/TH05-02-0140

Amma, L.L., Goodyear, R., Faris, J.S., Jones, I., Ng, L., Richardson, G., Forrest, D., 2003. An emilin family extracellular matrix protein identified in the cochlear basilar membrane. Mol. Cell. Neurosci. 23, 460–472. https://doi.org/10.1016/S1044-7431(03)00075-7

Andreuzzi, E., Capuano, A., Pellicani, R., Poletto, E., Doliana, R., Maiero, S., Fornasarig, M., Magris, R., Colombatti, A., Cannizzaro, R., Spessotto, P., Mongiat, M., 2018. Loss of Multimerin-2 and EMILIN-2 Expression in Gastric Cancer Associate with Altered Angiogenesis. Int. J. Mol. Sci. 19, 3983. https://doi.org/10.3390/ijms19123983

Andreuzzi, E., Capuano, A., Poletto, E., Pivetta, E., Fejza, A., Favero, A., Doliana, R., Cannizzaro, R., Spessotto, P., Mongiat, M., 2020. Role of Extracellular Matrix in Gastrointestinal Cancer-Associated Angiogenesis. Int. J. Mol. Sci. 21, 3686. https://doi.org/10.3390/ijms21103686

Andreuzzi, E., Colladel, R., Pellicani, R., Tarticchio, G., Cannizzaro, R., Spessotto, P., Bussolati, B., Brossa, A., De Paoli, P., Canzonieri, V., Iozzo, R.V., Colombatti, A., Mongiat, M., 2017. The angiostatic molecule Multimerin 2 is processed by MMP-9 to allow sprouting angiogenesis. Matrix Biol. 64, 40–53. https://doi.org/10.1016/j.matbio.2017.04.002

Apte, R.S., Chen, D.S., Ferrara, N., 2019. VEGF in Signaling and Disease: Beyond Discovery and Development. Cell 176, 1248–1264. https://doi.org/10.1016/j.cell.2019.01.021

Arroyo, A.G., Iruela-Arispe, M.L., 2010. Extracellular matrix, inflammation, and the angiogenic response. Cardiovasc. Res. 86, 226–235. https://doi.org/10.1093/cvr/cvq049

Ausprunk', D.H., Folkman, J., 1977. Migration and Proliferation of Endothelial Cells in Preformed and Newly Formed Blood Vessels during Tumor Angiogenesis. Migr. Prolif. Endothel. Cells Preformed New. Form. Blood Vessels Tumor Angiogenesis 14, 53-65 (13). https://doi.org/10.1016/0026-2862(77)90141-8

Bazzoni, G., Dejana, E., 2004. Endothelial Cell-to-Cell Junctions: Molecular Organization and Role in Vascular Homeostasis. Physiol. Rev. 84, 869–901. https://doi.org/10.1152/physrev.00035.2003

Bentley, K., Franco, C.A., Philippides, A., Blanco, R., Dierkes, M., Gebala, V., Stanchi, F., Jones, M., Aspalter, I.M., Cagna, G., Weström, S., Claesson-Welsh, L., Vestweber, D., Gerhardt, H., 2014. The role of differential VE-cadherin dynamics in cell rearrangement during angiogenesis. Nat. Cell Biol. 16, 309–321. https://doi.org/10.1038/ncb2926

Bergers, G., Brekken, R., McMahon, G., Vu, T.H., Itoh, T., Tamaki, K., Tanzawa, K., Thorpe, P., Itohara, S., Werb, Z., Hanahan, D., 2000. Matrix metalloproteinase-9 triggers the angiogenic switch during carcinogenesis. Nat. Cell Biol. 2, 737–744. https://doi.org/10.1038/35036374

Bertet, C., Sulak, L., Lecuit, T., 2004. Myosin-dependent junction remodelling controls planar cell intercalation and axis elongation. Nature 429, 667–671. https://doi.org/10.1038/nature02590

Bockhorn, M., Jain, R.K., Munn, L.L., 2007. Active versus passive mechanisms in metastasis: do cancer cells crawl into vessels, or are they pushed? Lancet Oncol. 8, 444–448. https://doi.org/10.1016/S1470-2045(07)70140-7

Bonnans, C., Chou, J., Werb, Z., 2014. Remodelling the extracellular matrix in development and disease. Nat. Rev. Mol. Cell Biol. 15, 786–801. https://doi.org/10.1038/nrm3904

Braghetta, P., Ferrari, A., de Gemmis, P., Zanetti, M., Volpin, D., Bonaldo, P., Bressan, G.M., 2002. Expression of the EMILIN-1 gene during mouse development. Matrix Biol. 21, 603–609. https://doi.org/10.1016/S0945-053X(02)00072-0

Braghetta, P., Ferrari, A., de Gemmis, P., Zanetti, M., Volpin, D., Bonaldo, P., Bressan, G.M., 2004. Overlapping, complementary and site-specific expression pattern of genes of the EMILINyMultimerin family. Matrix Biol. 22, 549–556.

Bressan, G.M., Daga-Gordini, D., Colombatti, A., Castellani, I., Marigo, V., 1993. Emilin, a Component of Elastic Fibers Preferentially Located at the Elastin-Microfibrils Interface 12.

Bronisz, A., 2012. Reprogramming of the tumour microenvironment by stromal PTEN-regulated miR-320 14, 19.

Burri, P.H., Djonov, V., 2002. Intussusceptive angiogenesis—the alternative to capillary sprouting. Mol. Aspects Med. 23, 1–27. https://doi.org/10.1016/S0098-2997(02)00096-1

Cantelmo, A.R., Conradi, L.-C., Brajic, A., Goveia, J., Kalucka, J., Pircher, A., Chaturvedi, P., Hol, J., Thienpont, B., Teuwen, L.-A., Schoors, S., Boeckx, B., Vriens, J., Kuchnio, A., Veys, K., Cruys, B., Finotto, L., Treps, L., Stav-Noraas, T.E., Bifari, F., Stapor, P., Decimo, I., Kampen, K., De Bock, K., Haraldsen, G., Schoonjans, L., Rabelink, T., Eelen, G., Ghesquière, B., Rehman, J., Lambrechts, D., Malik, A.B., Dewerchin, M., Carmeliet, P., 2016. Inhibition of the Glycolytic Activator PFKFB3 in Endothelium Induces Tumor Vessel Normalization, Impairs Metastasis, and Improves Chemotherapy. Cancer Cell 30, 968–985. https://doi.org/10.1016/j.ccell.2016.10.006

Cantelmo, A.R., Pircher, A., Kalucka, J., Carmeliet, P., 2017. Vessel pruning or healing: endothelial metabolism as a novel target? Expert Opin. Ther. Targets 21, 239–247. https://doi.org/10.1080/14728222.2017.1282465

Capuano, A., Pivetta, E., Sartori, G., Bosisio, G., Favero, A., Cover, E., Andreuzzi, E., Colombatti, A., Cannizzaro, R., Scanziani, E., Minoli, L., Bucciotti, F., Amor Lopez, A.I., Gaspardo, K., Doliana, R., Mongiat, M., Spessotto, P., 2019. Abrogation of EMILIN1-β1 integrin interaction promotes experimental colitis and colon carcinogenesis. Matrix Biol. 83, 97–115. https://doi.org/10.1016/j.matbio.2019.08.006

Carmeliet, P., 2005. VEGF as a Key Mediator of Angiogenesis in Cancer. Oncology 69, 4–10. https://doi.org/10.1159/000088478

Carmeliet, P., 2003. Angiogenesis in health and disease. Nat. Med. 9, 8.

Carmeliet, P., Jain, R.K., 2011. Principles and mechanisms of vessel normalization for cancer and other angiogenic diseases. Nat. Rev. Drug Discov. 10, 417–427. https://doi.org/10.1038/nrd3455

Carmeliet, P., Lampugnani, M.-G., Moons, L., Breviario, F., Compernolle, V., Bono, F., Balconi, G., Spagnuolo, R., Oosthuyse, B., Dewerchin, M., Zanetti, A., Angellilo, A., Mattot, V., Nuyens, D., Lutgens, E., Clotman, F., de Ruiter, M.C., Gittenberger-de Groot, A., Poelmann, R., Lupu, F., Herbert, J.-M., Collen, D., Dejana, E., 1999. Targeted Deficiency or Cytosolic Truncation of the VE-cadherin Gene in Mice Impairs VEGF-Mediated Endothelial Survival and Angiogenesis. Cell 98, 147–157. https://doi.org/10.1016/S0092-8674(00)81010-7

Christian, S., Ahorn, H., Novatchkova, M., Garin-Chesa, P., Park, J.E., Weber, G., Eisenhaber, F., Rettig, W.J., Lenter, M.C., 2001. Molecular Cloning and Characterization of EndoGlyx-1, an EMILIN-like Multisubunit Glycoprotein of Vascular Endothelium. J. Biol. Chem. 276, 48588–48595. https://doi.org/10.1074/jbc.M106152200

Claesson-Welsh, L., 2015. Vascular permeability—the essentials. Ups. J. Med. Sci. 120, 135–143. https://doi.org/10.3109/03009734.2015.1064501

Colladel, R., Pellicani, R., Andreuzzi, E., Paulitti, A., Tarticchio, G., Todaro, F., Colombatti, A., Mongiat, M., 2016. MULTIMERIN2 binds VEGF-A primarily via the carbohydrate chains exerting an angiostatic function and impairing tumor growth. Oncotarget 7, 2022–2037. https://doi.org/10.18632/oncotarget.6515

Colombatti, A., Bressan, G.M., Castellani, I., Volpin, D., 1985. Glycoprotein 115, a glycoprotein isolated from chick blood vessels, is widely distributed in connective tissue. J. Cell Biol. 100, 18–26. https://doi.org/10.1083/jcb.100.1.18

Colombatti, A., Spessotto, P., Doliana, R., Mongiat, M., Bressan, G.M., Esposito, G., 2012. The EMILIN/Multimerin Family. Front. Immunol. 2. https://doi.org/10.3389/fimmu.2011.00093

Coltrini, D., Ronca, R., Belleri, M., Zardi, L., Indraccolo, S., Scarlato, V., Giavazzi, R., Presta, M., 2009. Impact of VEGF-dependent tumour micro-environment on EDB fibronectin expression by subcutaneous human tumour xenografts in nude mice. J. Pathol. 219, 455–462. https://doi.org/10.1002/path.2626

Corallo, D., Schiavinato, A., Trapani, V., Moro, E., Argenton, F., Bonaldo, P., 2013. Emilin3 is required for notochord sheath integrity and interacts with Scube2 to regulate notochord-derived Hedgehog signals. Development 140, 4594–4601. https://doi.org/10.1242/dev.094078

Danussi, C., Petrucco, A., Wassermann, B., Modica, T.M.E., Pivetta, E., Belluz, L.D.B., Colombatti, A., Spessotto, P., 2012. An EMILIN1-Negative Microenvironment Promotes Tumor Cell Proliferation and Lymph Node Invasion. Cancer Prev. Res. (Phila. Pa.) 5, 1131–1143. https://doi.org/10.1158/1940-6207.CAPR-12-0076-T

Danussi, C., Petrucco, A., Wassermann, B., Pivetta, E., Modica, T.M.E., Belluz, L.D.B., Colombatti, A., Spessotto, P., 2011. EMILIN1–α4/α9 integrin interaction inhibits dermal fibroblast and keratinocyte proliferation. J. Cell Biol. 195, 131–145. https://doi.org/10.1083/jcb.201008013

Danussi, C., Spessotto, P., Petrucco, A., Wassermann, B., Sabatelli, P., Montesi, M., Doliana, R., Bressan, G.M., Colombatti, A., 2008. Emilin1 Deficiency Causes Structural and Functional Defects of Lymphatic Vasculature 28, 14.

Dejana, E., 2004. Endothelial cell–cell junctions: happy together. Nat. Rev. Mol. Cell Biol. 5, 261–270. https://doi.org/10.1038/nrm1357

Deok-Hoon Kong, Young Kim, Mi Kim, Ji Jang, Sukmook Lee, 2018. Emerging Roles of Vascular Cell Adhesion Molecule-1 (VCAM-1) in Immunological Disorders and Cancer. Int. J. Mol. Sci. 19, 1057. https://doi.org/10.3390/ijms19041057

Doliana, R., Bot, S., Mungiguerra, G., Canton, A., Cilli, S.P., Colombatti, A., 2001. Isolation and Characterization of EMILIN-2, a New Component of the Growing EMILINs Family and a Member of the EMI Domain-containing Superfamily. J. Biol. Chem. 276, 12003–12011. https://doi.org/10.1074/jbc.M011591200

Er, E.E., Valiente, M., Ganesh, K., Zou, Y., Agrawal, S., Hu, J., Griscom, B., Rosenblum, M., Boire, A., Brogi, E., Giancotti, F.G., Schachner, M., Malladi, S., Massagué, J., 2018. Pericyte-like spreading by disseminated cancer cells activates YAP and MRTF for metastatic colonization. Nat. Cell Biol. 20, 966–978. https://doi.org/10.1038/s41556-018-0138-8

Fearnley, G.W., Odell, A.F., Latham, A.M., Mughal, N.A., Bruns, A.F., Burgoyne, N.J., Homer-Vanniasinkam, S., Zachary, I.C., Hollstein, M.C., Wheatcroft, S.B., Ponnambalam, S., 2014. VEGF-A isoforms differentially regulate ATF-2–dependent VCAM-1 gene expression and endothelial–leukocyte interactions. Mol. Biol. Cell 25, 2509–2521. https://doi.org/10.1091/mbc.e14-05-0962

Ferrara, N., 2010. Binding to the Extracellular Matrix and Proteolytic Processing: Two Key Mechanisms Regulating Vascular Endothelial Growth Factor Action. Mol. Biol. Cell 21, 687–690. https://doi.org/10.1091/mbc.e09-07-0590

Folkman, J., Merler, E., Abernathy, C., Williams, G., 1971. Isolation of a tumor factor responsible for angiogenesis. J. Exp. Med. 133, 275–288. https://doi.org/10.1084/jem.133.2.275

Galvagni, F., Nardi, F., Spiga, O., Trezza, A., Tarticchio, G., Pellicani, R., Andreuzzi, E., Caldi, E., Toti, P., Tosi, G.M., Santucci, A., Iozzo, R.V., Mongiat, M., Orlandini, M., 2017. Dissecting the CD93-Multimerin 2 interaction involved in cell adhesion and migration of the activated endothelium. Matrix Biol. 64, 112–127. https://doi.org/10.1016/j.matbio.2017.08.003

Gavard, J., 2009. Breaking the VE-cadherin bonds. FEBS Lett. 583, 1–6. https://doi.org/10.1016/j.febslet.2008.11.032

Gerhardt, H., Golding, M., Fruttiger, M., Ruhrberg, C., Lundkvist, A., Abramsson, A., Jeltsch, M., Mitchell, C., Alitalo, K., Shima, D., Betsholtz, C., 2003. VEGF guides angiogenic sprouting utilizing endothelial tip cell filopodia. J. Cell Biol. 161, 1163–1177. https://doi.org/10.1083/jcb.200302047

Geudens, I., Gerhardt, H., 2011. Coordinating cell behaviour during blood vessel formation. Development 138, 4569–4583. https://doi.org/10.1242/dev.062323

Goel, S., Duda, D.G., Xu, L., Munn, L.L., Boucher, Y., Fukumura, D., Jain, R.K., 2011. Normalization of the Vasculature for Treatment of Cancer and Other Diseases. Physiol. Rev. 91, 1071–1121. https://doi.org/10.1152/physrev.00038.2010

Goveia, J., Rohlenova, K., Taverna, F., Treps, L., Conradi, L.-C., Pircher, A., Geldhof, V., de Rooij, L.P.M.H., Kalucka, J., Sokol, L., García-Caballero, M., Zheng, Y., Qian, J., Teuwen, L.-A., Khan, S., Boeckx, B., Wauters, E., Decaluwé, H., De Leyn, P., Vansteenkiste, J., Weynand, B., Sagaert, X., Verbeken, E., Wolthuis, A., Topal, B., Everaerts, W., Bohnenberger, H., Emmert, A., Panovska, D., De Smet, F., Staal, F.J.T., Mclaughlin, R.J., Impens, F., Lagani, V., Vinckier, S., Mazzone, M., Schoonjans, L., Dewerchin, M., Eelen, G., Karakach, T.K., Yang, H., Wang, J., Bolund, L., Lin, L., Thienpont, B., Li, X., Lambrechts, D., Luo, Y., Carmeliet, P., 2020. An Integrated Gene Expression Landscape Profiling Approach to Identify Lung Tumor Endothelial Cell Heterogeneity and Angiogenic Candidates. Cancer Cell 37, 21-36.e13. https://doi.org/10.1016/j.ccell.2019.12.001

Grant, M.A., Karsan, A., 2018. The Blood Vessel Wall, in: Hematology. Elsevier, pp. 1843-1856.e6. https://doi.org/10.1016/B978-0-323-35762-3.00123-2

Hale, M.D., Hayden, J.D., Grabsch, H.I., 2013. Tumour-microenvironment interactions: role of tumour stroma and proteins produced by cancer-associated fibroblasts in chemotherapy response. Cell. Oncol. 36, 95–112. https://doi.org/10.1007/s13402-013-0127-7

Hanahan, D., Weinberg, R.A., 2011. Hallmarks of Cancer: The Next Generation. Cell 144, 646–674. https://doi.org/10.1016/j.cell.2011.02.013

Hayward, C.P.M., Horsewood, P., Kelton, J.G., 1991. Multimerin: A Series of Large Disulfide-Linked Multimeric Proteins Within Platelets 5. Blood 77, 2556-2560

Hill, V.K., Hesson, L.B., Dansranjavin, T., Dallol, A., Bieche, I., Vacher, S., Tommasi, S., Dobbins, T., Gentle, D., Euhus, D., Lewis, C., Dammann, R., Ward, R.L., Minna, J., Maher, E.R., Pfeifer, G.P., Latif, F., 2010. Identification of 5 novel genes methylated in breast and other epithelial cancers. Mol. Cancer 9, 51. https://doi.org/10.1186/1476-4598-9-51

Hoskin, P.J., Sibtain, A., Daley, F.M., Wilson, G.D., 2003. GLUT1 and CAIX as intrinsic markers of hypoxia in bladder cancer: relationship with vascularity and proliferation as predictors of outcome of ARCON. Br. J. Cancer 89, 1290–1297. https://doi.org/10.1038/sj.bjc.6601260

Huang, Y., Yuan, J., Righi, E., Kamoun, W.S., Ancukiewicz, M., Nezivar, J., Santosuosso, M., Martin, J.D., Martin, M.R., Vianello, F., Leblanc, P., Munn, L.L., Huang, P., Duda, D.G., Fukumura, D., Jain, R.K., Poznansky, M.C., 2012. Vascular normalizing doses of antiangiogenic treatment reprogram the immunosuppressive tumor microenvironment and enhance immunotherapy. Proc. Natl. Acad. Sci. 109, 17561–17566. https://doi.org/10.1073/pnas.1215397109

Humphrey, J.D. Dufresne E.R. and Schwartz M.A., 2014. Mechanotransduction and extracellular matrix homeostasis. Nat Rev Mol Cell Biol 15, 802-812. http://doi: 10.1038/nrm3896.

Hurwitz, H., Fehrenbacher, L., Novotny, W., Cartwright, T., Hainsworth, J., Heim, W., Berlin, J., Baron, A., Griffing, S., Holmgren, E., Ferrara, N., Fyfe, G., Rogers, B., Ross, R., Kabbinavar, F., 2004. Bevacizumab plus Irinotecan, Fluorouracil, and Leucovorin for Metastatic Colorectal Cancer. N. Engl. J. Med. 350, 2335–2342. https://doi.org/10.1056/NEJMoa032691

Hynes, R.O., 2009. The Extracellular Matrix: Not Just Pretty Fibrils. Science 326, 1216–1219. https://doi.org/10.1126/science.1176009

Hynes, R.O., Naba, A., 2012. Overview of the Matrisome--An Inventory of Extracellular Matrix Constituents and Functions. Cold Spring Harb. Perspect. Biol. 4, a004903–a004903. https://doi.org/10.1101/cshperspect.a004903

Ito, N., Wernstedt, C., Engström, U., Claesson-Welsh, L., 1998. Identification of Vascular Endothelial Growth Factor Receptor-1 Tyrosine Phosphorylation Sites and Binding of SH2 Domain-containing Molecules. J. Biol. Chem. 273, 23410–23418. https://doi.org/10.1074/jbc.273.36.23410

Jaffe, E.A., Nachman, R.L., Becker, C.G., Minick, C.R., 1973. Culture of Human Endothelial Cells Derived from Umbilical Veins. Identification by morphologic and immunologic criteria. J. Clin. Invest. 52, 2745–2756. https://doi.org/10.1172/JCI107470

Jain, R.K., 2001. Normalizing tumor vasculature with anti-angiogenic therapy: A new paradigm for combination therapy. Nat. Med. 7, 987–989. https://doi.org/10.1038/nm0901-987

Jayson, G.C., Hicklin, D.J., Ellis, L.M., 2012. Antiangiogenic therapy—evolving view based on clinical trial results. Nat. Rev. Clin. Oncol. 9, 297–303. https://doi.org/10.1038/nrclinonc.2012.8

Jeimy, S.B., Fuller, N., Tasneem, S., Segers, K., Stafford, A.R., Weitz, J.I., Camire, R.M., Nicolaes, G.A.F., Hayward, C.P.M., 2008. Multimerin 1 binds factor V and activated factor V with high affinity and inhibits thrombin generation. Thromb. Haemost. 100, 1058–1067. https://doi.org/10.1160/TH08-05-0307

Juettner, V.V., Kruse, K., Dan, A., Vu, V.H., Khan, Y., Le, J., Leckband, D., Komarova, Y., Malik, A.B., 2019. VE-PTP stabilizes VE-cadherin junctions and the endothelial barrier via a phosphatase-independent mechanism. J. Cell Biol. 218, 1725–1742. https://doi.org/10.1083/jcb.201807210

Kai, F., Drain, A.P., Weaver, V.M., 2019. The Extracellular Matrix Modulates the Metastatic Journey. Dev. Cell 49, 332–346. https://doi.org/10.1016/j.devcel.2019.03.026

Khan, K.A., Naylor, A.J., Khan, A., Noy, P.J., Mambretti, M., Lodhia, P., Athwal, J., Korzystka, A., Buckley, C.D., Willcox, B.E., Mohammed, F., Bicknell, R., 2017. Multimerin-2 is a ligand for group 14 family C-type lectins CLEC14A, CD93 and CD248 spanning the endothelial pericyte interface. Oncogene 36, 6097–6108. https://doi.org/10.1038/onc.2017.214

Kim K.J., Li B., Winer J., Armanini M., Gillett N., Phillips H.S., Ferrara N., 1993. Inhibition of vascular endothelial growth factor-induced angiogenesis suppresses tumour growth in vivo. Nature, 362, 841-844. https://doi: 10.1038/362841a0

Koch, S., Claesson-Welsh, L., 2012. Signal Transduction by Vascular Endothelial Growth Factor Receptors. Cold Spring Harb. Perspect. Med. 2, a006502–a006502. https://doi.org/10.1101/cshperspect.a006502

Koh, Y.J., Kim, H.-Z., Hwang, S.-I., Lee, J.E., Oh, N., Jung, K., Kim, M., Kim, K.E., Kim, H., Lim, N.-K., Jeon, C.-J., Lee, G.M., Jeon, B.H., Nam, D.-H., Sung, H.K., Nagy, A., Yoo, O.J., Koh, G.Y., 2010. Double Antiangiogenic Protein, DAAP, Targeting VEGF-A and Angiopoietins in Tumor Angiogenesis, Metastasis, and Vascular Leakage. Cancer Cell 18, 171–184. https://doi.org/10.1016/j.ccr.2010.07.001

Kolte, D., McClung, J.A., Aronow, W.S., 2016. Vasculogenesis and Angiogenesis, in: Translational Research in Coronary Artery Disease. Elsevier, pp. 49–65. https://doi.org/10.1016/B978-0-12-802385-3.00006-1

Komarova, Y.A., Kruse, K., Mehta, D., Malik, A.B., 2017. Protein Interactions at Endothelial Junctions and Signaling Mechanisms Regulating Endothelial Permeability. Circ. Res. 120, 179–206. https://doi.org/10.1161/CIRCRESAHA.116.306534

Lambert, A.W., Pattabiraman, D.R., Weinberg, R.A., 2017. Emerging Biological Principles of Metastasis. Cell 168, 670–691. https://doi.org/10.1016/j.cell.2016.11.037

Leatherdale, A., Parker, D., Tasneem, S., Wang, Y., Bihan, D., Bonna, A., Hamaia, S.W., Gross, P.L., Ni, H., Doble, B.W., Lillicrap, D., Farndale, R.W., Hayward, C.P.M., 2020. Multimerin 1 supports platelet function *in vivo* and binds to specific GPAGPOGPX motifs in fibrillar collagens that enhance platelet adhesion. J. Thromb. Haemost. jth.15171. https://doi.org/10.1111/jth.15171

Leimeister, C., Steidl, C., Schumacher, N., Erhard, S., Gessler, M., 2002. Developmental Expression and Biochemical Characterization of Emu Family Members. Dev. Biol. 249, 204–218. https://doi.org/10.1006/dbio.2002.0764

Li, X., Padhan, N., Sjöström, E.O., Roche, F.P., Testini, C., Honkura, N., Sáinz-Jaspeado, M., Gordon, E., Bentley, K., Philippides, A., Tolmachev, V., Dejana, E., Stan, R.V., Vestweber, D., Ballmer-Hofer, K., Betsholtz, C., Pietras, K., Jansson, L., Claesson-Welsh, L., 2016. VEGFR2 pY949 signalling regulates adherens junction integrity and metastatic spread. Nat. Commun. 7, 11017. https://doi.org/10.1038/ncomms11017

Lorenzon, E., Colladel, R., Andreuzzi, E., Marastoni, S., Todaro, F., Schiappacassi, M., Ligresti, G., Colombatti, A., Mongiat, M., 2012. MULTIMERIN2 impairs tumor angiogenesis and growth by interfering with VEGF-A/VEGFR2 pathway. Oncogene 31, 3136–3147. https://doi.org/10.1038/onc.2011.487

Lugano, R., Ramachandran, M., Dimberg, A., 2020. Tumor angiogenesis: causes, consequences, challenges and opportunities. Cell. Mol. Life Sci. 77, 1745–1770. https://doi.org/10.1007/s00018-019-03351-7

Lugano, R., Vemuri, K., Yu, D., Bergqvist, M., Smits, A., Essand, M., Johansson, S., Dejana, E., Dimberg, A., 2018. CD93 promotes β1 integrin activation and fibronectin fibrillogenesis during tumor angiogenesis. J. Clin. Invest. 128, 3280–3297. https://doi.org/10.1172/JCI97459

Maes, H., Kuchnio, A., Peric, A., Moens, S., Nys, K., De Bock, K., Quaegebeur, A., Schoors, S., Georgiadou, M., Wouters, J., Vinckier, S., Vankelecom, H., Garmyn, M., Vion, A.-C., Radtke, F., Boulanger, C., Gerhardt, H., Dejana, E., Dewerchin, M., Ghesquière, B., Annaert, W., Agostinis, P., Carmeliet, P., 2014. Tumor Vessel Normalization by Chloroquine Independent of Autophagy. Cancer Cell 26, 190–206. https://doi.org/10.1016/j.ccr.2014.06.025

Mammoto, A., Connor, K.M., Mammoto, T., Yung, C.W., Huh, D., Aderman, C.M., Mostoslavsky, G., Smith, L.E.H., Ingber, D.E., 2009. A mechanosensitive transcriptional mechanism that controls angiogenesis. Nature 457, 1103–1108. https://doi.org/10.1038/nature07765

Marastoni, S., Andreuzzi, E., Paulitti, A., Colladel, R., Pellicani, R., Todaro, F., Schiavinato, A., Bonaldo, P., Colombatti, A., Mongiat, M., 2013. EMILIN2 down-modulates the Wnt signalling pathway and suppresses breast cancer cell growth and migration. J Pathol 14.

Mazzone, M., Dettori, D., Leite de Oliveira, R., Loges, S., Schmidt, T., Jonckx, B., Tian, Y.-M., Lanahan, A.A., Pollard, P., Ruiz de Almodovar, C., De Smet, F., Vinckier, S., Aragonés, J., Debackere, K., Luttun, A., Wyns, S., Jordan, B., Pisacane, A., Gallez, B., Lampugnani, M.G., Dejana, E., Simons, M., Ratcliffe, P., Maxwell, P., Carmeliet, P., 2009. Heterozygous Deficiency of PHD2 Restores Tumor Oxygenation and Inhibits Metastasis via Endothelial Normalization. Cell 136, 839–851. https://doi.org/10.1016/j.cell.2009.01.020

Mohan, V., 2020. Emerging roles of ECM remodeling processes in cancer. Semin. Cancer Biol. 9.

Mongiat, M., Andreuzzi, E., Tarticchio, G., Paulitti, A., 2016. Extracellular Matrix, a Hard Player in Angiogenesis. Int. J. Mol. Sci. 17, 1822. https://doi.org/10.3390/ijms17111822

Mongiat, M., Ligresti, G., Marastoni, S., Lorenzon, E., Doliana, R., Colombatti, A., 2007. Regulation of the Extrinsic Apoptotic Pathway by the Extracellular Matrix Glycoprotein EMILIN2. Mol Cell Biol 27, 7176-7187. http://doi: 10.1128/MCB.00696-07.

Mongiat, M., Marastoni, S., Ligresti, G., Lorenzon, E., Schiappacassi, M., Perris, R., Frustaci, S., Colombatti, A., 2010. The Extracellular Matrix Glycoprotein Elastin Microfibril Interface Located Protein 2: A Dual Role in the Tumor Microenvironment. Neoplasia 12, 294-IN1. https://doi.org/10.1593/neo.91930

Nitta, T., Hata, M., Gotoh, S., Seo, Y., Sasaki, H., Hashimoto, N., Furuse, M., Tsukita, S., 2003. Size-selective loosening of the blood-brain barrier in claudin-5–deficient mice. J. Cell Biol. 161, 653–660. https://doi.org/10.1083/jcb.200302070

Noy, P.J., Lodhia, P., Khan, K., Zhuang, X., Ward, D.G., Verissimo, A.R., Bacon, A., Bicknell, R., 2015. Blocking CLEC14A-MMRN2 binding inhibits sprouting angiogenesis and tumour growth. Oncogene 34, 5821–5831. https://doi.org/10.1038/onc.2015.34

Orlandini, M., Galvagni, F., Bardelli, M., Rocchigiani, M., Lentucci, C., Anselmi, F., Zippo, A., Bini, L., Oliviero, S., 2014. The characterization of a novel monoclonal antibody against CD93 unveils a new antiangiogenic target. Oncotarget 5, 2750–2760. https://doi.org/10.18632/oncotarget.1887

Orsenigo, F., Giampietro, C., Ferrari, A., Corada, M., Galaup, A., Sigismund, S., Ristagno, G., Maddaluno, L., Young Koh, G., Franco, D., Kurtcuoglu, V., Poulikakos, D., Baluk, P., McDonald, D., Grazia Lampugnani, M., Dejana, E., 2012. Phosphorylation of VE-cadherin is modulated by haemodynamic forces and contributes to the regulation of vascular permeability in vivo. Nat. Commun. 3, 1208. https://doi.org/10.1038/ncomms2199

Park, J.-S., Kim, I.-K., Han, S., Park, I., Kim, C., Bae, J., Oh, S.J., Lee, S., Kim, J.H., Woo, D.-C., He, Y., Augustin, H.G., Kim, I., Lee, D., Koh, G.Y., 2016. Normalization of Tumor Vessels by Tie2 Activation and Ang2 Inhibition Enhances Drug Delivery and Produces a Favorable Tumor Microenvironment. Cancer Cell 30, 953–967. https://doi.org/10.1016/j.ccell.2016.10.018

Paulitti, A., Andreuzzi, E., Bizzotto, D., Pellicani, R., Tarticchio, G., Marastoni, S., Pastrello, C., Jurisica, I., Ligresti, G., Bucciotti, F., Doliana, R., Colladel, R., Braghetta, P., Poletto, E., Di Silvestre, A., Bressan, G., Colombatti, A., Bonaldo, P., Mongiat, M., 2018. The ablation of the matricellular protein EMILIN2 causes defective vascularization due to impaired EGFR-dependent IL-8 production affecting tumor growth. Oncogene 37, 3399–3414. https://doi.org/10.1038/s41388-017-0107-x

Peach, C., Mignone, V., Arruda, M., Alcobia, D., Hill, S., Kilpatrick, L., Woolard, J., 2018. Molecular Pharmacology of VEGF-A Isoforms: Binding and Signalling at VEGFR2. Int. J. Mol. Sci. 19, 1264. https://doi.org/10.3390/ijms19041264

Pellicani, R., Poletto, E., Andreuzzi, E., Paulitti, A., Doliana, R., Bizzotto, D., Braghetta, P., Colladel, R., Tarticchio, G., Sabatelli, P., Bucciotti, F., Bressan, G., Iozzo, R.V., Colombatti, A., Bonaldo, P., **Mongiat, M.**, 2020. Multimerin-2 maintains vascular stability and permeability. Matrix Biol. 87, 11–25. https://doi.org/10.1016/j.matbio.2019.08.002

Phng, L.-K., Gerhardt, H., 2009. Angiogenesis: A Team Effort Coordinated by Notch. Dev. Cell 16, 196–208. https://doi.org/10.1016/j.devcel.2009.01.015

Pickup, M.W., Mouw, J.K., Weaver, V.M., 2014. The extracellular matrix modulates the hallmarks of cancer. EMBO Rep. 15, 1243–1253. https://doi.org/10.15252/embr.201439246

Potente, M., Gerhardt, H., Carmeliet, P., 2011. Basic and Therapeutic Aspects of Angiogenesis. Cell 146, 873–887. https://doi.org/10.1016/j.cell.2011.08.039

Potente, M., Mäkinen, T., 2017. Vascular heterogeneity and specialization in development and disease. Nat. Rev. Mol. Cell Biol. 18, 477–494. https://doi.org/10.1038/nrm.2017.36

Reid, S.E., Kay, E.J., Neilson, L.J., Henze, A., Serneels, J., McGhee, E.J., Dhayade, S., Nixon, C., Mackey, J.B., Santi, A., Swaminathan, K., Athineos, D., Papalazarou, V., Patella, F., Román-Fernández, Á., ElMaghloob, Y., Hernandez-Fernaud, J.R., Adams, R.H., Ismail, S., Bryant, D.M., Salmeron-Sanchez, M., Machesky, L.M., Carlin, L.M., Blyth, K., Mazzone, M., Zanivan, S., 2017. Tumor matrix stiffness promotes metastatic cancer cell interaction with the endothelium. EMBO J. 36, 2373–2389. https://doi.org/10.15252/embj.201694912

Reymond, N., d'Água, B.B., Ridley, A.J., 2013. Crossing the endothelial barrier during metastasis. Nat. Rev. Cancer 13, 858–870. https://doi.org/10.1038/nrc3628

Ribatti, D., 2013. Angiogenesis, in: Brenner's Encyclopedia of Genetics. Elsevier, pp. 130–132. https://doi.org/10.1016/B978-0-12-374984-0.00065-6

Rozario, T., DeSimone, D.W., 2010. The extracellular matrix in development and morphogenesis: A dynamic view. Dev. Biol. 341, 126–140. https://doi.org/10.1016/j.ydbio.2009.10.026

Sanz-Moncasi M.P., Garin-Chesa P., Stockert E., Jaffe E.A., Old L.J., Rettig W.J.
Identification of a high molecular weight endothelial cell surface glycoprotein, endoGlyx-1, in normal and tumor blood vessels Lab Invest 1994 71(3):366-73.

Schiavinato, A., Becker, A.-K.A., Zanetti, M., Corallo, D., Milanetto, M., Bizzotto, D., Bressan, G., Guljelmovic, M., Paulsson, M., Wagener, R., Braghetta, P., Bonaldo, P., 2012. EMILIN-3, Peculiar Member of Elastin Microfibril Interface-located Protein (EMILIN) Family, Has Distinct Expression Pattern, Forms Oligomeric Assemblies, and Serves as Transforming Growth Factor β (TGF-β) Antagonist. J. Biol. Chem. 287, 11498–11515. https://doi.org/10.1074/jbc.M111.303578

Schlesinger, M., Bendas, G., 2015. Vascular cell adhesion molecule-1 (VCAM-1)-An increasing insight into its role in tumorigenicity and metastasis: VCAM-1 in tumorigenicity. Int. J. Cancer 136, 2504–2514. https://doi.org/10.1002/ijc.28927

Shen, Q., Rigor, R.R., Pivetti, C.D., Wu, M.H., Yuan, S.Y., 2010. Myosin light chain kinase in microvascular endothelial barrier function. Cardiovasc. Res. 87, 272–280. https://doi.org/10.1093/cvr/cvq144

Spessotto, P., Cervi, M., Mucignat, M.T., Mungiguerra, G., Sartoretto, I., Doliana, R., Colombatti, A., 2003. β_1 Integrin-dependent Cell Adhesion to EMILIN-1 Is Mediated by the gC1q Domain. J. Biol. Chem. 278, 6160–6167. https://doi.org/10.1074/jbc.M208322200

Stegner, D., Dütting, S., Nieswandt, B., 2014. Mechanistic explanation for platelet contribution to cancer metastasis. Thromb. Res. 133, S149–S157. https://doi.org/10.1016/S0049-3848(14)50025-4

Strilić, B., Kučera, T., Eglinger, J., Hughes, M.R., McNagny, K.M., Tsukita, S., Dejana, E., Ferrara, N., Lammert, E., 2009. The Molecular Basis of Vascular Lumen Formation in the Developing Mouse Aorta. Dev. Cell 17, 505–515. https://doi.org/10.1016/j.devcel.2009.08.011

Sullivan, L.A., Brekken, R.A., 2010. The VEGF family in cancer and antibody-based strategies for their inhibition. mAbs 2, 165–175. https://doi.org/10.4161/mabs.2.2.11360

Tavora, B., Mederer, T., Wessel, K.J., Ruffing, S., Sadjadi, M., Missmahl, M., Ostendorf, B.N., Liu, X., Kim, J.-Y., Olsen, O., Welm, A.L., Goodarzi, H., Tavazoie, S.F., 2020. Tumoural activation of TLR3–SLIT2 axis in endothelium drives metastasis. Nature 586, 299–304. https://doi.org/10.1038/s41586-020-2774-y

Theocharis, A.D., Skandalis, S.S., Gialeli, C., Karamanos, N.K., 2016. Extracellular matrix **structure. Adv. Drug Deliv. Rev. 97, 4–27. https://doi.org/10.1016/j.addr.2015.11.001**

Thomas, M., Augustin, H.G., 2009. The role of the Angiopoietins in vascular morphogenesis. Angiogenesis 12, 125–137. https://doi.org/10.1007/s10456-009-9147-3

Tosi, G.M., Neri, G., Barbera, S., Mundo, L., Parolini, B., Lazzi, S., Lugano, R., Poletto, E., Leoncini, L., Pertile, G., Mongiat, M., Dimberg, A., Galvagni, F., Orlandini, M., 2020. The Binding of CD93 to Multimerin-2 Promotes Choroidal Neovascularization. Investig. Opthalmology Vis. Sci. 61, 30. https://doi.org/10.1167/iovs.61.8.30

Van Obberghen-Schilling, E., Tucker, R.P., Saupe, F., Gasser, I., Cseh, B., Orend, G., 2011. Fibronectin and tenascin-C: accomplices in vascular morphogenesis during development and tumor growth. Int. J. Dev. Biol. 55, 511–525. https://doi.org/10.1387/ijdb.103243eo

Wallez, Y., Cand, F., Cruzalegui, F., Wernstedt, C., Souchelnytskyi, S., Vilgrain, I., Huber, P., 2007. Src kinase phosphorylates vascular endothelial-cadherin in response to vascular endothelial growth factor: identification of tyrosine 685 as the unique target site. Oncogene 26, 1067–1077. https://doi.org/10.1038/sj.onc.1209855

Warmke, N., Walker, A.M.N., Cubbon, R.M., 2018. Angiogenesis, in: Encyclopedia of Cardiovascular Research and Medicine. Elsevier, pp. 85–96. https://doi.org/10.1016/B978-0-12-809657-4.99736-9

Wessel, F., Winderlich, M., Holm, M., Frye, M., Rivera-Galdos, R., Vockel, M., Linnepe, R., Ipe, U., Stadtmann, A., Zarbock, A., Nottebaum, A.F., Vestweber, D., 2014. Leukocyte extravasation and vascular permeability are each controlled in vivo by different tyrosine residues of VE-cadherin. Nat. Immunol. 15, 223–230. https://doi.org/10.1038/ni.2824

Wieland, E., Rodriguez-Vita, J., Liebler, S.S., Mogler, C., Moll, I., Herberich, S.E., Espinet, E., Herpel, E., Menuchin, A., Chang-Claude, J., Hoffmeister, M., Gebhardt, C., Brenner, H., Trumpp, A., Siebel, C.W., Hecker, M., Utikal, J., Sprinzak, D., Fischer, A., 2017. Endothelial Notch1 Activity Facilitates Metastasis. Cancer Cell 31, 355–367. https://doi.org/10.1016/j.ccell.2017.01.007

Wolf, M., Hoos, A., Bauer, J., Boettcher, S., Knust, M., Weber, A., Simonavicius, N., Schneider, C., Lang, M., StUrzl, M., Croner, R., Konrad, A., Manz, M.G., Moch, H., Aguzzi, A., 2012. Endothelial CCR2 Signaling Induced by Colon Carcinoma Cells Enables Extravasation via the JAK2-Stat5 and p38MAPK Pathway. Cancer Cell 22, 91-105. http://dx.doi.org/10.1016/j.ccr.2012.05.023

Wu, X., Giobbie-Hurder, A., Liao, X., Lawrence, D., McDermott, D., Zhou, J., Rodig, S., Hodi, F.S., 2016. VEGF Neutralization Plus CTLA-4 Blockade Alters Soluble and Cellular Factors Associated with Enhancing Lymphocyte Infiltration and Humoral Recognition in Melanoma. Cancer Immunol. Res. 4, 858–868. https://doi.org/10.1158/2326-6066.CIR-16-0084

Zacchigna, L., Vecchione, C., Notte, A., Cordenonsi, M., Dupont, S., Maretto, S., Cifelli, G., Ferrari, A., Maffei, A., Fabbro, C., Braghetta, P., Marino, G., Selvetella, G., Aretini, A., Colonnese, C., Bettarini, U., Russo, G., Soligo, S., Adorno, M., Bonaldo, P., Volpin, D., Piccolo, S., Lembo, G., Bressan, G.M., 2006. Emilin1 Links TGF-b Maturation to Blood Pressure Homeostasis. Cell 124, 929-942. doi: 10.1016/j.cell.2005.12.035.

Zhang, S., Xie, B., Wang, L., Yang, H., Zhang, H., Chen, Y., Wang, F., Liu, C., He, H., 2020. Macrophage-mediated vascular permeability via VLA4/VCAM1 pathway dictates ascites development in ovarian cancer. J. Clin. Invest. https://doi.org/10.1172/JCI140315

Zhu, X., Zhou, W., 2015. The Emerging Regulation of VEGFR-2 in Triple-Negative Breast Cancer. Front. Endocrinol. 6, 159. https://doi.org/10.3389/fendo.2015.00159

8. PUBLICATIONS

1. **The Binding of CD93 to Multimerin-2 Promotes Choroidal Neovascularization.**
   Tosi GM, Neri G, Barbera S, Mundo L, Parolini B, Lazzi S, Lugano R, Poletto E, Leoncini L, Pertile G, Mongiat M, Dimberg A, Galvagni F, Orlandini M. - Invest Ophthalmol Vis Sci. 2020 Jul 1;61(8):30 - doi: 10.1167/iovs.61.8.30.

2. **Role of Extracellular Matrix in Gastrointestinal Cancer-Associated Angiogenesis.**
   Andreuzzi E, Capuano A, Poletto E, Pivetta E, Fejza A, Favero A, Doliana R, Cannizzaro R, Spessotto P, Mongiat M.- Int J Mol Sci. 2020 May 23;21(10):3686 - doi: 10.3390/ijms21103686.

3. **Deregulated expression of Elastin Microfibril Interfacer 2 (EMILIN2) in gastric cancer affects tumor growth and angiogenesis**
   Andreuzzi E, Fejza A, Capuano A, Poletto E, Pivetta E, Doliana R, Pellicani R, Favero A, Maiero S, Fornasarig M, Cannizzaro R, Iozzo RV, Spessotto P, Mongiat M. – Matrix Biol Plus. May 2020, Volume 6-7 - doi.10.1016/j.mbplus.2020.100029

4. **TIMP-1 is Overexpressed and Secreted by Platinum Resistant Epithelial Ovarian Cancer Cells.**
   Sonego M, Poletto E, Pivetta E, Nicoloso MS, Pellicani R, Vinciguerra GLR, Citron F, Sorio R, Mongiat M, Baldassarre G.- Cells. 2019 Dec 18;9(1):6 - doi: 10.3390/cells9010006.

5. **Multimerin-2 maintains vascular stability and permeability.**
   Pellicani R, Poletto E, Andreuzzi E, Paulitti A, Doliana R, Bizzotto D, Braghetta P, Colladel R, Tarticchio G, Sabatelli P, Bucciotti F, Bressan G, Iozzo RV, Colombatti A, Bonaldo P, Mongiat M. - Matrix Biol. 2020 May;87:11-25 - doi: 10.1016/j.matbio.2019.08.002 - Epub 2019 Aug 15

6. **Sleeping beauty genetic screen identifies miR-23b::BTBD7 gene interaction as crucial for colorectal cancer metastasis**.
   Grisard E, Coan M, Cesaratto L, Rigo I, Zandonà L, Paulitti A, Andreuzzi E, Rampioni Vinciguerra GL, Poletto E, Del Ben F, Brisotto G, Biscontin E, Turetta M, Dassi E, Mirnezami A, Canzonieri V, Vecchione A, Baldassarre G, Mongiat M, Spizzo R, Nicoloso MS. - EBioMedicine. 2019 Aug;46:79-93 - doi: 10.1016/j.ebiom.2019.06.044 - Epub 2019 Jul 11.

7. **Loss of Multimerin-2 and EMILIN-2 Expression in Gastric Cancer Associate with Altered Angiogenesis**.
   Andreuzzi E, Capuano A, Pellicani R, Poletto E, Doliana R, Maiero S, Fornasarig M, Magris R, Colombatti A, Cannizzaro R, Spessotto P, Mongiat M. - Int J Mol Sci. 2018 Dec 11;19(12):3983 - doi: 10.3390/ijms19123983.

8. **The ablation of the matricellular protein EMILIN2 causes defective vascularization due to impaired EGFR-dependent IL-8 production affecting tumor growth.**
   Paulitti A, Andreuzzi E, Bizzotto D, Pellicani R, Tarticchio G, Marastoni S, Pastrello C, Jurisica I, Ligresti G, Bucciotti F, Doliana R, Colladel R, Braghetta P, Poletto E, Di Silvestre A, Bressan G, Colombatti A, Bonaldo P, Mongiat M. - Oncogene. 2018 Jun;37(25):3399-3414 - doi: 10.1038/s41388-017-0107-x - Epub 2018 Feb 27

9. ACKNOWLEDGMENTS

This work was carried out in the Division of Molecular Oncology and Preclinical Models of Tumor Progression at CRO-IRCSS Institute of Aviano (Italy), directed by Dr. Gustavo Baldassarre.

I would like to acknowledge all the members of the “Tumor Microenvironment and Angiogenesis” group and a special thanks to my supervisors Dr. Maurizio Mongiat and Dr. Paola Spessotto for the support given me in these three years.